

FELIPE DE QUEIROZ PIRES

IMPRESSÃO TRIDIMENSIONAL NO CAMPO FARMACÊUTICO E A  
APLICAÇÃO DA NANOTECNOLOGIA

BRASÍLIA

2023

UNIVERSIDADE DE BRASÍLIA  
FACULDADE DE CIÊNCIAS DA SAÚDE  
PROGRAMA DE PÓS-GRADUAÇÃO EM CIÊNCIAS DA SAÚDE

FELIPE DE QUEIROZ PIRES

IMPRESSÃO TRIDIMENSIONAL NO CAMPO FARMACÊUTICO E A  
APLICAÇÃO DA NANOTECNOLOGIA

Tese de doutorado apresentada ao Programa de Pós-Graduação em Ciências da Saúde da Universidade de Brasília como parte dos requisitos para obtenção do título de doutor.

Orientador: Prof. Dr. Marcílio Sérgio Soares da Cunha Filho

Co-orientador: Prof. Dr. Álvaro Goyanes Goyanes

BRASÍLIA

2023

FELIPE DE QUEIROZ PIRES

IMPRESSÃO TRIDIMENSIONAL NO CAMPO FARMACÊUTICO E A  
APLICAÇÃO DA NANOTECNOLOGIA

Tese de doutorado apresentada ao Programa  
de Pós-Graduação em Ciências da Saúde da  
Universidade de Brasília como parte dos  
requisitos para obtenção do título de doutor.

Aprovado em:

BANCA EXAMINADORA

Dr. Marcílio Sérgio Soares da Cunha Filho  
Universidade de Brasília – presidente

Dr. Paulo César de Moraes  
Universidade Católica de Brasília

Dr. João Paulo Longo  
Universidade de Brasília

Dr. Breno Noronha Matos  
Centro Universitário Unieuro

Dra. Idejan Padilha Gross  
Universidade de Brasília – suplente

## **AGRADECIMENTOS**

Agradeço toda a minha família e amigos por todo apoio, confiança e paciência.

Agradeço ao meu orientador, professor Marcílio Cunha-Filho pela orientação e o esforço em moldar este trabalho até a melhor forma possível. A todos os professores que colaboraram com o trabalho, em especial os professores Guilherme Gelfuso, Taís Gratieri e Lívia Sá Barreto pela colaboração tanto intelectual quanto pessoal, incentivando a manutenção do bom trabalho.

E por fim, agradeço aos meus colegas do LTMAC, em especial à Ludmila Alvim, Ana Luiza Lima, Idejan Gross, Jéssika Rocha, Camila Cardoso, Breno Noronha e Ricardo Nunes que não só me ajudaram em diversos trabalhos, mas contribuíram sempre com ideias e palavras de incentivo.

“The world always seems brighter when you´re just made something that wasn´t there before.”

Neil Gaiman

## RESUMO

A utilização da impressão 3D na área farmacêutica promete revolucionar a forma de se utilizar um medicamento, tendo a completa personalização como uma das principais vantagens do seu uso, com destaque para a impressão 3D por modelagem de fusão e deposição que incorpora no seu processo técnicas já utilizadas na indústria farmacêutica, como a termoextrusão. Com essa tecnologia se ampliou as possibilidades terapêuticas, visto que mudanças nos parâmetros de impressão, podem afetar características importantes do medicamento como a dosagem e o perfil de liberação. Os avanços nessa aplicação medicinal da tecnologia 3D vêm trazendo também novas vertentes de terapia, como a combinação com outras tecnologias de grande impacto, como a nanotecnologia. A nanotecnologia já vem demonstrando seu impacto há anos na área farmacêutica e se amplia ainda mais quando existe o envolvimento de materiais poliméricos associados a fármacos, devido a tendência destes materiais de formarem nanopartículas de forma espontânea em determinadas condições de dissolução. Com isso, o presente trabalho tem objetivo de investigar a impressão 3D por modelagem de fusão e deposição como uma forma confiável de obtenção de formas farmacêuticas e sua correlação com a nanotecnologia, seja pela formação espontânea de nanocompostos ou pela inclusão de nanopartículas em formulações que serão impressas. A primeira parte do estudo avaliou o impacto dos parâmetros de impressão na obtenção de protótipos de medicamentos, evidenciando a necessidade de protocolos de validação para incorporar a tecnologia na produção de medicamentos. Na segunda parte do estudo foi feita uma investigação da formação de nanopartículas *in situ*, pela dissolução de comprimidos feitos por impressão 3D, formulados com três diferentes polímeros e utilizando a naringenina como o fármaco modelo. O resultado demonstrou a formação das partículas nos três polímeros testados, encapsulando uma quantidade considerável do fármaco, demonstrando a necessidade de conhecer esse processo como uma forma de prever como estas partículas podem afetar a absorção oral destes compostos. Por fim, na terceira parte foi feita a inserção de nanopartículas de óxido de ferro em comprimidos feitos por impressão 3D com o objetivo de avaliar a compatibilidade das duas tecnologia para a aplicação no tratamento oral de deficiência de ferro. Os resultados obtidos mostraram que os processos de extrusão impressão são capazes de gerar interações importantes entre o polímero e as nanopartículas, resultando na formação *in situ* de um revestimento polimérico nas partículas capaz de mudar suas características físico-químicas e biológicas

Palavras-chave: Impressão 3D; Nanotecnologia; Administração oral; Polímeros; Termoextrusão.

## ABSTRACT

The use of 3D printing in the pharmaceutical area promises to revolutionize the drug therapy, having the complete customization of the dosage form as one of the main advantages of its use, with emphasis on the fused deposit modeling technique (FDM) that incorporates in its process technologies already used in the pharmaceutical industry, such as hot melt extrusion. With this technology the therapeutic possibilities have been expanded, since changes in the printing parameters can affect important characteristics of the drug, such as dosage and release profile. With the advances in this medicinal application of 3D technology, new aspects of therapy are being developed, such as the combination with other technologies of great impact, like nanotechnology. Nanotechnology has been demonstrating its impact for years in the pharmaceutical area, becoming even more important when polymeric materials associated with drugs are involved, due to the tendency of these materials to spontaneously form nanoparticles under certain dissolution conditions. With this, the present work aims to investigate 3D printing FDM as a reliable way to obtain pharmaceutical dosage forms and its correlation with nanotechnology, either by the spontaneous formation of the nanoparticles or by the inclusion of nanoparticles in formulations that will be printed. The first part of the study evaluated the impact of the 3D printing parameters in obtaining drug prototypes, highlighting the need for validation protocols to incorporate the technology in drug production. The second part of the study investigated the *in-situ* formation of nanoparticles by the dissolution of 3D-printed tablets formulated with three different polymers and using naringenin as the model drug. The result demonstrated the formation of the particles in all the tested polymers, encapsulating a considerable amount of the drug, demonstrating the necessity to understand this process as a way to predict how these particles may affect the oral drug absorption. Finally, in the third part iron oxide nanoparticles were inserted into an oral pharmaceutical form made by 3D printing, investigating their dissolution process and the possibility of their use for the oral treatment of iron deficiency. The results proved that the extrusion and 3D printing processes were capable to enhance the interaction between polymer and particles resulting in an *in-situ* coating process changing physical-chemical and biological characteristics of the particles.

**Keywords:** 3D printing; Nanotechnology; Oral administration; Polymers; Hot Melt Extrusion.

## FIGURES LIST

### Chapter I

**Figure 1.** 3D printing techniques (Source: Adapted from Miller and Burdick, 2016)...20

### Chapter II

**Figure 1.** Model planning phases using DOE.....48

**Figure 2.** Photomicrography of generic Mesalazine 500 mg tablet (A and B); printlets in cylindrical (C, D, G, H, K, and L) and torus (E, F, I, J, M, and N) format produced using the polymers ABS, HIPS, and PLA. Top (A, C, E, G, I, K, and M) and lateral (B, D, F, H, J, L, and N) views. ....51

**Figure 3.** The surface responses for the printlets' average mass using the filaments ABS, HIPS, or PLA, their predictive equations, and correlation coefficients. A–printlets per plate; B–size scale; C–infill density; D–printing speed; F–temperature; H–shape; J–printer brand.....53

**Figure 4.** 3D model of unfinished printlets showing details of the inner space, infill pattern, and infill density of torus (B, D, F, and H) and cylindrical (A, C, E, and G) printlets with 10 and 50% infill density.....55

**Figure 5.** The surface responses for the mass variation coefficient of the printlets use the filaments ABS, HIPS, or PLA, their predictive equations, and correlation coefficients. A–printlets per plate; B–size scale; E–layer height; G–infill pattern; H–shape; J–printer brand.....56

**Figure 6.** The surface responses for printing time of printlets using the filaments ABS, HIPS, or PLA, their predictive equations, and correlation coefficients. B–size scale; D–printing speed; E–layer height.....58

**Figure 7.** The surface responses for porosity (%) of the printlets using the filaments ABS, HIPS, or PLA, their predictive equations, and correlation coefficients. B–size scale; C–infill density; D–printing speed; H–shape.....60

**Figure 8.** Surface response, predictive equations, correlation coefficients, and adeq. precision values for average mass (mg) response of ABS, HIPS, and PLA polymers. A–amount of printlets per plate, B–size scale, C–infill density.....63



**Figure 9.** Surface response, predictive equations, correlation coefficients, and adequacy precision values for porosity (%) response of ABS, HIPS, and PLA polymers. A—amount of printlets per plate, B—size scale, C—infill density.....65

### Chapter III

**Figure 1.** Variation of the total Hansen solubility parameter ( $\Delta\delta_t$ ) of each combination of materials related to the polymer-based formulations of hydroxypropylmethylcellulose acetate succinate (HPMCAS) and the plasticizer triethyl citrate (TEC) (A), Polyvinyl alcohol (PVA) and the plasticizer Glycerin (GLY) (B), and Eudragit RL PO<sup>®</sup> (EUD RL) and the plasticizer TEC (C). The blue line represents the limit for high interactions (up to 7.0 MPa<sup>1/2</sup>), and the green line is the limit for low interactions (up to 10.0 MPa<sup>1/2</sup>).....85

**Figure 2.** FTIR spectra of the selected samples: a) hydroxypropylmethylcellulose acetate succinate (HPMCAS) and Naringenin (NAR); b) HPMCAS and triethyl citrate (TEC); c) Glycerin (GLY) and NAR; and d) Eudragit RL PO<sup>®</sup> (EUD RL) and TEC. The theoretical average spectrum, was obtained by the combination of the pure material spectra data considering the proportion of each component.....86

**Figure 3.** a) FTIR spectra of the physical mixture and calculated average spectrum for PVA/GLY/NAR ternary system; b) Zoom of the highlighted gray shaded rectangle region, from 1,300 to 900 cm<sup>-1</sup>. PVA - Polyvinyl alcohol, GLY – Glycerin and NAR – Naringenin.....87

**Figure 4.** Dissolution profile and mean encapsulation of the released Naringenin (NAR) through 24 h experiment for the printlets produced with the polymers hydroxypropylmethylcellulose acetate succinate (HPMCAS), Polyvinyl alcohol (PVA), and Eudragit RL PO<sup>®</sup> (EUD RL) and the control samples, pure NAR, and physical mixture. Since the drug encapsulation values were stable, the mean drug encapsulation considers the values obtained during the experiment.....90

**Figure 5.** Graphical representation of the pathways of particle formation, phase separation and erosion.....92

**Figure 6.** Particle diameter and zeta potential of the particles arose spontaneously from the dissolution of the physical mixtures and the printlets over 24h, produced with the polymers hydroxypropylmethylcellulose acetate succinate (HPMCAS), Polyvinyl alcohol (PVA), and Eudragit RL PO<sup>®</sup> (EUD RL).....95

**Figure 7.** TEM images of the particles arose spontaneously from the dissolution of the physical mixtures and the printlets after 24h produced with the polymers hydroxypropylmethylcellulose acetate succinate (HPMCAS), Polyvinyl alcohol (PVA), and Eudragit RL PO<sup>®</sup> (EUD RL).....97

#### **Chapter IV**

**Figure 1.** Diameter analysis by dynamic light scattering and transmission electronic microscopy analysis of the iron oxide nanoparticles.....113

**Figure 2.** Mechanical properties of the filament. Highlighted the elastic and plastic deformation phases, the fracture and the minimal fracture force for a quality filament for fused deposit modeling 3D printing , at 5.0 N.....114

**Figure 3.** Theoretical and experimental TGA analyses of printlets formulations on the filament and printlet made with the iron oxide nanoparticles. The theoretical thermogram was obtained considering the contribution of each formulation compound on the mass loss events.....115

**Figure 4.** FTIR of the iron oxide nanoparticles (IONP), filament and printing. Highlighted the most identifiable peaks of the IONP, the polymer Polyvinyl alcohol (PVA) and the plasticizer glycerin (GLY) on all the spectrums.....116

**Figure 5.** Particle diameter of the particles released from the dissolution of the iron oxide nanoparticles (IONP) powder and printlets along 6h. Additionally, transmission electronic microscopy images of printlets aliquots.....118

**Figure 6.** Zeta potential analysis in three different pH, 2.0, 7.0 and 10.0 of the particles released from the dissolution of the iron oxide nanoparticles (IONP) powder and printlets along 6h.....119

**Figure 7.** Illustration of the erosion process of the polymeric matrix of the printlets, forming polymeric nanosized structures that can carry the iron oxide nanoparticles (IONP) agglomerations.....121

**Figure 8.** Dissolution profile of the iron oxide nanoparticles (IONP) powder and printlets along 6h.....124

## Appendix B

<b>Figure 1.</b> FTIR spectrum of naringenin (NAR) as supplied.....	139
<b>Figure 2.</b> FTIR spectrum of hydroxypropylmethylcellulose acetate succinate (HPMCAS) as supplied.....	139
<b>Figure 3.</b> FTIR spectrum of Polyvinyl alcohol (PVA) as supplied.....	140
<b>Figure 4.</b> FTIR spectrum of Eudragit RL PO (EUD RL) as supplied.....	140
<b>Figure 5.</b> FTIR spectrum of Triethyl citrate (TEC) as supplied.....	141
<b>Figure 6.</b> FTIR spectrum of glycerin (GLY) as supplied.....	141

## Appendix C

<b>Figure 1.</b> Particle diameter and zeta potential of the particles arose spontaneously from the dissolution of the physical mixtures and the printlets over 24h, produced with the polymers hydroxypropylmethylcellulose acetate succinate (HPMCAS) and Eudragit RL PO <sup>®</sup> (EUD RL) without the model drug naringenin (NAR). The highlighted data are the only ones with count rate higher than 100 keps, been the only reliable data.....	142
---	-----

## TABLES LIST

### Chapter II

<b>Table 1.</b> Polymer filaments characteristics.....	51
<b>Table 2.</b> Predicted and experimental results of the simulated prescriptions #1 and #2 obtained using ABS, HIPS, and PLA filaments, with 95% of confidence interval (CI) of prediction.....	66

### Chapter III

<b>Table 1.</b> Formulations composition (% , m/m) with the amount of plasticizer and model drug. HPMCAS - hydroxypropylmethylcellulose acetate succinate, PVA - Polyvinyl alcohol, EUD RL - Eudragit RL PO <sup>®</sup> , TEC - Triethyl citrate, GLY – Glycerin and NAR.....	77
<b>Table 2.</b> Hansen solubility parameters. $\delta_d$ – Dispersion parameter; $\delta_p$ – Polar parameter; $\delta_h$ – Hydrogen bonds parameter; $\delta_t$ – Total Hansen solubility parameter. HPMCAS - hydroxypropylmethylcellulose acetate succinate, PVA - Polyvinyl alcohol, EUD RL - Eudragit RL PO <sup>®</sup> , TEC - triethyl citrate and GLY - Glycerin.....	78
<b>Table 3.</b> Filaments manufacturing specifications and characterization data of all formulations with and without naringenin (NAR). HPMCAS - hydroxypropylmethylcellulose acetate succinate, PVA - Polyvinyl alcohol, EUD RL - Eudragit RL PO <sup>®</sup> , $T_{\text{extrusion}}$ – Extrusion temperature and $V_{\text{rotation}}$ - Velocity of the screws rotation.....	79
<b>Table 4.</b> Printlets manufacturing specifications and characterization data of all formulations with and without naringenin (NAR). HPMCAS - hydroxypropylmethylcellulose acetate succinate, PVA - Polyvinyl alcohol, EUD RL - Eudragit RL PO <sup>®</sup> and $T_{\text{printing}}$ – printing temperature.....	81

### Chapter IV

<b>Table 1.</b> Filaments and printlets made with the iron oxide nanoparticles (IONP) manufacturing specifications and characterization data. $T_{\text{extrusion}}$ – Extrusion temperature; $V_{\text{rotation}}$ = Velocity of the screw rotation; $T_{\text{printing}}$ – Printing temperature; $T_{\text{printing platform}}$ – Printing platform temperature.....	108
---	-----

## **Appendix A**

<b>Table 1.</b> Bibliographic search on polymeric based 3D printed dosage forms evaluating the investigation on the in-situ formation of nano/micro compounds.....	132
--	-----

## ABREVIATIONS

3D	Three-Dimensional
3DP	Three-dimensional printing
ABS	Acrylonitrile butadiene styrene
API	Active pharmaceutical ingredients
CIJ	Continuous inkjet
DE	Dissolution efficiency
DOD	Drop-on-demand
DOE	Design of experiments
DSC	Differential scanning calorimetry
EUD	Eudragit <sup>®</sup>
FDM	Fused deposit modeling
GLY	Glycerin
GNP	Gold nanoparticles
HIPS	High impact polystyrene
HME	Hot Melt Extrusion
HPC	Hydroxypropyl cellulose
HPMC	Hydroxypropyl methylcellulose
HPMCAS	Hydroxypropyl methylcellulose acetate succinate
IONP	Iron oxide nanoparticles
NAR	Naringenin
pdI	Polydispersity index
PET-G	Polyethylene terephthalate glycol-modified
PLA	Poly(lactic acid)
PLGA	Poly (lactic-co-glycolic acid)
PVA	Poly(vinyl alcohol)
SLA	Stereolithography
SLN	Solid lipid nanoparticles
SLS	Selective laser sintering
SSE	Semisolid extrusion
TEC	Triethyl citrate
TGA	Thermogravimetry
WHO	World health organization

## SUMMARY

<b>1. CHAPTER I: OBJECTIVES AND LITERATURE REVIEW.....</b>	<b>17</b>
<b>1.1 INTRODUCTION .....</b>	<b>17</b>
<b>1.2 OBJECTIVES.....</b>	<b>19</b>
1.2.1 Specific objectives .....	19
<b>1.3 LITERATURE REVIEW .....</b>	<b>20</b>
1.3.1 Three-dimensional printing .....	20
1.3.2 Nanotechnology and the application in oral drug delivery .....	27
1.3.3 Nanotechnology Applied to FDM 3D printing for oral delivery .....	32
<b>1.4. REFERENCES .....</b>	<b>36</b>
<b>2. CHAPTER II: PREDICTIVE MODELS OF FDM 3D PRINTING USING EXPERIMENTAL DESIGN BASED ON PHARMACEUTICAL REQUIREMENTS FOR TABLETS PRODUCTION .....</b>	<b>45</b>
<b>2.1 INTRODUCTION .....</b>	<b>45</b>
<b>2.2 MATERIAL AND METHODS .....</b>	<b>46</b>
2.2.1 Material.....	46
2.2.2 Thermal characterization of polymeric filaments .....	47
2.2.3. Model planning using DOE .....	47
2.2.4 Printlets characterization .....	50
<b>2.3 RESULTS AND DISCUSSION .....</b>	<b>50</b>
2.3.1 Characterization of the filaments .....	50
2.3.2. Model planning: Screening design.....	52
2.3.3 Optimization process .....	61
2.3.4 Model Checking .....	66
<b>2.4 CONCLUSION .....</b>	<b>68</b>
<b>2.5 REFERENCES .....</b>	<b>68</b>
<b>3. CHAPTER III: IN-SITU FORMATION OF NANOPARTICLES FROM DRUG-LOADED 3D POLYMERIC MATRICES.....</b>	<b>74</b>
<b>3.1. INTRODUCTION .....</b>	<b>74</b>
<b>3.2. MATERIALS AND METHODS .....</b>	<b>76</b>
3.2.1. Materials .....	76
3.2.2. Preformulation studies .....	76
3.2.3. Filament production by HME.....	79
3.2.4. Filament characterization .....	80
3.2.5. Printlets production by FDM 3D printing .....	80
3.2.6. Printlets characterization .....	81
3.2.7. Dissolution studies and drug encapsulation.....	82
3.2.8. Characterization of the <i>in situ</i> formed particles.....	83
3.2.9. Drug determination .....	83

<b>3.3. RESULTS AND DISCUSSION .....</b>	<b>84</b>
<b>3.3.1. Preformulation studies .....</b>	<b>84</b>
<b>3.3.2. The HME filaments.....</b>	<b>88</b>
<b>3.3.2. The printlets characterization.....</b>	<b>89</b>
<b>3.3.3. The dissolution assays .....</b>	<b>89</b>
<b>3.3.4. The particles characterization .....</b>	<b>93</b>
<b>3.4. CONCLUSIONS .....</b>	<b>99</b>
<b>3.5. REFERENCES .....</b>	<b>99</b>
<b>4. CHAPTER IV: PRELIMINARY STUDIES ON THE COMBINATION OF IRON OXIDE NANOPARTICLES AND FDM 3D PRINTING ON THE ORAL TREATMENT OF IRON DEFICIENCY.....</b>	<b>105</b>
<b>4.1. INTRODUCTION .....</b>	<b>105</b>
<b>4.2. MATERIALS AND METHODS .....</b>	<b>107</b>
<b>4.2.1. Materials .....</b>	<b>107</b>
<b>4.2.2. Iron oxide nanoparticles production .....</b>	<b>107</b>
<b>4.2.3 Filament production by hot-melt extrusion .....</b>	<b>107</b>
<b>4.2.4 Printlets production by FDM 3D printing .....</b>	<b>109</b>
<b>4.2.5. Characterizations .....</b>	<b>109</b>
<b>4.2.6. Released particles characterization .....</b>	<b>110</b>
<b>4.2.7. Dissolution studies.....</b>	<b>111</b>
<b>4.2.8. Iron determination.....</b>	<b>112</b>
<b>4.3. RESULTS AND DISCUSSION .....</b>	<b>112</b>
<b>4.3.1. Characterization studies.....</b>	<b>112</b>
<b>4.3.2. Characterization of the released particles .....</b>	<b>117</b>
<b>4.3.3. The dissolution assays .....</b>	<b>123</b>
<b>4.4. CONCLUSIONS .....</b>	<b>125</b>
<b>4.5. REFERENCES .....</b>	<b>125</b>
<b>5. CONCLUSION .....</b>	<b>130</b>
<b>APPENDIX A – Bibliographical search .....</b>	<b>132</b>
<b>APPENDIX B – FTIR Isolated materials.....</b>	<b>139</b>
<b>APPENDIX C – PArticle release of saples without naringenin.....</b>	<b>142</b>



## **1. CHAPTER I: OBJECTIVES AND LITERATURE REVIEW**

### **1.1 INTRODUCTION**

The use of three-dimensional printing (3DP) in the pharmaceutical field is promised to be one of the main trends of the market on the future, revolutionizing the way to consume medications (Araújo et al., 2019). The complete customization of the dosage form is the main advantage of its use, making possible the production of a dosage form completely adapted to the necessities of the user and the health professional (Tamil Ponni et al., 2020).

With this technology the administration possibilities have been expanded, since changes in the shape of the printed material and the printing parameters can affect important characteristics of the medication, such as dosage, release profile, and comfort of administration (Pires et al., 2020).

Of the various 3DP techniques, fused deposit modeling (FDM) has been increasingly employed in this area, due to its precision, diversity of raw materials, and direct relationship with the Hot Melt Extrusion technique (HME), already widely used in the pharmaceutical industry (Nukala et al., 2019b).

With the advances in this medicinal application of 3D technology, new possibilities of therapy are being developed, such as the combination with other technologies of great impact, like nanotechnology (Elder et al., 2020).

Nanotechnology has been demonstrating its impact for years in several areas. In the pharmaceutical field, a highlight can be given to its use on drug delivery, applied in various routes of administration, including the oral route. With the nanoparticles the drug is capable to be absorbed and achieve the action site in a more efficient and direct way, contributing to a more focus and beneficial action (Mitchell et al., 2021).

The participation of nanotechnology expands even more with the involvement of polymeric materials associated with drugs, in formulations like solid dispersions and dosage forms made with 3DP, due to the tendency of these materials to form nanoparticles spontaneously under certain dissolution conditions, affecting the pharmacokinetics of the drug (Schittny et al., 2020).

With that, the relationship between 3DP and nanotechnology is already established by this spontaneous formation, although studies on this regard are lacking. However, the beneficials of the combination of those technologies are already being recognized by the scientific community, with many studies attempting to combine the versatility of the 3DP,

with the beneficial properties of the nanoparticles for many different purposes. (dos Santos et al., 2021).

Therefore, the object of this study is to expand on the understanding of the relationship of 3DP and nanotechnology. Firstly, by understanding the 3DP technology through the study of the impact of the 3D printing parameters in obtaining drug prototypes. Secondly, describing the spontaneous formation of nanoparticles from the dissolution of 3D printed oral dosage forms. And finally, the insertion of iron oxide nanoparticles in 3D printed oral dosage forms, investigating their dissolution process and the possibility of its use for the oral treatment of iron deficiency

## 1.2 OBJECTIVES

Investigate FDM 3D printing as a reliable way to obtain pharmaceutical dosage forms and its correlation with nanotechnology, either by the spontaneous formation of the nanoparticles or by the inclusion of nanoparticles in formulations that will be printed.

### 1.2.1 Specific objectives

- Review the available data on 3D printing of oral dosage forms, nanotechnology and the combination of both technologies.
- Understand the 3D printing FDM technique by the evaluation of the impact of the printing parameters on printed dosage forms.
- Use the dosage forms developed to describe the *in-situ* formation of nanoparticles from 3D printed oral dosage forms made with different polymers.
- Insert iron oxide nanoparticles on the developed formulation of 3D printed oral dosage forms, evaluating the interaction between nanoparticles and polymers during the dissolution process.

## 1.3 LITERATURE REVIEW

### 1.3.1 Three-dimensional printing

Three dimensional printing (3DP) is the technique that makes use of computational programs to modeling and programming the construction of a 3D model by layering materials on a surface (Tamil Ponni et al., 2020). This technology started to getting shape in the early 1980's, having the first commercial debut in the end of this decade, mostly selling fabrication machinery used on different manufactory industries (Savini and Savini, 2015).

With the rising popularity of the technique the research for new forms of 3DP originated the several different printing methods that are available on the market today. The most popular methods are the ink-jet based, extrusion based and laser based 3DP (Figure 1) (Mohammed et al., 2021).

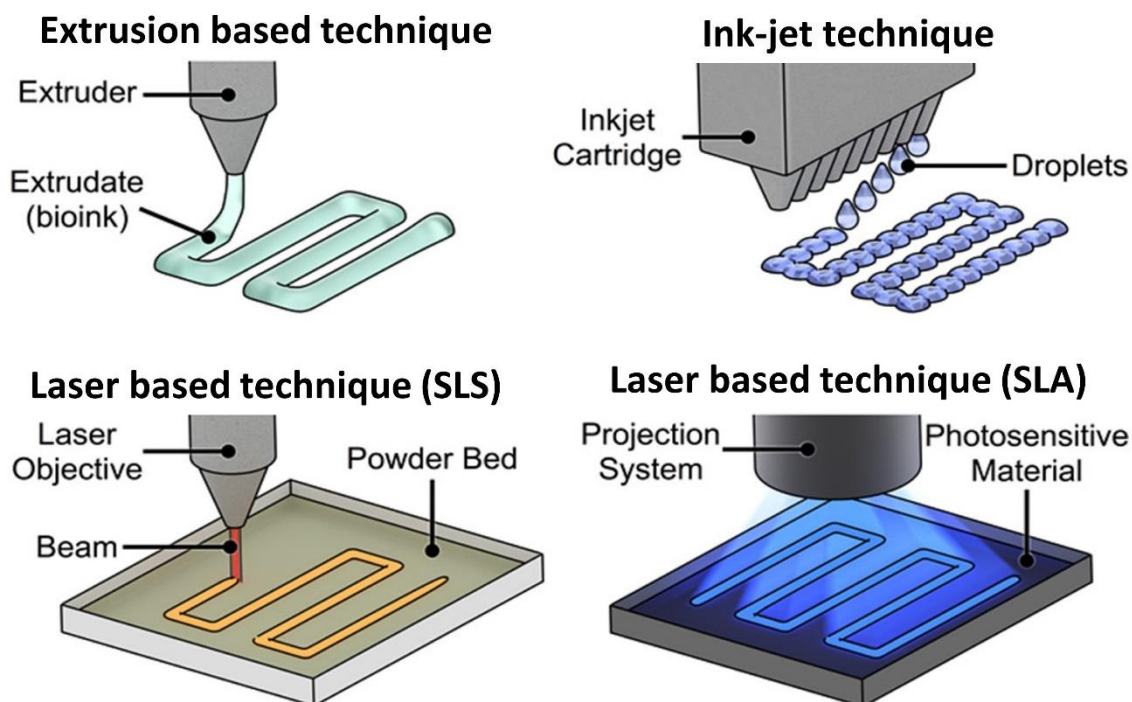


**Figure 1.** 3D printing techniques ( Source: Adapted from Miller and Burdick, 2016)

The ink-jet technique is grounded by the idea of a traditional desktop inkjet printer, using a liquid material to impregnate a different material, forming the printed model (Sen et al., 2020). Two different ink-jet printing techniques are available, continuous inkjet printing (CIJ) and drop-on-demand printing (DOD), both based on the

deposition of a liquid adhesive material on a powder, binding the powder particles on the shape previously defined by the computer modulation. The difference between the techniques is the deposition flow of the liquid, on the CIJ the liquid is deposited in a continuous flow on an orifice containing the powder and on the DOD the deposition is controlled by a trigger signal only on the areas necessary for the 3D model construction (Mohammed et al., 2021). The many possibilities of materials used in both the powder and the liquid binder formulations make this technique very attractive for many different areas.

The extrusion based 3DP is based on the extrusion of a material through a narrow nozzle by pressure, characterizing the semisolid extrusion technique (SSE), or by the melting of a solid filament, characterizing the fused deposit modeling technique (FDM). In both techniques the material is deposited in layers in a surface and forming the 3D model after solidification (Tamil Ponni et al., 2020). The differences between the techniques are just the type of substrate and the extrusion method. Those techniques have been a focus of research and development in many areas because of the great variety of materials that can be used as substrate and the precision of the printed model (Kristiawan et al., 2021).

The laser based 3DP uses a high energy UV laser to bind materials in layers, forming the 3D model. The type of materials bound by the laser beam characterize the different techniques that use this type of 3DP technology. If the material is a liquid polymeric resin that are bound by the laser beam on the precise areas necessary for the formation of the 3D model, the technique used is called stereolithography (SLA). If the material is a powder that is sintered in a temperature below the melting point and the laser beam is responsible to melting and fusion of the material particles in the shape of the 3D model, the used technique is called selective laser sintering (SLS) (Palo et al., 2017). Those techniques have been also widely explored due to the high precision of the printing, resulting in very detailed models (Martinez et al., 2018).

The nature of the materials used for all the techniques are also a subject of intense research, that made possible the expansion of the technology beyond the engineering area. The polymers are the focus material because of its versatile physical and chemical characteristics, capable to be applied to different techniques and fields, but it's not the only possibility (Stansbury and Idacavage, 2016). For example, the extrusion technique can be applied to the 3DP of different materials like metals, ceramic and food, expanding even more the possibilities of application (Chen et al., 2019; Ni et al., 2019; Piyush et al., 2019).

As it can be implied by the great variety of techniques and materials, the versatility is the main attractive point for several areas that can benefit from the use of the 3DP technology. The models can be printed on different shapes and sizes, with levels of details that are becoming more precise each day, with the evolution of the processes (Tamil Ponni et al., 2020). Besides that, other advantages like the low investment cost, since the technique dispenses the use of additional accessories, and the possibility of complete personalization of the final product, add new layers to the benefits of the 3DP use (Araújo et al., 2019; Jiménez et al., 2019).

The biomedical area was one of the fields that embraced the 3DP and are innovating each day on its use. For example, the 3DP is already used to print prosthetic pieces to substitute bones and cartilages when it is necessary, it is also possible to print tissues and organs to substitute defected ones and the printing of pharmaceutical dosage forms, with several advantages compared to the traditional forms (Jin et al., 2021; Manero et al., 2019; Parhi and Jena, 2021). In particular, the use of 3D printing for the manufacturing of pharmaceutical dosage forms is a field that are rapidly growing, and it is considered a possible next trend on the pharmaceutical area.

#### 1.3.1.1 Three-dimensional printing on the pharmaceutical field

The application of 3DP on the pharmaceutical field was made possible by the use of biodegradable polymeric plastic materials that for years has already been applied to other types of pharmaceutical products, like solid dispersion in oral dosage forms and patches in topic and transdermic products (Monschke and Wagner, 2020; Sabbagh and Kim, 2022). Besides that, the incorporation of methods, like hot melt extrusion (HME), to the pharmaceutical practice narrow the distance between the pharmaceutical field and 3DP since this method is used in both areas (Tambe et al., 2021)ta.

Several 3DP techniques were already explored on the pharmaceutical field. The inkjet technic was already applied for the manufacture of dosage forms like oral films and controlled released tablets, including the first FDA approved tablet made by 3DP, “spritam”, made using the DOD 3DP technique (Sen et al., 2020). The laser based 3DP method are also the subject of studies for the formulation of different pharmaceutical forms, like microneedles for transdermic release and other devices (Economidou et al., 2019). However today on the pharmaceutical field the dominant 3DP technology,

responsible to about 80% of the studies made on this area, are the extrusion based 3DP, especially the FDM technique (Mohammed et al., 2021).

On the extrusion based FDM technique a pre-produced thermoplastic filament is used as substrate of the printer. The filament is melted and extruded through a nozzle forming the model defined by the 3D modeling software. The filament is produced mixing a polymeric material and additional components using HME, a technology that combine high temperatures and intense shear to change the thermoplastic characteristics of the materials, extruding it through an orifice that can be adapted to different shapes, including filaments of approximately 1.75 mm, one of the patterns to FDM 3DP use (Kristiawan et al., 2021).

The HME technology is already consolidated in many types of industries, including the pharmaceutical, producing, for example, solid dispersions and films for oral dosage. For the pharmaceutical use of 3DP the filaments produced are formed by a biodegradable pharmaceutical-grade polymer, the active pharmaceutical ingredients (API) and other additives to enhance the formulation performance physically and pharmaceutically (Tan et al., 2018).

On a traditional non-medicinal application of 3DP the polymers used are normally thermoplastic materials well adapted to the printing process, like acrylonitrile butadiene styrene (ABS), poly(lactic acid) (PLA), high impact polystyrene (HIPS), polyethylene terephthalate glycol-modified (PET-G) and poly(vinyl alcohol) (PVA). Some of those polymers, such as PLA and PVA, are biodegradable medically graded materials that can be used to some medical application, like prosthetics, but in the market there are no options of filament containing some kind of API material for pharmaceutical purposes (Rahim et al., 2019).

On the pharmaceutical research a huge variety of polymers are being tested for the 3DP of many types of pharmaceutical dosage forms with great results, including PLA, PVA, hydroxypropyl cellulose (HPC), hydroxypropyl methylcellulose (HPMC), hydroxypropyl methylcellulose acetate succinate (HPMCAS), Eudragit® and Soluplus® (Azad et al., 2020). The polymer is selected mostly by its thermoplastic characteristics and the interaction with the API that is going to be incorporated on the product. The API can be melted and/or dissolved in the polymeric matrix, depending on the polymer properties and the HME and 3DP parameters, affecting directly the release of the drug from the pharmaceutical dosage form (Seoane-Viaño et al., 2021). With that it is

important a rational selection of the polymeric material, evaluating the interaction not only with the API, but with the additional components.

As mentioned earlier, with the HME and 3DP processes the API can be melted and/or dissolved in the polymeric matrix, possibly suffering an amorphization process, transformation that can be very positive for the formulation, since the dissolution rate of the drug can be enhanced (Buyukgoz et al., 2021). However, both the HME and 3DP are processes made in high temperatures, consequently API with low thermal resistance are not viable candidates for integrate a dosage form made with 3DP FDM.

The additional components of the filament and 3D printed pharmaceutical dosage forms formulation can have many functions for physical characteristics and/or for pharmaceutical performance. The most used additives are plasticizers and lubricants. The plasticizers are used mainly for achieving a filament with a good balance of viscoelasticity, important characteristic for the filament printability, but an effect on the release profile of the API from the pharmaceutical dosage form can also be expected since it can change the dissolution of the 3D model (Lima et al., 2022; Zhao et al., 2019). The lubricant is used to facilitate the feeding of the formulation powder during the HME process and help to prevent the adhesion of the filament on the walls of the printer extruder (Aziz et al., 2020). The use of one or more of those additives are conditioned mainly on the characteristics of the chosen polymer and previews tests attesting the compatibility between the two materials are a necessary step.

In the end of the manufacture process the filament must have a good balance on its viscoelasticity characteristics. Parameters like plasticity, brittleness and rigidity can directly affect the printing processes, meaning that any disbalance on one of those characteristics can make the filament unprintable or can affect the quality of the final printed model (Lima et al., 2022).

With a filament in hand, the printing parameters are the other critical point of the printing process. The changeable parameters of the 3DP FDM are numerous, being some of the more important, the printing temperature, layer height, infill density, infill pattern and the general format of the 3D model.

The printing temperature must be determined based mainly on the melting characteristics of the components, ideally been above the melting point of the polymer. The temperature can affect both the printing process and the final printed model. In low temperatures the melting of the filament does not occur properly, and the printing is not possible and in high temperatures the fluidity of the melted filament can be affected,



changing the precision of the printer and the characteristics of the final model, altering parameters like the density (Pires et al., 2020).

Printing parameters like printing speed, layer height, infill density and infill pattern are capable to change the density and porosity of the printed model. Changing those parameters is a way to alter the amount of material used during the printing process and how the model is going to be filled (Zhang et al., 2020). It is possible to print both a completely hollow model and a 100% filled one, changing completely the amount of material, including the API, present on the final product. Besides that, on a pharmaceutical dosage form, the way how the API is released on the action site is another important factor altered by those parameters. A completely filled dosage form is denser, consequently is going to release a higher dosage of the API in a more controlled way, and a hollow form is going to release a low amount of API in a faster way (Gültekin et al., 2019). Hence, changes on these parameters are a way to personalize both dosage and release profile of a pharmaceutical dosage form.

The format of the final product is also a parameter that can be important, especially for pharmaceutical products. The size is one of the main factors that impact on the API dosage and the format can change how the model is going to interact with the release site, affect how the API is going to be released (Goyanes et al., 2017b).

With a good filament and ideal setting of the printing parameters the chance of success on the 3D printing of the pharmaceutical dosage form is high and that is applied to every type of dosage forms possible. It is reported a great number of different types of pharmaceutical dosage forms developed for the 3DP FDM, but the main focus is still the production of oral delivery forms.

#### 1.3.1.2 Application of three-dimensional printing in oral drug delivery

The oral drug delivery is one of the main focuses of the researches made with 3DP, especially using FDM technique. This is happening because this technology is capable to overcome many limitations of the current oral delivery systems that represents problems for the patient therapy. Problems like the limitation of dosages, tablet subdivision, and polypharmacy are examples of limitations that can be addressed using 3DP (Pandey et al., 2020).

As it was seen before, with 3DP is possible to obtain a dosage form with completely personalized characteristics. Through modifications on the size, infill density

and other printing parameters by a modeling computation system, it is possible to print a dosage form in different dosages and even different dissolution profiles of the API. It is proved that variations on the infill characteristic, size and form of oral dosage forms made by FDM 3DP are capable to alter the dissolution profile of the API, since those variation impact directly on the density and the porosity of the dosage form (Thakkar et al., 2020). With that, problems like the lack of specific dosages of API on the market can be addressed by the printing of tablets in the exact dosage necessary for each patient, with the additional possibility of modulating the dissolution profile of the drug.

In the same way the subdivision problem can also be addressed. It is proved that even on ideal scenarios the subdivision of tablets is a risky practice, resulting on loss of important components and functionality of the dosage forms, representing a font of bad consequences to the patients (Temer et al., 2018). Using the 3DP the partition can be substituted to the obtention of complete dosage forms containing the exact dosage necessary for the patient (Zheng et al., 2020).

Other possibility of the 3DP is the incorporation of multiple materials to the same dosage forms. A 3D printed tablet (printlet), for example, can be printed using different filaments made with different API, each filament been substrate for the printing of specific layers of the printlet, resulting in a dosage form that can make a precise administration of multiple API in a single use, addressing the problem of polypharmacy by facilitating the adhesion to the treatment (B. C. Pereira et al., 2020).

The use of 3DP is entering on the market recently, but most of the projects are still in development and clinical studies phases. Many problems are yet to be addresses in order to make this technology a reality on the current pharmaceutical field. One of those problems is the difficulty on making a large-scale production possible, seen that the 3DP techniques are no known for been fast production methods. And are also the limited number of drugs that can be used on these products, especially in techniques like FDM, that require the use of high temperature on its processes (Seoane-Viaño et al., 2021).

Another important matter that are being addressed recently, that can enhance the impact of the 3DP technology on the pharmaceutical field is the combination with other advanced technologies. The nanotechnology represents a revolution on the drug delivery in different areas including the oral drug delivery and combining the benefits of both the technologies can be an opportunity to advance even more the possibilities of patient treatment.

### 1.3.2 Nanotechnology and the application in oral drug delivery

Nanotechnology can be defined as any technology operating in nanoscale, been the nanoparticles an example of these technology. It can be considered nanoparticles particulate compounds with dimensions less than 1000 nm, depending on the nanoparticle type (Wilczewska et al., 2012).

These nanoparticles started to get attention with the observation that in nanoscale, materials can change completely some of its chemical, physical and biological properties. With that, the nanostructure of a material to change its properties and improve its performance on processes, compared to the bulk material, became a possibility (Medina et al., 2007). For example, one of the first applications of these technology was the nanostructure of catalytic materials, changing some of its physical-chemical properties and improving its performance on chemical reactions (Astruc, 2020).

With the years, the rapid expansion on the nanotechnology field resulted on the discovery of new types of nanoparticles made with different materials, like metals, polymers, and lipids. With that, other possibilities started to be discovered, like the complexation with other compounds by an encapsulation process inside the nanoparticles or bonded to the surface of the particles, transforming the nanoparticles in carriers of other substances like API's (Mitchell et al., 2021).

As carriers, nanoparticles can not only transport the compounds but also use its structure to protect and stabilize it. In a biological environment, for example, nanoparticles made with biodegradable materials can carry an API to a specific location using its properties to penetrate more efficiently through biological barriers and improving the API stability protecting it from the environment before and after the administration (Reinholz et al., 2018).

With that, a biomedical application of the nanoparticles became a subject of intense research, and today it can be found applications in many biomedical areas, like diagnosis, cosmetology and pharmacology. Inside the pharmacology area, the oral drug delivery of API is one of the more researched subjects, mainly due to the potential of the nanoparticle to improve the process (Chenthamara et al., 2019).

Oral delivery is the most common route of API administration, mainly due to the high level of patient compliance. This route stands out, comparing to the parenteral route, for avoid painful administration procedures, equivalent efficacy, and low risk of cross contamination. However, the oral administration is dependent of specific characteristics

of the API in terms of solubility and permeability. In addition, it must trespass all the gastrointestinal tract without losing its properties (Alqahtani et al., 2021).

The API must be capable to overcome the multiple compartments of the system, starting with the stomach, with an overly acidic environment and with the presence of important enzymes that can degrade the compound. Once the API surpass the stomach the next compartment in the small intestine, preceded by the duodenum, environments with massive enzymatic activity, making even higher the chances of degradation. Upon surviving both environments, the API still must contact the enterocyte and survive the absorption process and get to the bloodstream. With that, it's justified the high amount of API's with low resorption percentage, resulting in poor bioavailable (Reinholz et al., 2018).

To overcome those obstacles, many strategies have been used. The enteric coating is one of the main strategies and consist of contain the medication inside layers of polymeric materials that can resist to the gastric environment, avoiding the loss of API. The API is released only on the alkaline environment of the small intestine, becoming available to absorption. However, even with enteric coating many API's have a low bioavailability, probably due to degradation on the intestine or weak interaction with the enterocytes (Maderuelo et al., 2019).

Another strong strategy is the use of nanoparticles to potentially provide protection for the API from the aggressive environment of the gastrointestinal tract, increase the intestinal absorption into the bloodstream, target specific cells and guaranty a control release on the target cell. In this scenario, in many cases, the drug is released directly inside the intestinal cell, the bloodstream or in the cell target of the pharmacological activity, significantly enhancing the bioavailability (Chenthamara et al., 2019).

In general, a nanoparticle, after administration, is capable to protect the API against the acidic medium of the stomach, achieving the small intestines. On the intestines the particles can resist to the environment due to its structure and is available to be absorbed by the enteric cells as a whole. After the absorption the particles trespass the enteric cell and the lamina propria, achieving the bloodstream, open the possibility to go anywhere in the body. Advanced in development nanoparticles are capable even to leave the bloodstream and diffuse through the cellular structures to achieve the action site (Reinholz et al., 2018).

Depending on the type of nanoparticles and the objective of the treatment the API can be released on the intestinal lumen, acting similarly to the enteric coating, inside the enterocyte, on the bloodstream or directly on the action site, requiring the nanoparticle to be adapted to each situation. Hence, in most of these cases it is required that particles are capable to trespass all those biological barriers without losing its properties, and that is one of the many challenges on the development of new nanoparticles for oral administration (Cao et al., 2019).

Many types of materials had shown the potential to become the main ingredient on a nanoparticle formulation. For oral administrations three types of materials can be highlighted: polymers, lipids and metals.

Polymeric nanoparticles are particles made with polymeric materials of synthetic or natural origins, with sizes that can range between 1-1000 nm, although the lower size particles (between 20 nm and 250 nm) have been a more applied alternative for the biomedical application, especially for oral delivery (Chenthamara et al., 2019).

The most important properties of those particle are the biocompatibility, biodegradability and the high stability in different environments, including biological ones. For drug delivery applications, the API can be entrapped onto the polymeric core of the nanoparticle or adsorbed to its surface, being released only on the target site by diffusion or desorption mechanisms, with the potential for a controlled release of the API (Pridgen et al., 2014).

Nanoparticles made with synthetic polymers have the advantage of being easily produces, with no risk of biological contamination. Besides that, studies show that for controlled release the nanoparticles made with synthetic polymers are more efficient for a sustained API release, since the balance of hydrophilicity is more controlled on those polymers, compared to the natural ones (Dmour and Taha, 2018). Poly (lactic-co-glycolic acid (PLGA) nanoparticles is an example of a tested polymeric nanoparticles for oral delivery, showing positive results on the endocytoses of the full particle on epithelial enteric cell model (Caco-2 cell line) and the stabilization of encapsulated DNA, successfully protecting the material against the action of the nuclease enzymes inside the cells (Chenthamara et al., 2019).

Nanoparticles made with natural polymers, in turn, have the advantage of an expressive mucoadhesivity, facilitating processes of uptake in different cells, fact that contributes to a direct delivery in specific sites (Mumuni et al., 2020). Chitosan is one of the most common natural polymers used to produce nanoparticles. It is a linear

polysaccharide extract from the shrimp and other crustaceans by the treatment of its chitin shells. Studies made with chitosan nanoparticles show a superior potential of delivering macromolecules through biological barriers like the enteric epithelium (studies made with Caco-2 cell line), the polymeric core of those particles is capable to create an environment that can more efficiently protect those molecules generating great uptake results, if compared to PLGA nanoparticle (Cao et al., 2022).

Lipid nanoparticles are spherical vesicles made with different types of lipidic molecular structures. The use of those particles became a focus of research because of the extensive biocompatibility characteristics since most of these particles have in the composition common human body lipids like cholesterol and phospholipids molecules (Chaudhari et al., 2020). Additionally, the structure of these particles counts with an outer lipid layer, compatible with the also lipidic outer cells membrane facilitating the uptake process of the particles. Many different lipid particles are being study for an oral drug delivery application, some of the more promising are the liposomes and the solid lipid nanoparticles (SLN) (Mitchell et al., 2021).

Liposomes are formed by a lipid bilayer encapsulating an aqueous core in with the API can be dispersed (Large et al., 2021). Initially, liposomes are not the most appropriated strategy for oral delivery because of the instability on the gastrointestinal environment, structure instability during the process of crossing biological membranes and the difficulty on large scale producing. However, studies show that by applying modifications to the structure of the liposomes, like adding a polymeric coating to add on resistance, can make the particle viable and make use of its properties to a better oral delivery of drugs (He et al., 2019).

SLN in other hand, are formed by a lipid monolayer encapsulating a solid lipid core that can contain an API dispersed (Scioli Montoto et al., 2020). Like the liposomes, the SLN have stability limitations for oral delivery, especially on the gastrointestinal environment, however its structure is more capable to resist the cellular uptake process and the large-scale production is facilitated. Again, similarly to the liposomes, the SLN was already modified with enhancements like a polymeric coating, to overcome these limitations and being able to achieve results like the increase of the bioavailability of API like antidiabetics and anticancer drugs (Ganesan et al., 2018).

Metallic nanoparticles are particles made with inorganic metallic materials like iron, gold, and zinc. Those nanoparticles are known for being very small particles (10 nm and 100 nm) that can enhance some of the metallic material properties like optical

characteristics, magnetic potential, fluorescence and specific electromagnetic absorption, that can be applied, for example, on the biomedical area on image-guided therapies as image contrast agents (Chenthamara et al., 2019).

Another great potential of the metallic nanoparticles is the functionalization of its core by an API molecule, by coating or by a bidding process. That functionalization turns the nanoparticle on a delivery system that can stabilize the API and delivery it to a specific site. For many years the focus of research was the use of these functionalize nanoparticles for parenteral delivery. However recently the use of those particles for oral administration have been gain attention, specialty gold and iron oxide nanoparticles (Lin et al., 2015).

Gold nanoparticles (GNP) are easily synthesized particles, with size and format that can be altered according to changes on the synthesis process. The possible variation of size and shape also bring an adaptability to the particle since changes on these parameters can modify optical and electrical properties of the nanoparticles. Additionally, the negative surface charge of the particle makes easy the functionalization by many types of molecules and biomolecules (Kong et al., 2017).

All those characteristics, added to the biocompatibility and nontoxicity, make the GNP a viable option for directed drug delivery, including by oral administration. Studies show that GNP with low sizes are capable to be internalized by human endothelial cells from the blood vessels and the brain, showing a potential to be delivery in multiple sites is an oral administration (Kumari et al., 2020).

Iron oxide nanoparticles (IONP) are spherical particle with sizes that can range between 10 nm and 200 nm. It is one of the more accepted metallic nanoparticle, having many approved products available on the pharmaceutical market. It is a stablished biocompatible particle, with a relatively easy synthesis process and a high capacity of being functionalized by different types of molecules. The paramagnetic characteristics of its core structure is another important featuring, adding to the many possibilities of use (Ali et al., 2016).

In oral delivery the IONP have being tested in many ways as a drug delivery mechanism, however the use of the particle as source of supplementary iron for iron deficient patients is a recent application that deserve some attention. The use of iron nanoparticles for treatment of iron deficiency it is a stablished treatment made by parenteral administration, with several commercial products available (Alphandéry, 2020). However, the efficiency of parenteral delivery comes with the many disadvantages of this type of administration, like pain, difficulty on self-administration and high cost of

production. In response to that, the oral use of the IONP as iron supplement have been a source of investigation, with the objective of produced a more comfortable for the patient and less costly delivery system (Zanella et al., 2017) .

Many research have been made on this new use of the IONP in the last fell years and additionally to the obvious advantages of the administration form, some advantages on the efficacy of the IONP, in comparison with the current way to treat iron deficiency by oral delivery, has being reported (Alphandéry, 2020). The current oral iron deficiency treatment, mainly composed of ferrous salts, suffers with problems like the low bioavailability and side effects like inflammation on the gastrointestinal epithelial cells caused by the free iron accumulated on the regions. The studies with IONP, show that small sized particles can have a superior bioavailability on the intestinal cells and with less adverse effects associated with the treatment (Garcia-Fernandez et al., 2020).

The increase on bioavailability is duo to a more efficient absorption process on the enterocytes. The IONP probably enter the enteric cells by an endocytosis mechanism through the cell membrane apical pole and diffuse inside the cell until the release on the interstitial space through the basolateral pole. It is reported that after this step the particles access the hepatic portal vein. In this vein, the particles are capable to transferred across the vessel basolateral membrane and achieve the systemic distribution, fact confirmed by the particles founded on the blood and organs like the spleen (Garcia-Fernandez et al., 2020).

During this process the particles presents a loss in size, evidencing a release of free iron during the whole trajectory, but it's still found structured in the organs, maintaining the release of free iron for some time. Furthermore, no sign of cellular damage was funded in any of the body sites, where the particles where capable to reach, including the gastrointestinal tract, demonstrating the possible reduction on the adverse effects (Garcia-Fernandez et al., 2020).

With those examples it is clear the impact of nanoparticles on the pharmaceutical area in general. On oral delivery the use of those nanoparticles are still limited, however the potential is demonstrated and it can change how to approach oral administration in the future.

### **1.3.3 Nanotechnology Applied to FDM 3D printing for oral delivery**



On a pharmaceutical perspective 3D printing and nanotechnology can be complementary in their improvement of medicines efficiency. On oral delivery, 3D printing is capable to make a difference on administration and release profile of the API on the gastrointestinal tract, personalizing the dosage form according to the necessity of the therapy and making the experience more comfortable to the user. This personalization is made by changes on parameters like the type of material, size, shape, and density of the dosage form (Thakkar et al., 2020).

The nanotechnology can also make a difference on the release profile of the API on the gastrointestinal tract, however the main focuses of the application is to improve the uptake by the gastrointestinal cells, enhancing the bioavailability, and a direct and controlled delivery on specific sites of the body. Those improvements are made by the selection of the type of nanoparticles, based on the core material, the functionalization process, and additives like coating (Chenthamara et al., 2019).

Therefore, the possibilities of improvement are numerous with the combination of both technologies, with several studies already being made in this area combining several types of particles inserted in 3D models made with different 3DP techniques (dos Santos et al., 2021). On the oral delivery field, a more restrict amount of information is founded on the literature and the combination of nanoparticles for oral delivery and FDM 3DP technique is even more restrict.

The combination of the FDM 3DP and nanotechnology for oral delivery was tested on a study that tried to incorporate Eudragit® RL PO nanoparticles on printlets made with the same polymer as base. On the study the particle was added to the printlets by a soaking procedure, meaning that the nanoparticles did not participate as an ingredient nether to the filament production nor the printing. That is due to the fact that the polymeric nanoparticle used on the study would not resist to the high temperature and intense sheer of both processes, loosing completely its structure (Beck et al., 2017).

With that, the study highlights one of the more expressive limitations of the combination of FDM 3DP and nanotechnology, the lack of stability of the nanoparticles on the processes of extrusion and printing, presenting the soaking as a viable alternative for the combination of the technologies. Although, the results suggest the necessity of a more efficient soaking process, capable to load a high amount of particle into the printlets structure (Beck et al., 2017).

When the search is made outside of the oral delivery area it is possible to find studies that presents other possibilities for the combination of FDM 3DP and

nanotechnology, for example, the use of nanoparticles that can resist to the high temperature and intense shear processes.

Nanoparticles made with inorganic materials like hydroxyapatite, magnesium oxide, zinc, titanium dioxide and iron oxide are known to be resistant to high temperature and mechanical stress. This resistance was proved by several studies that applied those materials, in nanoparticles forms, to the FDM 3DP procedure. The nanoparticles were incorporated on the formulation during the filament production and printed on FDM printers, resisting to both processes (Luo et al., 2020; Rasoulianboroujeni et al., 2019; Roh et al., 2017; Senatov et al., 2017; Wang et al., 2017).

On most of those studies, the incorporation of the nanoparticles was a strategy to provide resistance and additional properties, like antimicrobial activity and tissue regeneration to materials like prosthetics and tissue substitutes. However, many of those materials can also be applied to other areas, for example, magnesium oxide and iron oxide nanoparticles are already being applied to oral delivery (Garcia-Fernandez et al., 2020; Somanathan et al., 2016).

With that, the conclusion is that it is possible to combine FDM 3DP and nanotechnology for the obtention of an oral delivery dosage form by the application on alternative techniques, like soaking and even during the normal process of filament production and printing, with the use of nanoparticles that can resist to the thermal and mechanical stress.

#### 1.3.3.1 Spontaneous formation of nanoparticles and the possible association with 3D printing

So far, the discussion centered on the insertion of nanoparticles in a 3D model used for drug delivery purposes. However, another important discussion in the spontaneous formation of nanosized compounds during the solubilization of API and the polymeric materials on a dissolution medium.

On the oral drug delivery, the importance of those spontaneous formed nanoparticles is the capacity of interfere on the release of the free API and its absorption by the gastrointestinal cells. It is reported cases that the particles are capable to increase and decrease the release of the free API, affecting in different ways the absorption and even the bioavailability (Sironi et al., 2017; Stewart and Grass, 2020).

This phenomenon is mainly described on solid dispersion and is connected to dissolution mechanisms of the formulation. The formation of the nanomaterials can be described in three different mechanisms: the erosion of the polymeric dosage form, the carrier-controlled release and the dissolution-controlled release (Schittny et al., 2020).

On the erosion process the dissolution medium enters the polymeric matrix, resulting in a swelling process that causes a fragilization of the polymeric structure. With that, the material starts to erode and nanosized pieces are released on the medium retaining its structure by the molecular bonds between the components. If an API is part of the formulations its going to be trapped inside this structure (Göpferich, 1996).

On the carrier-controlled release the solvent penetrates through the polymeric matrix and induces the formation of a gel layer. The API must diffuse through the polymer, including the highly viscous gel layer, to be released in the medium, making this a slow procedure. When the API concentration exceed the amorphous solubility, it forms a colloidal solution composed of drug rich nanosized particles stabilized by the polymer (Schittny et al., 2020).

On the dissolution-controlled release the formation of the particles occurs by the same mechanism, the only difference being the rapid release of both polymer and API. This mechanism is more common when a more soluble polymeric material is applied on the formulation (Nunes et al., 2022).

With that, it is possible to observe that the formation of those particles is dependent of the API and polymer solubility on the dissolution medium and theoretically can be controlled. Hence, if the objective is a modification on the release profile and the absorption of the API, the formation of this spontaneous particles can be an important control mechanism. However, can also be a factor that interfere negatively with other mechanisms that are being tested (Schittny et al., 2020).

The dosage forms produced by 3DP are mostly polymeric material incorporated whith different API's. Therefore the possibility of spontaneous nanoparticle formation is real for those dosage forms, however studies describing this phenomenon of those materials are lacking.

#### 1.4. REFERENCES

- Ali, A., Zafar, H., Zia, M., ul Haq, I., Phull, A.R., Ali, J.S., Hussain, A., 2016. Synthesis, characterization, applications, and challenges of iron oxide nanoparticles. *Nanotechnol. Sci. Appl.* 9, 49–67. <https://doi.org/10.2147/NSA.S99986>
- Alphandéry, E., 2020. Iron oxide nanoparticles for therapeutic applications. *Drug Discov. Today* 25, 141–149. <https://doi.org/10.1016/j.drudis.2019.09.020>
- Alqahtani, M.S., Kazi, M., Alsenaidy, M.A., Ahmad, M.Z., 2021. Advances in Oral Drug Delivery. *Front. Pharmacol.* 12. <https://doi.org/10.3389/fphar.2021.618411>
- Araújo, M.R.P., Sa-Barreto, L.L., Gratieri, T., Gelfuso, G.M., Cunha-Filho, M., 2019. The digital pharmacies era: How 3D printing technology using fused deposition modeling can become a reality. *Pharmaceutics* 11. <https://doi.org/10.3390/pharmaceutics11030128>
- Astruc, D., 2020. Introduction: Nanoparticles in Catalysis. *Chem. Rev.* 120, 461–463. <https://doi.org/10.1021/acs.chemrev.8b00696>
- Azad, M.A., Olawuni, D., Kimbell, G., Badruddoza, A.Z.M., Hossain, M.S., Sultana, T., 2020. Polymers for extrusion-based 3D printing of pharmaceuticals: A holistic materials–process perspective, *Pharmaceutics*. <https://doi.org/10.3390/pharmaceutics12020124>
- Aziz, R., Ul Haq, M.I., Raina, A., 2020. Effect of surface texturing on friction behaviour of 3D printed polylactic acid (PLA). *Polym. Test.* 85, 106434. <https://doi.org/10.1016/j.polymertesting.2020.106434>
- Beck, R.C.R., Chaves, P.S., Goyanes, A., Vukosavljevic, B., Buanz, A., Windbergs, M., Basit, A.W., Gaisford, S., 2017. 3D printed tablets loaded with polymeric nanocapsules: An innovative approach to produce customized drug delivery systems. *Int. J. Pharm.* 528, 268–279. <https://doi.org/10.1016/j.ijpharm.2017.05.074>
- Buyukgoz, G.G., Kossor, C.G., Davé, R.N., 2021. Enhanced supersaturation via fusion-assisted amorphization during fdm 3d printing of crystalline poorly soluble drug loaded filaments. *Pharmaceutics* 13, 28–33. <https://doi.org/10.3390/pharmaceutics13111857>
- Cao, S., Deng, Y., Zhang, L., Aleahmad, M., 2022. Chitosan nanoparticles, as biological

- macromolecule-based drug delivery systems to improve the healing potential of artificial neural guidance channels: A review. *Int. J. Biol. Macromol.* 201, 569–579. <https://doi.org/10.1016/j.ijbiomac.2022.01.017>
- Cao, S. jun, Xu, S., Wang, H. ming, Ling, Y., Dong, J., Xia, R. dong, Sun, X. hong, 2019. Nanoparticles: Oral Delivery for Protein and Peptide Drugs. *AAPS PharmSciTech* 20, 1–11. <https://doi.org/10.1208/s12249-019-1325-z>
- Chaudhari, V.S., Murty, U.S., Banerjee, S., 2020. Lipidic nanomaterials to deliver natural compounds against cancer: a review. *Environ. Chem. Lett.* 18, 1803–1812. <https://doi.org/10.1007/s10311-020-01042-5>
- Chen, Z., Li, Z., Li, J., Liu, Chengbo, Lao, C., Fu, Y., Liu, Changyong, Li, Y., Wang, P., He, Y., 2019. 3D printing of ceramics: A review. *J. Eur. Ceram. Soc.* 39, 661–687. <https://doi.org/10.1016/j.jeurceramsoc.2018.11.013>
- Chenthamara, D., Subramaniam, S., Ramakrishnan, S.G., Krishnaswamy, S., Essa, M.M., Lin, F.H., Qoronfleh, M.W., 2019. Therapeutic efficacy of nanoparticles and routes of administration. *Biomater. Res.* 23, 1–29. <https://doi.org/10.1186/s40824-019-0166-x>
- Dmour, I., Taha, M.O., 2018. Natural and semisynthetic polymers in pharmaceutical nanotechnology, *Organic Materials as Smart Nanocarriers for Drug Delivery*. Elsevier Inc. <https://doi.org/10.1016/B978-0-12-813663-8.00002-6>
- dos Santos, J., de Oliveira, R.S., de Oliveira, T. V., Velho, M.C., Konrad, M. V., da Silva, G.S., Deon, M., Beck, R.C.R., 2021. 3D Printing and Nanotechnology: A Multiscale Alliance in Personalized Medicine. *Adv. Funct. Mater.* 31, 1–35. <https://doi.org/10.1002/adfm.202009691>
- Economidou, S.N., Pere, C.P.P., Reid, A., Uddin, M.J., Windmill, J.F.C., Lamprou, D.A., Douroumis, D., 2019. 3D printed microneedle patches using stereolithography (SLA) for intradermal insulin delivery. *Mater. Sci. Eng. C* 102, 743–755. <https://doi.org/10.1016/j.msec.2019.04.063>
- Elder, B., Neupane, R., Tokita, E., Ghosh, U., Hales, S., Kong, Y.L., 2020. Nanomaterial Patterning in 3D Printing. *Adv. Mater.* 32, 1–42. <https://doi.org/10.1002/adma.201907142>
- Ganesan, P., Ramalingam, P., Karthivashan, G., Ko, Y.T., Choi, D.K., 2018. Recent

- developments in solid lipid nanoparticle and surface-modified solid lipid nanoparticle delivery systems for oral delivery of phyto-bioactive compounds in various chronic diseases. *Int. J. Nanomedicine* 13, 1569–1583. <https://doi.org/10.2147/IJN.S155593>
- Garcia-Fernandez, J., Turiel, D., Bettmer, J., Jakubowski, N., Panne, U., Rivas García, L., Llopis, J., Sánchez González, C., Montes-Bayón, M., 2020. In vitro and in situ experiments to evaluate the biodistribution and cellular toxicity of ultrasmall iron oxide nanoparticles potentially used as oral iron supplements. *Nanotoxicology* 14, 388–403. <https://doi.org/10.1080/17435390.2019.1710613>
- Göpferich, A., 1996. Mechanisms of polymer degradation and erosion1. *Biomater. Silver Jubil. Compend.* 17, 117–128. <https://doi.org/10.1016/B978-008045154-1.50016-2>
- Goyanes, A., Scarpa, M., Kamlow, M., Gaisford, S., Basit, A.W., Orlu, M., 2017. Patient acceptability of 3D printed medicines. *Int. J. Pharm.* 530, 71–78. <https://doi.org/10.1016/j.ijpharm.2017.07.064>
- Gültekin, H.E., Tort, S., Acartürk, F., 2019. An Effective Technology for the Development of Immediate Release Solid Dosage Forms Containing Low-Dose Drug: Fused Deposition Modeling 3D Printing. *Pharm. Res.* 36. <https://doi.org/10.1007/s11095-019-2655-y>
- He, H., Lu, Y., Qi, J., Zhu, Q., Chen, Z., Wu, W., 2019. Adapting liposomes for oral drug delivery. *Acta Pharm. Sin. B* 9, 36–48. <https://doi.org/10.1016/j.apsb.2018.06.005>
- Jiménez, M., Romero, L., Domínguez, I.A., Espinosa, M.D.M., Domínguez, M., 2019. Additive Manufacturing Technologies: An Overview about 3D Printing Methods and Future Prospects. *Complexity* 2019. <https://doi.org/10.1155/2019/9656938>
- Jin, Z., Li, Y., Yu, K., Liu, L., Fu, J., Yao, X., Zhang, A., He, Y., 2021. 3D Printing of Physical Organ Models: Recent Developments and Challenges. *Adv. Sci.* 8, 1–27. <https://doi.org/10.1002/advs.202101394>
- Kong, F.Y., Zhang, J.W., Li, R.F., Wang, Z.X., Wang, W.J., Wang, W., 2017. Unique roles of gold nanoparticles in drug delivery, targeting and imaging applications. *Molecules* 22. <https://doi.org/10.3390/molecules22091445>
- Kristiawan, R.B., Imaduddin, F., Ariawan, D., Ubaidillah, Arifin, Z., 2021. A review on the fused deposition modeling (FDM) 3D printing: Filament processing, materials,

and printing parameters. *Open Eng.* 11, 639–649. <https://doi.org/10.1515/eng-2021-0063>

- Kumari, Y., Singh, S.K., Kumar, Rajesh, Kumar, B., Kaur, G., Gulati, M., Tewari, D., Gowthamarajan, K., Karri, V.V.S.N.R., Ayinkamiye, C., Khursheed, R., Awasthi, A., Pandey, N.K., Mohanta, S., Gupta, S., Corrie, L., Patni, P., Kumar, Rajan, Kumar, Rakesh, 2020. Modified apple polysaccharide capped gold nanoparticles for oral delivery of insulin. *Int. J. Biol. Macromol.* 149, 976–988. <https://doi.org/10.1016/j.ijbiomac.2020.01.302>
- Large, D.E., Abdelmessih, R.G., Fink, E.A., Auguste, D.T., 2021. Liposome composition in drug delivery design, synthesis, characterization, and clinical application. *Adv. Drug Deliv. Rev.* 176, 113851. <https://doi.org/10.1016/j.addr.2021.113851>
- Lima, A.L., Pires, F.Q., Hilgert, L.A., Sa-Barreto, L.L., Gratieri, T., Gelfuso, G.M., Cunha-Filho, M., 2022. Oscillatory shear rheology as an in-process control tool for 3D printing medicines production by fused deposition modeling. *J. Manuf. Process.* 76, 850–862. <https://doi.org/10.1016/j.jmapro.2022.03.001>
- Lin, Z., Monteiro-Riviere, N.A., Riviere, J.E., 2015. Pharmacokinetics of metallic nanoparticles. *Wiley Interdiscip. Rev. Nanomedicine Nanobiotechnology* 7, 189–217. <https://doi.org/10.1002/wnan.1304>
- Luo, Y., Humayun, A., Mills, D.K., 2020. Surface Modification of 3D Printed PLA / Halloysite Composite Scaffolds with Antibacterial and Osteogenic Capabilities. *Appl. Sci.* 10.
- Maderuelo, C., Lanao, J.M., Zarzuelo, A., 2019. Enteric coating of oral solid dosage forms as a tool to improve drug bioavailability. *Eur. J. Pharm. Sci.* 138, 105019. <https://doi.org/10.1016/j.ejps.2019.105019>
- Manero, A., Smith, P., Sparkman, J., Dombrowski, M., Courbin, D., Kester, A., Womack, I., Chi, A., 2019. Implementation of 3D printing technology in the field of prosthetics: Past, present, and future. *Int. J. Environ. Res. Public Health* 16. <https://doi.org/10.3390/ijerph16091641>
- Martinez, P.R., Goyanes, A., Basit, A.W., Gaisford, S., 2018. Influence of Geometry on the Drug Release Profiles of Stereolithographic (SLA) 3D-Printed Tablets. *AAPS PharmSciTech* 19, 3355–3361. <https://doi.org/10.1208/s12249-018-1075-3>

- Medina, C., Santos-Martinez, M.J., Radomski, A., Corrigan, O.I., Radomski, M.W., 2007. Nanoparticles: Pharmacological and toxicological significance. *Br. J. Pharmacol.* 150, 552–558. <https://doi.org/10.1038/sj.bjp.0707130>
- Miller, J.S., Burdick, J.A., 2016. Editorial: Special Issue on 3D Printing of Biomaterials. *ACS Biomater. Sci. Eng.* 2, 1658–1661. <https://doi.org/10.1021/acsbiomaterials.6b00566>
- Mitchell, M.J., Billingsley, M.M., Haley, R.M., Wechsler, M.E., Peppas, N.A., Langer, R., 2021. Engineering precision nanoparticles for drug delivery. *Nat. Rev. Drug Discov.* 20, 101–124. <https://doi.org/10.1038/s41573-020-0090-8>
- Mohammed, A.A., Algahtani, M.S., Ahmad, M.Z., Ahmad, J., Kotta, S., 2021. 3D Printing in medicine: Technology overview and drug delivery applications. *Ann. 3D Print. Med.* 4, 100037. <https://doi.org/10.1016/j.stlm.2021.100037>
- Monschke, M., Wagner, K.G., 2020. Impact of HPMCAS on the dissolution performance of polyvinyl alcohol celecoxib amorphous solid dispersions. *Pharmaceutics* 12, 1–17. <https://doi.org/10.3390/pharmaceutics12060541>
- Mumuni, M.A., Kenechukwu, F.C., Ofokansi, K.C., Attama, A.A., Díaz, D.D., 2020. Insulin-loaded mucoadhesive nanoparticles based on mucin-chitosan complexes for oral delivery and diabetes treatment. *Carbohydr. Polym.* 229, 115506. <https://doi.org/10.1016/j.carbpol.2019.115506>
- Ni, J., Ling, H., Zhang, S., Wang, Z., Peng, Z., Benyshek, C., Zan, R., Miri, A.K., Li, Z., Zhang, X., Lee, J., Lee, K.J., Kim, H.J., Tebon, P., Hoffman, T., Dokmeci, M.R., Ashammakhi, N., Li, X., Khademhosseini, A., 2019. Three-dimensional printing of metals for biomedical applications. *Mater. Today Bio* 3. <https://doi.org/10.1016/j.mtbio.2019.100024>
- Nukala, P.K., Palekar, S., Solanki, N., Fu, Y., Patki, M., Shohatee, A.A., Trombetta, L., Patel, K., 2019. Investigating the application of FDM 3D printing pattern in preparation of patient-tailored dosage forms. *J. 3D Print. Med.* 3, 23–37. <https://doi.org/10.2217/3dp-2018-0028>
- Nunes, P.D., Pinto, J.F., Henriques, J., Paiva, A.M., 2022. Insights into the Release Mechanisms of ITZ:HPMCAS Amorphous Solid Dispersions: The Role of Drug-Rich Colloids. *Mol. Pharm.* 19, 51–66.



<https://doi.org/10.1021/acs.molpharmaceut.1c00578>

- Palo, M., Holländer, J., Suominen, J., Yliruusi, J., Sandler, N., 2017. 3D printed drug delivery devices: perspectives and technical challenges. *Expert Rev. Med. Devices* 14, 685–696. <https://doi.org/10.1080/17434440.2017.1363647>
- Pandey, M., Choudhury, H., Fern, J.L.C., Kee, A.T.K., Kou, J., Jing, J.L.J., Her, H.C., Yong, H.S., Ming, H.C., Bhattamisra, S.K., Gorain, B., 2020. 3D printing for oral drug delivery: a new tool to customize drug delivery. *Drug Deliv. Transl. Res.* 10, 986–1001. <https://doi.org/10.1007/s13346-020-00737-0>
- Parhi, R., Jena, G.K., 2021. An updated review on application of 3D printing in fabricating pharmaceutical dosage forms, *Drug Delivery and Translational Research*. Springer US. <https://doi.org/10.1007/s13346-021-01074-6>
- Pereira, B.C., Isreb, A., Isreb, M., Forbes, R.T., Oga, E.F., Alhnan, M.A., 2020. Additive Manufacturing of a Point-of-Care “Polypill:” Fabrication of Concept Capsules of Complex Geometry with Bespoke Release against Cardiovascular Disease. *Adv. Healthc. Mater.* 9, 1–12. <https://doi.org/10.1002/adhm.202000236>
- Pires, F.Q., Alves-Silva, I., Pinho, L.A.G., Chaker, J.A., Sa-Barreto, L.L., Gelfuso, G.M., Gratieri, T., Cunha-Filho, M., 2020. Predictive models of FDM 3D printing using experimental design based on pharmaceutical requirements for tablet production. *Int. J. Pharm.* 588, 119728. <https://doi.org/10.1016/j.ijpharm.2020.119728>
- Piyush, Kumar, Raman, Kumar, Ranvijay, 2019. 3D printing of food materials: A state of art review and future applications. *Mater. Today Proc.* 33, 1463–1467. <https://doi.org/10.1016/j.matpr.2020.02.005>
- Pridgen, E.M., Alexis, F., Farokhzad, O.C., 2014. Polymeric Nanoparticle Technologies for Oral Drug Delivery. *Clin. Gastroenterol. Hepatol.* 12, 1605–1610. <https://doi.org/10.1016/j.cgh.2014.06.018>
- Rahim, T.N.A.T., Abdullah, A.M., Md Akil, H., 2019. Recent Developments in Fused Deposition Modeling-Based 3D Printing of Polymers and Their Composites. *Polym. Rev.* 59, 589–624. <https://doi.org/10.1080/15583724.2019.1597883>
- Rasoulianboroujeni, M., Fahimipour, F., Shah, P., Khoshroo, K., Tahriri, M., Eslami, H., Yadegari, A., Dashtimoghadam, E., Tayebi, L., 2019. Development of 3D-printed PLGA/TiO<sub>2</sub> nanocomposite scaffolds for bone tissue engineering applications.

- Mater. Sci. Eng. C 96, 105–113. <https://doi.org/10.1016/j.msec.2018.10.077>
- Reinholz, J., Landfester, K., Mailänder, V., 2018. The challenges of oral drug delivery via nanocarriers. *Drug Deliv.* 25, 1694–1705. <https://doi.org/10.1080/10717544.2018.1501119>
- Roh, H.S., Lee, C.M., Hwang, Y.H., Kook, M.S., Yang, S.W., Lee, D., Kim, B.H., 2017. Addition of MgO nanoparticles and plasma surface treatment of three-dimensional printed polycaprolactone/hydroxyapatite scaffolds for improving bone regeneration. *Mater. Sci. Eng. C* 74, 525–535. <https://doi.org/10.1016/j.msec.2016.12.054>
- Sabbagh, F., Kim, B.S., 2022. Recent advances in polymeric transdermal drug delivery systems. *J. Control. Release* 341, 132–146. <https://doi.org/10.1016/j.jconrel.2021.11.025>
- Savini, A., Savini, G.G., 2015. A short history of 3D printing, a technological revolution just started. *Proc. 2015 ICOHTEC/IEEE Int. Hist. High-Technologies their Socio-Cultural Context. Conf. HISTELCON 2015 4th IEEE Reg. 8 Conf. Hist. Electrotechnol.* <https://doi.org/10.1109/HISTELCON.2015.7307314>
- Schittny, A., Huwyler, J., Puchkov, M., 2020. Mechanisms of increased bioavailability through amorphous solid dispersions: a review. *Drug Deliv.* 27, 110–127. <https://doi.org/10.1080/10717544.2019.1704940>
- Scioli Montoto, S., Muraca, G., Ruiz, M.E., 2020. Solid Lipid Nanoparticles for Drug Delivery: Pharmacological and Biopharmaceutical Aspects. *Front. Mol. Biosci.* 7, 1–24. <https://doi.org/10.3389/fmolb.2020.587997>
- Sen, K., Manchanda, A., Mehta, T., Ma, A.W.K., Chaudhuri, B., 2020. Formulation design for inkjet-based 3D printed tablets. *Int. J. Pharm.* 584, 119430. <https://doi.org/10.1016/j.ijpharm.2020.119430>
- Senatov, F.S., Zadorozhnyy, M.Y., Niaza, K. V., Medvedev, V. V., Kaloshkin, S.D., Anisimova, N.Y., Kiselevskiy, M. V., Yang, K.C., 2017. Shape memory effect in 3D-printed scaffolds for self-fitting implants. *Eur. Polym. J.* 93, 222–231. <https://doi.org/10.1016/j.eurpolymj.2017.06.011>
- Seoane-Viaño, I., Trenfield, S.J., Basit, A.W., Goyanes, A., 2021. Translating 3D printed pharmaceuticals: From hype to real-world clinical applications. *Adv. Drug Deliv. Rev.* 174, 553–575. <https://doi.org/10.1016/j.addr.2021.05.003>

- Sironi, D., Rosenberg, J., Bauer-Brandl, A., Brandl, M., 2017. Dynamic dissolution-/permeation-testing of nano- and microparticle formulations of fenofibrate. *Eur. J. Pharm. Sci.* 96, 20–27. <https://doi.org/10.1016/j.ejps.2016.09.001>
- Somanathan, T., Krishna, V.M., Saravanan, V., Kumar, Raju, Kumar, Randhir, 2016. MgO nanoparticles for effective uptake and release of doxorubicin drug: PH sensitive controlled drug release. *J. Nanosci. Nanotechnol.* 16, 9421–9431. <https://doi.org/10.1166/jnn.2016.12164>
- Stansbury, J.W., Idacavage, M.J., 2016. 3D printing with polymers: Challenges among expanding options and opportunities. *Dent. Mater.* 32, 54–64. <https://doi.org/10.1016/j.dental.2015.09.018>
- Stewart, A.M., Grass, M.E., 2020. Practical Approach to Modeling the Impact of Amorphous Drug Nanoparticles on the Oral Absorption of Poorly Soluble Drugs. *Mol. Pharm.* 17, 180–189. <https://doi.org/10.1021/acs.molpharmaceut.9b00889>
- Tambe, S., Jain, D., Agarwal, Y., Amin, P., 2021. Hot-melt extrusion: Highlighting recent advances in pharmaceutical applications. *J. Drug Deliv. Sci. Technol.* 63, 102452. <https://doi.org/10.1016/j.jddst.2021.102452>
- Tamil Ponni, R., Swamivelmanickam, M., Sivakrishnan, S., 2020. 3D Printing in Pharmaceutical Technology – A Review. *Int. J. Pharm. Investig.* 10, 8–12. <https://doi.org/10.5530/ijpi.2020.1.2>
- Tan, D.K., Maniruzzaman, M., Nokhodchi, A., 2018. Advanced pharmaceutical applications of hot-melt extrusion coupled with fused deposition modelling (FDM) 3D printing for personalised drug delivery. *Pharmaceutics* 10. <https://doi.org/10.3390/pharmaceutics10040203>
- Temer, A.C., Teixeira, M.T., Sa-Barreto, L.L., Gratieri, T., Gelfuso, G.M., Silva, I.C., Taveira, S.F., Marreto, R.N., Cunha-Filho, M., 2018. Subdivision of Tablets Containing Modified Delivery Technology: the Case of Orally Disintegrating Tablets. *J. Pharm. Innov.* 13, 261–269. <https://doi.org/10.1007/s12247-018-9323-3>
- Thakkar, R., Pillai, A.R., Zhang, J., Zhang, Y., Kulkarni, V., Maniruzzaman, M., 2020. Novel on-demand 3-dimensional (3-d) printed tablets using fill density as an effective release-controlling tool. *Polymers (Basel)*. 12, 1–21. <https://doi.org/10.3390/POLYM12091872>

- Wang, H.T., Chiang, P.C., Tzeng, J.J., Wu, T.L., Pan, Y.H., Chang, W.J., Huang, H.M., 2017. In vitro biocompatibility, radiopacity, and physical property tests of nano-Fe<sub>3</sub>O<sub>4</sub> incorporated poly-L-lactide bone screws. *Polymers (Basel)*. 9, 1–11. <https://doi.org/10.3390/polym9060191>
- Wilczewska, A.Z., Niemirowicz, K., Markiewicz, K.H., Car, H., 2012. Nanoparticles as drug delivery systems. *Pharmacol. Reports* 64, 1020–1037. [https://doi.org/10.1016/S1734-1140\(12\)70901-5](https://doi.org/10.1016/S1734-1140(12)70901-5)
- Zanella, D., Bossi, E., Gornati, R., Bastos, C., Faria, N., Bernardini, G., 2017. Iron oxide nanoparticles can cross plasma membranes. *Sci. Rep.* 7, 1–10. <https://doi.org/10.1038/s41598-017-11535-z>
- Zhang, J., Thakkar, R., Zhang, Y., Maniruzzaman, M., 2020. Structure-function correlation and personalized 3D printed tablets using a quality by design (QbD) approach. *Int. J. Pharm.* 590, 119945. <https://doi.org/10.1016/j.ijpharm.2020.119945>
- Zhao, Yanna, Xie, X., Zhao, Yuping, Gao, Y., Cai, C., Zhang, Q., Ding, Z., Fan, Z., Zhang, H., Liu, M., Han, J., 2019. Effect of plasticizers on manufacturing ritonavir/copovidone solid dispersions via hot-melt extrusion: Preformulation, physicochemical characterization, and pharmacokinetics in rats. *Eur. J. Pharm. Sci.* 127, 60–70. <https://doi.org/10.1016/j.ejps.2018.10.020>
- Zheng, Z., Lv, J., Yang, W., Pi, X., Lin, W., Lin, Z., Zhang, W., Pang, J., Zeng, Y., Lv, Z., Lao, H., Chen, Y., Yang, F., 2020. Preparation and application of subdivided tablets using 3D printing for precise hospital dispensing. *Eur. J. Pharm. Sci.* 149, 105293. <https://doi.org/10.1016/j.ejps.2020.105293>

## **2. CHAPTER II: PREDICTIVE MODELS OF FDM 3D PRINTING USING EXPERIMENTAL DESIGN BASED ON PHARMACEUTICAL REQUIREMENTS FOR TABLETS PRODUCTION**

### **2.1 INTRODUCTION**

The technology of three-dimensional (3D) printing, which was developed for rapid prototyping, has been widely explored in the pharmaceutical field over the last five years (Mathew et al., 2020). During this short period, a consistent research activity occurred worldwide in the development of the most diverse drug delivery systems including devices for oral, dermal, and implantable administration. This demonstrates the potential of 3D printing not as an accessory technology, but also as a significant player in the production of medicines (Araújo et al., 2019; Trenfield et al., 2018; Warsi et al., 2018).

One of the most vaunted benefits of 3D printing for the pharmaceutical field is the possibility of generating drug products for a personalized therapy, since inadequate dosages is a recognized health problem (Alhnan et al., 2016). In particular, 3D printing by fusion deposition modeling (FDM) has enormous potential for therapeutic customization due to its operational simplicity, low cost, high precision, and versatility to produce different solid dosage forms, as tablets, capsules, films, adhesives, and implants (Cunha-Filho et al., 2017).

Despite the advantages and benefits of developing personalized patient-specific dosage forms with tailored release profiles, just one 3D-printed drug product has been approved by FDA up to date – Spritam<sup>®</sup> (Norman et al., 2017). This may be related to the regulatory requirements, once a pharmaceutical product, regardless of the technology involved in its elaboration, needs to follow *Good Manufacturing Practices* and pharmacopeia specifications in production, and these are more associated with already-established industries (Jamróz et al., 2018; Li Chew et al., 2019; Richey et al., 2017).

The FDM 3D printing process involves a large number of technical print configurations, such as extrusion speed, extrusion nozzle temperature, platform temperature, layer height, wall thickness, infill density, object size, among others, which show a decisive impact on the characteristic of the final printed object (Alhijaj et al., 2019). These basic settings, in turn, can be subdivided into even more specific commands. For example, the print speed can be configured in different steps of printing, including

print tip speed between extrusions; print speed of the first layer; print speed of the infill; print speed of the last layer; print speed of the outer wall; print speed of the inner side of the object and so on (Fernandez-Vicente et al., 2016; Gendviliene et al., 2020; Hernandez, 2015).

Most of the 3D printing studies are focused on the field of engineering; however, the pharmaceutical manufacturing process has distinct particularities that demand further and appropriate experimental experimentation. Indeed, studies in the pharmaceutical field have shown an intricate relationship among print settings (input variable) and product quality parameters (output variable). Input variables include: the geometric shape of a printed object, which has shown to influence its release profile (Goyanes et al., 2015); the infill density, which modifies tablet porosity and consequently the drug release kinetics (Goyanes et al., 2015); the infill pattern, which is related to printlet hardness and affects disintegration time (NUKALA *et al.*, 2019); and variations of temperatures of the printing nozzle and platform, which – along with changes of printing speed – significantly affect printlet mass uniformity (Alhijaj et al., 2019). Moreover, the same drug filament produced immediate, controlled, and combined release kinetics by only modifying a few printing parameters (Jamróz et al., 2020).

In this scenario, in which pharmaceutical characteristics are influenced by the printing variables in a non-linear and little-understood relationship, the application of quality-by-design tools, such as the use of a design of experiments (DOE), could be used to guide the manufacturing process while predicting product's output (Pires et al., 2017). The purpose of the present study was to evaluate the feasibility of DOE tools for planning and conducting experiments over multiple variables of the 3D FDM printing process. The aim was to obtain a predictive model that might be able to set the printing configuration to meet random medical prescriptions, including drug release specifications.

## **2.2 MATERIAL AND METHODS**

### **2.2.1 Material**

Commercial 3D printing 1.75mm filaments of acrylonitrile butadiene styrene (ABS, lot 017127011) and polylactic acid (PLA, lot 217187012) were supplied by 3DFila (Belo Horizonte, Brazil). High impact polystyrene 1.75mm filament (HIPS, lot 18I24) was provided by Faz3D (São Paulo, Brazil).

### 2.2.2 Thermal characterization of polymeric filaments

Differential scanning calorimetry (DSC) analyses were performed in aluminum pans using a DSC-60H (Shimadzu, Tokyo, Japan), which operated at a heating rate of 10 °C min<sup>-1</sup> ranging from 30 to 350 °C. Thermogravimetry (TGA) analyses were carried out in platinum pans using a DTG-60 (Shimadzu, Tokyo, Japan), which operated at a heating rate of 10 °C min<sup>-1</sup> from 30 to 500 °C. Analyses were performed using samples of the polymers in the range of 3-6 mg. Additionally, the water content of each polymer was determined using TGA by heating the samples until 105 °C and holding this temperature for 120 min (Malaquias et al., 2018). All assays were performed under a nitrogen atmosphere (flow rate of 50 mL min<sup>-1</sup>).

The possible mass loss in printing conditions was evaluated with TGA in isothermal conditions of analysis for 60 min at the printing temperature of each polymer—i.e., 195 °C, 225 °C, and 230 °C for PLA, ABS, and HIPS, respectively.

### 2.2.3. Model planning using DOE

DOE-based model building for each selected filament followed the stages described in Fig. 1. The 3D-printed (3DP) FDM tablets, called printlets (GOYANES *et al.*, 2017), were graphically designed and sliced using free versions of Tinkercad<sup>®</sup> (Autodesk<sup>®</sup> Inc, San Rafael, CA, USA) and Slic3r<sup>®</sup> (Rome, Italy) software, respectively.

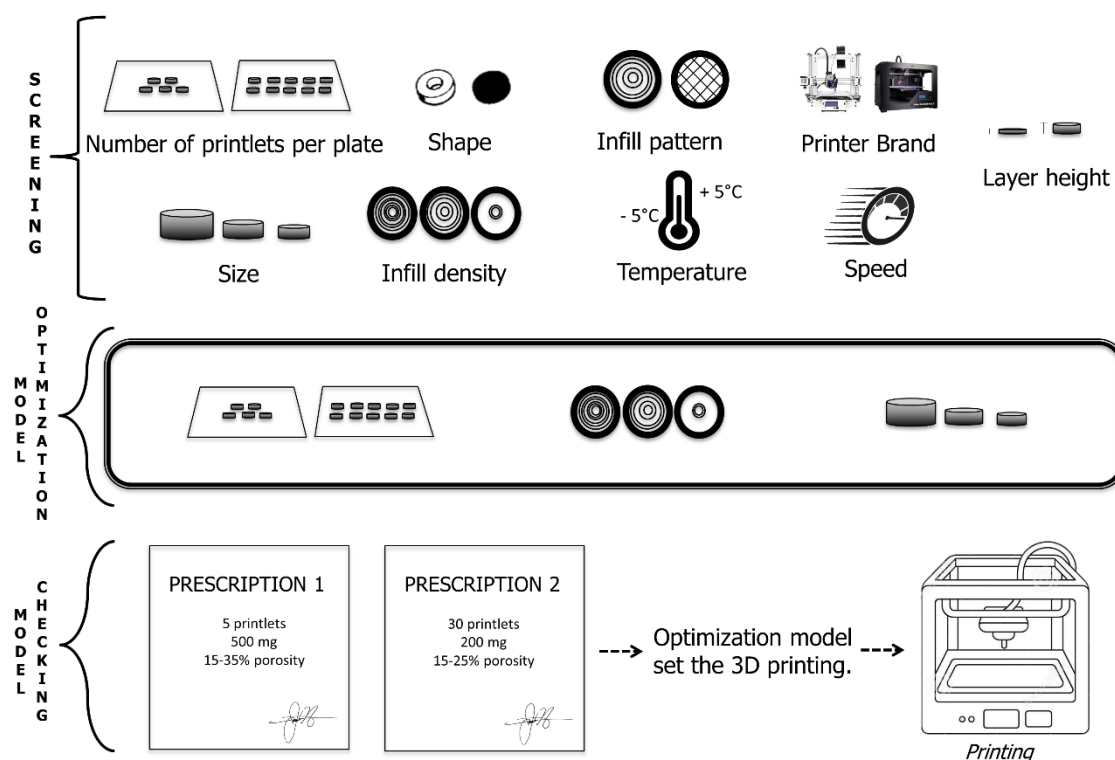


**Figure 1.** Model planning phases using DOE.

### 2.2.3.1 Screening design

From the several of the 3D FDM printing parameters that are possible to be set, nine of them were selected for the first modeling phase based on recent studies, which pointed out relevant printing configurations for 3DP of drug products (ALHIJJAJ *et al.*, 2019; GOYANES *et al.*, 2015; NUKALA *et al.*, 2019). Six continuous and three discrete factors were selected to be studied in the screening design phase, comprising twenty experiments for each filament.

The continuous factors were: a) number of printlets per plate (from 5 to 10); b) size scale (from 50 to 100%); c) printing speed (from 30 and 100  $\text{mm s}^{-1}$  to 60 and 200  $\text{mm s}^{-1}$  for printing moves and travel, respectively); d) layer height (from 0.1 to 0.2 mm); e) infill density (from 10 to 90%); and f) printing temperature (variations of  $\pm 5^{\circ}\text{C}$  of printing temperature). The discrete factors were: i) infill pattern (concentric or rectilinear); ii) printlet shape (cylindric or torus); and iii) printer brand (Makerbot Replicator 2, New York, NY, USA; or Voolt 3D model Gi3, São Paulo, Brazil).

Relevant measurements for a tablet were selected as responses for this study, including assays related to the accuracy and precision of drug product dosage (*mass* and



*mass variation coefficient*), the manufacturing time (*printing time*), and the drug release performance (*porosity*).

#### 2.2.3.2 Model optimization

Based on the most significant factors in terms of modifying the responses assessed during the phase of screening design, a further experimental design was carried out. In this next phase, the following three factors were more intensively studied: the number of printlets per plate, the size scale, and the infill density. The remaining print parameters were fixed as printing speed (60 mm s<sup>-1</sup> for printing moves and 150 mm s<sup>-1</sup> for travel speed), layer height (0.2 mm), printing temperature (225 °C for ABS, 230 °C for HIPS and 195 °C for PLA), infill pattern (rectilinear), printlet shape (cylindric) and printer brand (Voolts3D). In this design, twenty-five experiments were planned for each filament, and the same responses previously described were evaluated.

#### 2.2.3.3 Model checking

In order to test the predictive equation built for each filament from the optimization design, two different simulated prescriptions for a compounding pharmacy were proposed. Prescription #1 prescribed five printlets of 500 mg each with porosity in a range of 15-35% were prescribed, while in prescription #2, it was prescribed thirty printlets of 200 mg each with porosity in the range of 15-25%. All prescriptions were printed in triplicate for each filament.

#### 2.2.3.4 Statistical analysis of DOE

All screening and optimization experiments were planned and analyzed using the Design Expert<sup>®</sup> 11 software (Stat-Ease, Minneapolis, MN, USA). The models were examined using one-way ANOVA. The best-fitting model was selected for each response based on F-values and p-values, and the predictive equations were established by stepwise multiple regression analysis.

The simulated prescriptions responses for printlets were inserted in the software set with the optimized model for each polymer. Once the data were inserted, the software

provided all the 3D printer parameters that were needed to meet the predicted responses. The correlations among the predicted and the experimental values were evaluated (Malaquias et al., 2017).

#### 2.2.4 Printlets characterization

The variation coefficients of printlet's average mass and mass were determined using an analytical balance (Shimadzu, Tokyo, Japan). A digital caliper rule (Mitutoyo, São Paulo, Brazil) was used for volume assessment. The morphology of the tablets was assessed by optical microscopy using a stereoscope (SZ—SZT, BEL Engineering®, Milan, Italy) coupled to a video camera. All assays were performed taking five replicates.

The skeletal density ( $\rho_{skeletal}$ ) of printlets was measured by helium pycnometry using an AccuPyc II 1340 pycnometer (Micromeritics, Norcross, GA, USA). The apparent density ( $\rho_{ap}$ ) was calculated by dividing the printlet mass by the volume. All analyses were performed in triplicate. The porosity was calculated with Equation (1) (Cunha-Filho et al., 2019):

$$Tablet\ porosity\ (\%) = (1 - (\rho_{ap}/\rho_{skeletal})) * 100 \quad (1)$$

Determinations were performed only in the screening phase of the study in which was verified that the skeletal density of each polymer did not change after the printing process, which were 1.28, 1.18, and 1.45 g cm<sup>-3</sup> for ABS, HIPS, and PLA, respectively.

## 2.3 RESULTS AND DISCUSSION

### 2.3.1 Characterization of the filaments

The selected filaments (ABS, PLA, and HIPS) are well-known commercial polymers used in 3D FDM printing and recognized by their superior stability and printability. Moreover, most of these polymers are biocompatible (Mazzanti et al., 2019; Micó-Vicent et al., 2019; Ou-Yang et al., 2018) and have been used for pharmaceutical purposes (Jamróz et al., 2020; Zhao et al., 2018). The thermal analysis of the filaments (Table 1) confirmed their favourable characteristics for pharmaceutical use, e.g., all polymers presented less than 1.5% of mass loss at printing temperature and low water content (around 0.5%). This mass loss during the printing process has been described to occur due to the unbound moisture and the thermal decomposition of the polymers

(Solanki et al., 2018). Hence, reducing this occurrence is essential to preserve the stability of the printlet.

**Table 1.** Polymer filaments characteristics.

Polymer	Printing temperature	Glass transition	Mass loss at printing temperature	Water content	Specific heat
ABS	225 °C	105 °C	1.4 %	0.51 %	1060 J/kg K
HIPS	230 °C	100 °C	1.0 %	0.52 %	1400 J/kg K
PLA	195 °C	60 °C	1.2 %	0.52 %	1800 J/kg K

For establishing a standard for printlet size, the dimensions of the generic Mesalazine 500 mg flat circular tablet were used as a model. Based on the acceptability by the patients (Goyanes et al., 2015), the cylindrical and torus printlets format with a volume of 5.903 cm<sup>3</sup> were used as prototypes (Figure 2).

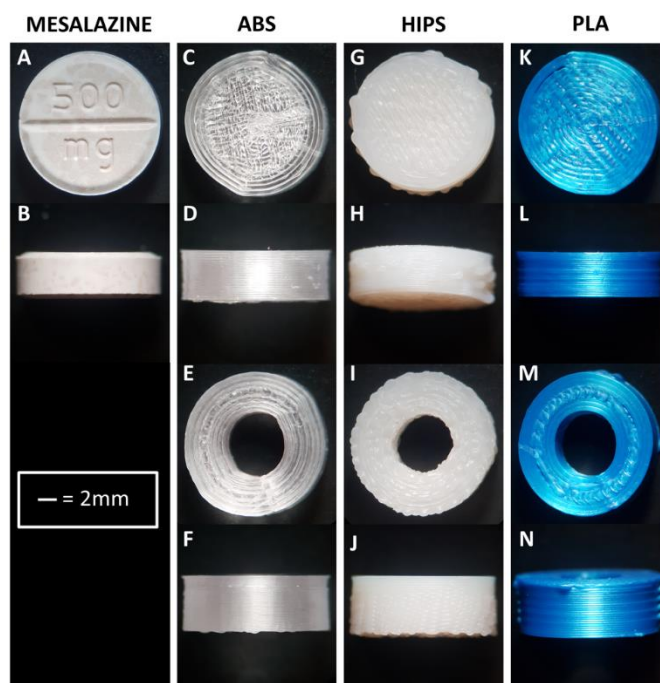


**Figure 2.** Photomicrography of generic Mesalazine 500 mg tablet (A and B); printlets in cylindrical (C, D, G, H, K, and L) and torus (E, F, I, J, M, and N) format produced using the polymers ABS, HIPS, and PLA. Top (A, C, E, G, I, K, and M) and lateral (B, D, F, H, J, L, and N) views.

### **2.3.2. Model planning: Screening design**

In the first stage of the model development, an experimental screening design was employed, enabling the simultaneous study of many factors related to the FDM 3D printing process. This type of experimental design has a low predictive capacity due to the limited hierarchy between the factors; however, it is useful to measure the contribution of each factor in the responses, guiding the selection of the most important ones to be applied in a higher hierarchy experimental design (Durakovic, 2017).

#### **2.3.2.1. Average mass**

In consideration of the premise that drug presentation of the pharmaceutical filaments must be uniformly distributed in their polymeric matrix, one of the main responses obtained for the printlets was the average mass. Average mass is directly related to the dosage of the drug product; thus, developing a predictive model that can fully control this response is a prerequisite for pharmaceutical use of this technology.

As expected, the size scale presented the highest influence on printlets mass (Figure 3). Indeed, the coefficient for size scale in the predictive equation was ten times higher than the coefficients found for the other factors.

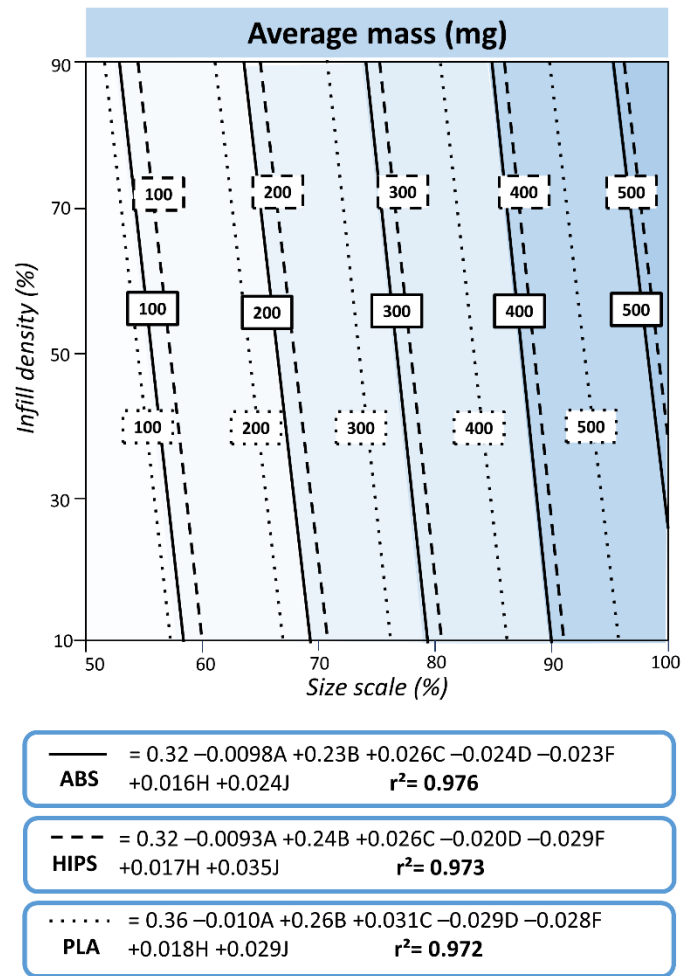


**Figure 3.** The surface responses for the printlets' average mass using the filaments ABS, HIPS, or PLA, their predictive equations, and correlation coefficients. A—printlets per plate; B—size scale; C—infill density; D—printing speed; F—temperature; H—shape; J—printer brand.

Different studies already observed this same relationship, which could present a non-linear behavior, depending on other parameters such as the type of polymer and infill density (Öblom et al., 2019). In our study, a non-linear behavior was found for all polymers. For example, for PLA filament, once all printing parameters are constant, and the size scale is reduced from 100 to 50%, the mass changes from 541 to 87 mg. This occurs due to the deposition of layers in the 3D object, which is not homogeneous since the printlet structure has a thicker and compact shell and a heterogeneous infill that depends on its pattern and density (Galeja et al., 2020).

In such cases, the use of DOE is a valuable tool to reach a reliable predictive model. In the present study, for the mass response, size scale is a crucial parameter to be set in the 3D printer to obtain printlets with different dosages. In fact, shifts in the size scale axis produce notable changes in mass, as observed in the response surface presented in Figure 3. Also, the infill density is a parameter that is clearly related to mass since it determines the space that is freely available inside of the printlets (Fernandez-Vicente et al., 2016).

The number of printlets per plate had a small but significant impact on this response, i.e., the increase in the number of printed tablets caused a reduction of their average mass. Since the 3DP pieces are built layer by layer, increasing the number of printlets per plate leads to an increase in the itinerary of the nozzle to put a subsequent layer in all the printlets, causing a cooling of the last printed layer and a consequent small volumetric contraction (coefficient of thermal expansion in the range of 70-90  $\mu\text{m}/\text{m } ^\circ\text{C}$ ) (Alsoufi and Elsayed, 2017). When this occurs, the extra gap between the nozzle and the object leads to an adherence failure, causing insufficient traction in the feeding mechanism and consequently promoting a lower volumetric flow rate of the filament that reduces printlets mass (Feuerbach et al., 2018).

Furthermore, a small reduction in printlets mass was seen with an increase in the printing speed—which was expected, considering that higher speeds of nozzle movement result in shorter times for material deposition in each layer (Feuerbach et al., 2018). In addition, a reduction in printlets mass was observed with the increase of the print temperature. This can be explained based on the decrease of the polymer's density at higher temperatures due to polymer expansion, which means that the same volume of filament used in the construction of the printlets will result in a lower mass deposition (Alhijjaj et al., 2019).

The significant impact of the printlets' format on their mass is a result of the difference in the inner space of each structure. As shown in Figure 4, although torus and cylindrical printlets have the same volume and external layers, the internal space left over for the filling greatly differs. In cylindrical printlets the inner space represents most of the built structure, while in the torus format it constitutes only a small part of the object. Thus, torus-shape printlets may have a mass of up to 49% higher than cylindrical. This finding somewhat limits one of the most vaunted advantages of 3D medicine printing technology, which is the freedom to print them in any desired format. In fact, the format needs to be

considered together with other printing variables in the validation of the predictive model, in order to guarantee the correct dosage of the intended drug product.

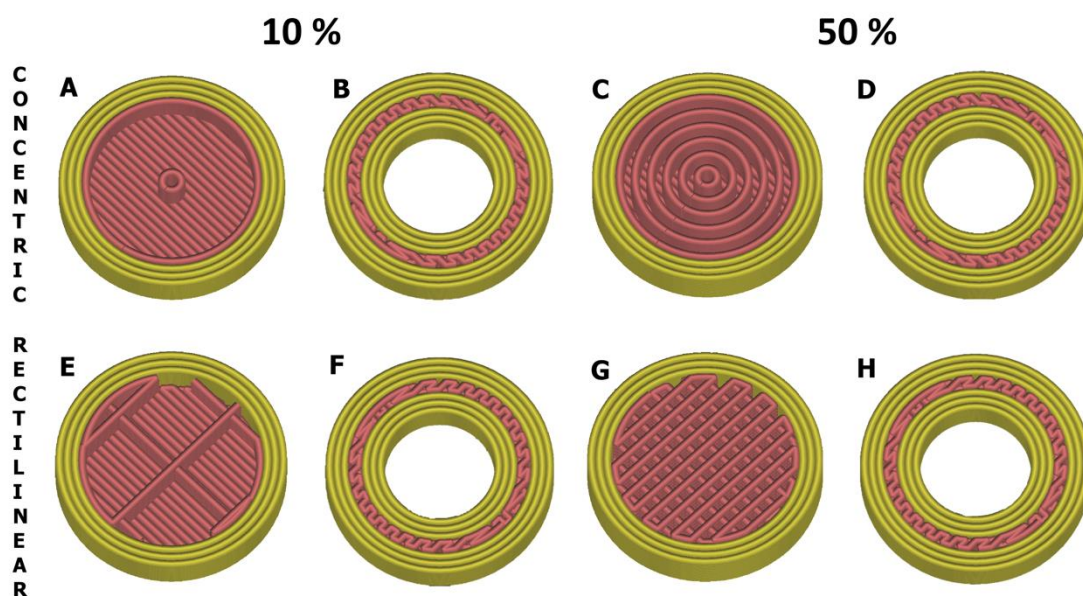


**Figure 4.** 3D model of unfinished printlets showing details of the inner space, infill pattern, and infill density of torus (B, D, F, and H) and cylindrical (A, C, E, and G) printlets with 10 and 50% infill density.

The printer brand significantly impacted the mass of the final product. Differences in the mechanical structures, especially in heating and traction mechanisms, lead to changes in material deposition (Feuerbach et al., 2018; Gendviliene et al., 2020). The results showed for printlet mass variations by the Makerbot Replicator 2X<sup>®</sup> printer were slightly higher than those provided by the Voolt3D Gi3<sup>®</sup>. Based on this, it is possible to anticipate that a specific validation process will be required for each printer brand. Lastly, layer height and infill pattern presented no significant impact on the mass response ( $p>0.05$ ) of the resulted tablets.

### 2.3.2.2. Mass variation coefficient

The variability of the printing process was assessed by the variation coefficient of the tablets' mass. In brief, the mass variation coefficients of printlets were always below 2% in all specific conditions studied regardless the tested material. Moreover, the result of the average mass variation was 0.81%, 0.79%, and 0.77% for ABS, HIPS, and PLA filaments, respectively. These values are lower than those usually found in conventional tablet production and are also far below the limits set for a tablet containing more than 250 mg (<5%) (WHO, 2019).

Figure 5 shows that by increasing the number of printlets per plate and the size of the printlets, the mass variation coefficient decreases. This behavior is verified with tablets produced by conventional methods since the production variables have less impact on larger pharmaceutical units (Bakar et al., 2010).

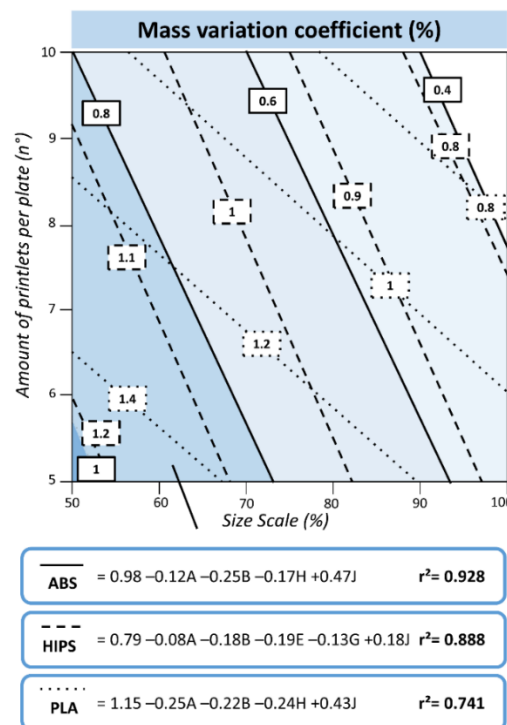


**Figure 5.** The surface responses for the mass variation coefficient of the printlets using the filaments ABS, HIPS, or PLA, their predictive equations, and correlation coefficients. A–printlets per plate; B–size scale; E–layer height; G–infill pattern; H–shape; J–printer brand.



Moreover, layer height showed a statistical impact on the mass variation coefficient, due to the tendency of the polymers to undergo deformation; still, the mass variation was low and irrelevant for printing robustness. Printlets' shape, in turn, presented influence on mass variation coefficient for ABS and PLA possible due to the differences in inner space as commented before. Finally, the 3D printer brand had a significant impact on the mass variation coefficient, which was 0.53% and 1.30% for Voolt3D Gi3® and Makerbot Replicator 2X®, respectively, still in acceptable levels for pharmaceutical production (<5%) (WHO, 2019).

#### 2.3.2.3. Printing time

The printing speed of the dosage forms is a limitation for the pharmaceutical use of the FDM 3DP technology. Indeed, while modern industrial tablets' machines can manufacture a pharmaceutical unit in milliseconds, a 3D printer can take a few mins to obtain a printlet (Melocchi et al., 2016). Hence, understanding the operational variables that are involved in this response and adjusting them to optimize the printing time of the formulation can be decisive to enable the popularization of such technology.

The parameters that significantly influenced the printing time in this study were the size scale, the printing speed, and the layer height (Figure 6). In this way, depending on the printer configuration, printlets can be produced over a wide time interval, ranging from 28 to 420 s per pharmaceutical unit.

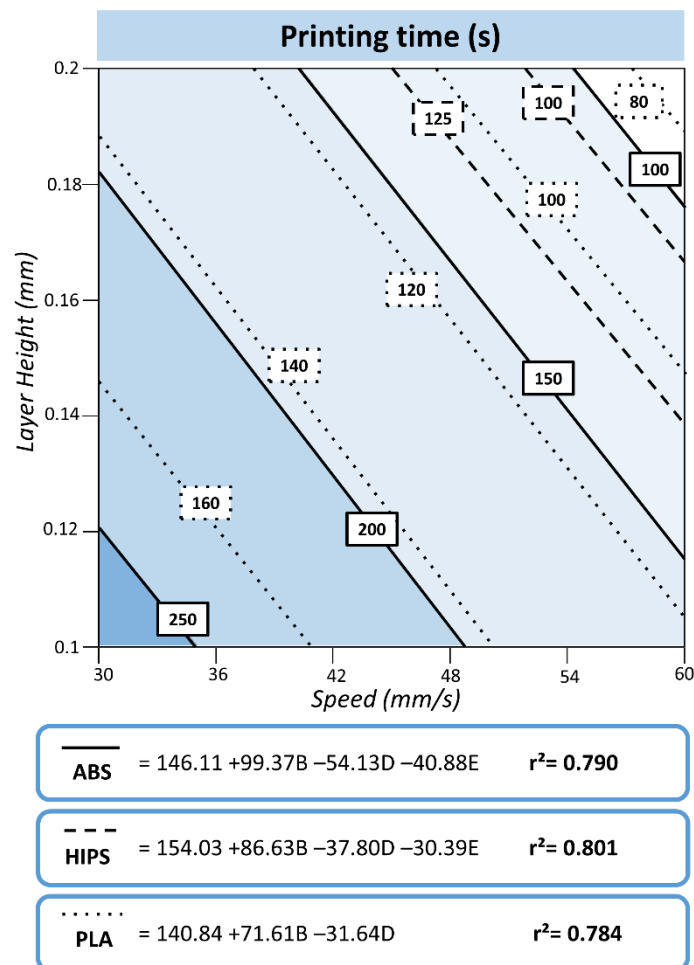


**Figure 6.** The surface responses for printing time of printlets using the filaments ABS, HIPS, or PLA, their predictive equations, and correlation coefficients. B–size scale; D–printing speed; E–layer height.

The size scale is linked to the amount of material necessary to build the printlet. Larger tablets require more layers of deposition and, therefore, take more time to be built. Increasing the layer height implies a reduction in the number of layers required to build the tablet and, therefore, lower the printing time. An increase of printing speed, in turn, makes the print nozzle move more quickly while the layers are deposited, which also understandably accelerate the construction of the tablet. The latter two parameters, when adjusted concomitantly, can reduce the printlet construction time by a factor of more than five (Figure 6). However, these parameters can also alter relevant quality parameters,

such as the mass and porosity of the printlets, and thus must be optimized in coordination with other parameters.

The evaluation over printing time results of different polymers showed that a printlet with an average mass of 267 mg and a porosity around 20% took about 102 seconds to be printed using ABS, 101 seconds for HIPS, and 103 seconds for PLA. The low variation observed is an evidence that the printing time is mostly unaffected by the polymer type itself, although it is affected by other printing parameters, such as layer height and printlet size.

Undeniably, in the current state of the art for 3D FDM printing, production performances cannot be compared with traditional high-performance tablets machines. Still, when the focus is personalizing the medicines in compounding pharmacies, predictive models could be employed to optimize the printing time through the use of higher printing speeds or larger dimensions layers at levels, which do not compromise the other quality parameters of the drug product.

On the other hand, the number of printlets per plate did not affect the printing time per unit. This occurs because the equipment adjusts the trajectory of the nozzle during the printing process in order to optimize displacements (Fok et al., 2017). However, the time spent to set-up the printer before starting the production should be considered, which involves heating the nozzle and plate and calibrating the position of the nozzle. These variables were not included in this study, which only focuses on the tablets' printing time itself.

#### 2.3.2.4. Porosity

As anticipated, the infill density had the highest impact on printlets' porosity since this factor is directly related to the amount of material deposited inside the printed object (Cheng et al., 2018). Despite the noticeable influence observed, the relationship between infill density and porosity is not linear, similarly to the relationship between printlet mass and size scale.

Moreover, the influence of the infill density on this response depends on the polymer used, i.e., the infill density impacts almost twice the PLA printlets porosity than those produced using HIPS and ABS (Figure 7). Other research has established that different materials are deposited on the layer in different ways. The uniformity of a layer

can vary, with irregularities leading to gaps in the structure, which affects the porosity (Abeykoon et al., 2020). This concept should be connected to the physicochemical characteristics of each polymer, for example, ABS and HIPS are processed at higher temperatures (225 and 230 °C, respectively) and show higher coefficients of thermal expansion (98 and 80  $\mu\text{m}/\text{m } ^\circ\text{C}$ ) than the PLA, which is processed at 195 °C and has a thermal expansion coefficient of 68  $\mu\text{m}/\text{m } ^\circ\text{C}$  (Billah et al., 2019; Messimer et al., 2018; Spina, 2019). Because of these differences, the thin layer of material can be deformed by the cooling process in different ways, probably resulting in deformations on the structure that differently affect the porosity for each polymer. That phenomenon, added to the structural changes made by the modifications of the infill density (Figure 4) explain the observed polymer-dependent behaviour.

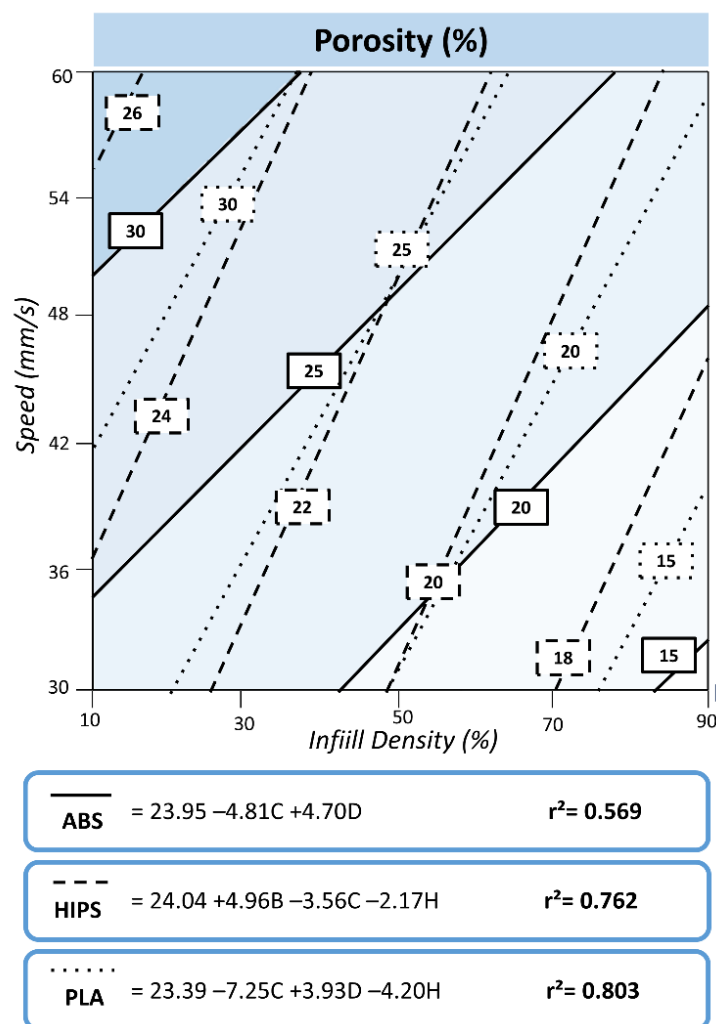


**Figure 7.** The surface responses for porosity (%) of the printlets using the filaments ABS, HIPS, or PLA, their predictive equations, and correlation coefficients. B–size scale; C–infill density; D–printing speed; H–shape.

In addition, the printlets shape significantly affected the porosity responses for most of the polymers. In fact, torus printlets have almost no space for the infill printed mass because of their compact double-shell layers (inner and outer), as shown in Figure 4. Thus, the design of the torus printlet enhances the mass to form the object but reduces porosity in the other hand. These results corroborate the need for a predictive model for each printlet format.

Finally, an increase in printing speed leads to more porous printlets (Figure 7). This is because a non-homogeneous filament deposition and a layer-by-layer cohesion deficiency, which results in construction failures and, consequently, printlets with higher porosity (Hernandez, 2015; Shie et al., 2019).

### **2.3.3 Optimization process**

The models obtained in the screening phase showed a significant influence of the printing parameters on the pharmaceutical variables of the printed medicines. Although some studies have already shown the impact of some of these printing parameters on the mass or porosity of printlets (Chai et al., 2017; Pietrzak et al., 2015; Tagami et al., 2017), this is the first study to integrate several variables in an evaluation using DOE. This allowed us to determine the intricate and complex relationships among the printing factors for different filaments. Thus, the results obtained up to this point make it clear that, in order to obtain a personalized medicine by this technology, mathematical models with high predictive quality are essential. Such models should be capable of integrating the operational variables of 3D printing to obtain a drug product with the expected quality specifications.

Virtually all of the studied printing parameters affect the responses to some degree. With this information, a predictive model was planned with a high hierarchy and broad predictive capacity that can be used in the practices of compounding pharmacies. Only the printing factors that caused the most considerable changes to the responses were chosen, especially in the average mass and the porosity—namely, size scale and infill density. Additionally, the printlets per plate variable was included since this has shown to be a factor that significantly impacts the responses along with being an inherent variable of the patient's prescriptions. The other printing parameters were fixed to avoid

inconsistencies in the final product. A full validation process must follow any changes in those parameters.

In this optimization phase, the tests were performed by combining these three factors in a factorial design planned for twenty-five runs. The response surface combining the two more important factors are exhibited for each polymer in Figures 8 and 9. All the obtained predictive models obtained fitted a cubic model. According to the statistical parameters, the best predictive capacity was acquired for the average mass response, which showed an adjusted correlation close to 1 and adequate precision greater than 80. The statistical values for the other measured responses met the recommended requirements (Ferreira-Nunes et al., 2018).

Based on the response surface for average mass (Figure 8), it is possible to obtain mass measurements over a wide range of values (<100 mg to >600 mg), simply by moving between the operational variables studied. Similarly, for porosity response, it is possible to move within the response surface and obtain printlets with porosity below 20% up to values above 40% (Figure 9). The ample mobility in the aforementioned responses is one of the main objectives of the intended models due to the need to meet the medical prescriptions of different patients regarding their individualities, including different dosages and drug delivery kinetics.

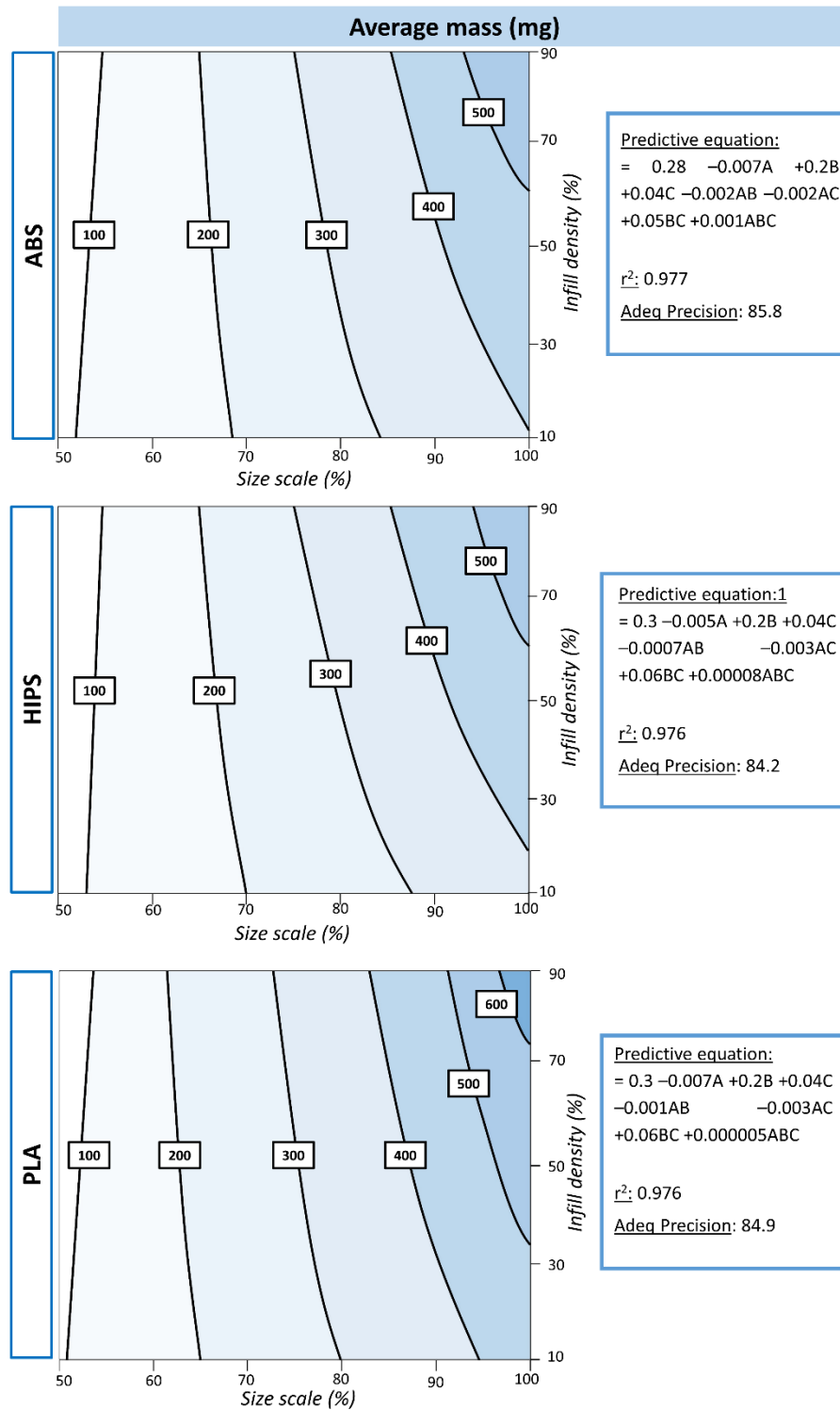


**Figure 8.** Surface response, predictive equations, correlation coefficients, and adeq. precision values for average mass (mg) response of ABS, HIPS, and PLA polymers. A– amount of printlets per plate, B–size scale, C–infill density.

As already verified in the first phase of this study, the size scale factor showed absolute predominance regarding the printlets average mass. Indeed, the size scale

coefficients were more than five times higher than that found for the other factors (Figure 8). For porosity, the size and the infill density showed equivalent relevance. In this response, the absolute coefficient values for these factors were similar in the predictive equations but with different signs (Figure 9). The negative sign for the infill density coefficient indicates an increase in this parameter causes a reduction in the porosity of the printlet. The combination of both factors was used to control printlets drug release with repercussions in its bioavailability, as demonstrated by previous studies (Goyanes et al., 2016; Kempin et al., 2018; Solanki et al., 2018).

Importantly, a significant contribution of the interaction between size scale and infill density was denoted by the predictive models for average mass and porosity (Figures 8 and 9). This interaction resulted in larger average mass and smaller porosity than what was predicted by the simple relationship between the factors in the linear hierarchy equation. This led to errors in predicting responses, which confirms the importance of an experimental optimization planning.

Differences in the predictive equations concerning the material used were also noticed. ABS and HIPS filaments showed similar predictive equations which should be related to their similar physical-mechanical and thermal properties (Table 1). Still, these differences can be important when considering the accuracy of the responses required for a pharmaceutical product. For example, on a printing process of a batch comprised of 5 printlets, with a size scale of 75% and an infill density of 55%, the average mass obtained was  $268 \pm 1.15$  mg,  $254 \pm 0.60$  mg, and  $294 \pm 0.82$  mg, for ABS, HIPS, and PLA, respectively. The observed differences would make a considerable quality issue if it were observed on the production of a precise dosage pharmaceutical device. The influence of the polymer has already been described as an important factor (Kempin et al., 2018; Melocchi et al., 2016); therefore, the establishment of a specific predictive tool for each material is advisable.

Finally, it was observed that the mobility within the response surfaces varies depending on the filament type. In terms of average mass, larger coefficients of the predictive equations indicate easier adjustment of this response through the printing parameters for the PLA filaments than other polymers (Figure 8). However, the printlets' porosity can be more easily adjusted in the ABS and HIPS filaments, which both showed higher values of the predictive equation coefficients for this response (Figure 9).



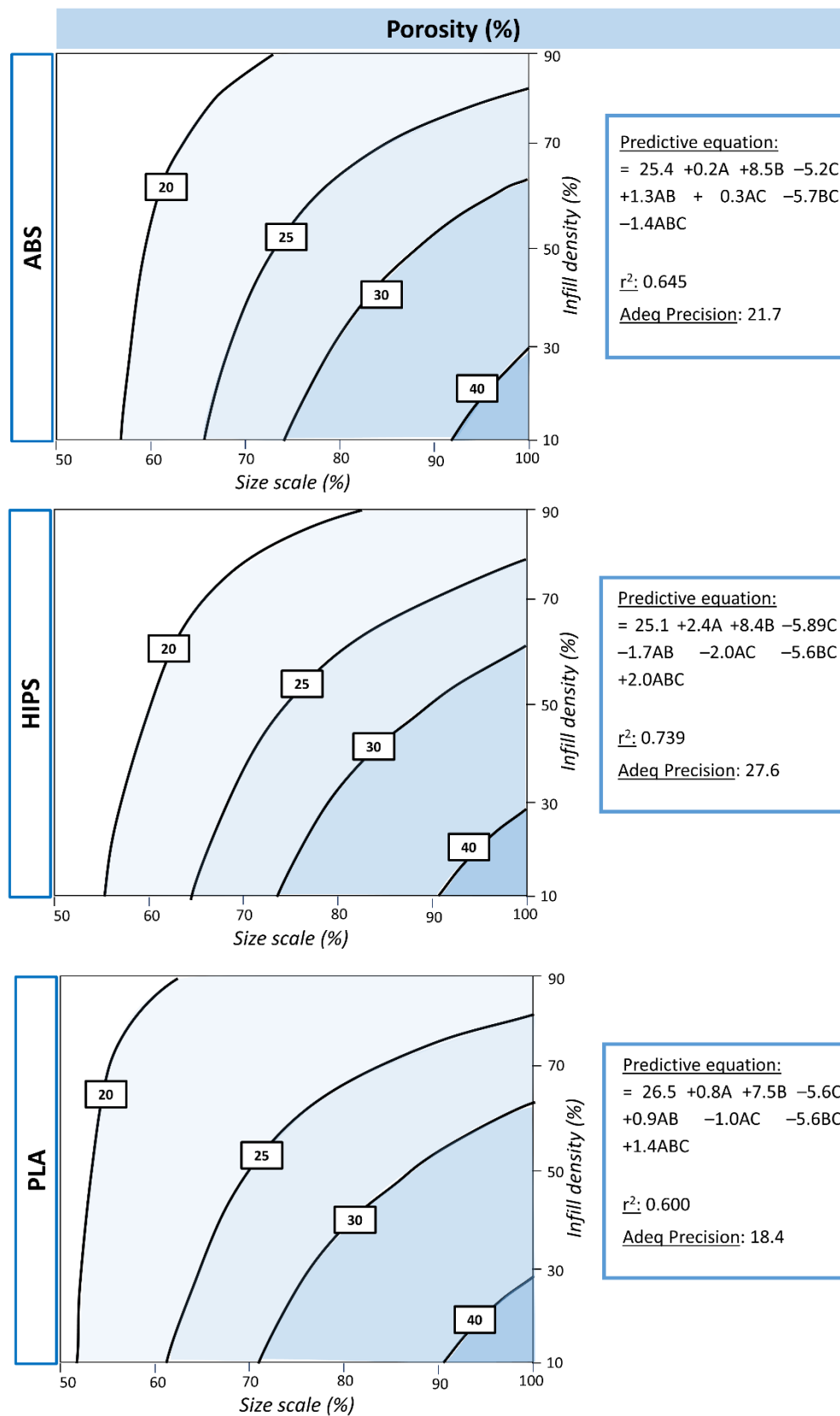


**Figure 9.** Surface response, predictive equations, correlation coefficients, and adeq. precision values for porosity (%) response of ABS, HIPS, and PLA polymers. A—amount of printlets per plate, B—size scale, C—infill density.

### 2.3.4 Model Checking

The optimized predictive equations for the studied responses were integrated to generate solutions containing the printing conditions capable of meeting the demands of a medical prescription. This involved setting the average mass of the printlets, the number of pharmaceutical units to be produced (according to the treatment needs of the patient), and the right porosity range (for the appropriate drug release kinetics). Additionally, the parameters of mass variation and printing time were adjusted for the lowest possible values, inducing smart solutions to meet the other printlet quality requirements.

In order to test the models' ability to meet randomized clinical demands, two prescriptions for printlets were simulated and printed using the three studied filaments - namely, *Prescription #1*, requiring the preparation of five 500 mg printlets in a porosity range of 15 to 35%; and *Prescription #2*, involving thirty 200 mg printlets in a narrower porosity range (15-25%). The results of the model's solutions, as well as the experimental results of their printing are described in Table 2.

**Table 2.** Predicted and experimental results of the simulated prescriptions #1 and #2 obtained using ABS, HIPS, and PLA filaments, with 95% of confidence interval (CI) of prediction.

	<b>Prescription #1</b>		<b>Prescription #2</b>	
<b>Average mass (mg)</b>	<i>in target 500</i>		<i>in target 200</i>	
	<i>Predicted (CI)</i>	Observed	<i>Predicted</i>	Observed
ABS	500 (450-550)	500 ± 7.0	200 (140 -250)	200 ± 4.0
HIPS	500 (460-570)	480 ± 2.0	200 (150-250)	190 ± 1.0
PLA	500 (460 -540)	479 ± 3.0	200 (170-240)	189 ± 1.0
	<i>equal to 5</i>		<i>equal to 30</i>	
<b>Printlets per plate</b>	<i>Predicted</i>	Observed	<i>Predicted</i>	Observed
ABS	5	5	30	30
HIPS	5	5	30	30
PLA	5	5	30	30
	<i>in target 15 - 35</i>		<i>in target 15 - 25</i>	
<b>Porosity (%)</b>	<i>Predicted (CI)</i>	Observed	<i>Predicted (CI)</i>	Observed
ABS	30.0 (17.3-42.7)	30.5 ± 5.1	24.8 (12.2-4.5)	21.4 ± 5.1

HIPS	20.6 (09.8-31.5)	16.4 ± 2.0	25.0 (14.4-35.5)	15.5 ± 3.7
PLA	30.0 (22.0-38.1)	36.1 ± 1.4	25.2 (17.3-33.0)	21.4 ± 2.3
<b>Mass variation (%)</b>	<i>minimize</i>		<i>minimize</i>	
	<i>Predicted</i>	Observed	<i>Predicted</i>	Observed
ABS	0.32 (0.0-0.83)	0.31	0.50 (0.0-1.00)	0.79
HIPS	0.33 (0.0-1.32)	0.45	0.47 (0.0-1.34)	0.51
PLA	0.19 (0.0-0.52)	0.24	0.44 (0.0-0.8)	0.40
<b>Time (s/printlet)</b>	<i>in range</i>		<i>in range</i>	
	<i>Predicted</i>	Observed	<i>Predicted</i>	Observed
ABS	138 (118-158)	137.6 ± 0.2	60 (40-79)	61.7 ± 0.07
HIPS	146 (126-167)	137.1 ± 0.2	62 (43-80)	61.0 ± 0.02
PLA	126 (112-139)	119.5 ± 0.1	55 (43-68)	56.6 ± 0.05

The printing settings that met the simulated prescriptions resulted in average masses precisely equal to those specified in the prescriptions for all filaments, thereby indicating the ability of the optimized DOE employed in this study to meet the random demands of medical prescriptions (Table 2). Moreover, the experimental average mass results for both prescriptions showed very close values to the predicted ones, within the 95% confidence interval and that fulfilled pharmacopeia requirements for tablet production of uniformity of mass method for single-dose preparations (WHO, 2019).

In terms of porosity results, despite the low predictive precision, all proposed prescriptions produced printlets within the established confidence interval—including Prescription #2, which had a narrower interval for this response (Table 2). The ability to predict the time spent manufacturing the printlets was quite high, confirming that it is possible to establish a Process Control Plan from the predictive equations that can rationalize and optimize the use of 3D printers in digital pharmacies.

Finally, the mass variations found for the prescriptions preparation repeated the pattern observed throughout all the experiments carried out in this study, with values mostly below 0.5%. In addition, this parameter showed a high correlation between the expected and observed mass variations (Table 2). These results reaffirm the consistent production precision of pharmaceutical units using 3D FDM printing that is far superior to the artisanal drug product production in compounding pharmacies, which achieve mass variation levels higher than 4% and, in some cases, as high as 20% (Green et al., 2012; Neumann et al., 2017).

## 2.4 CONCLUSION

This study is a proof-of-concept on the feasibility of using the quality-by-design DOE tools to integrate the 3D FDM printing operational variables and to obtain tablets that can meet the prescribing demands of each patient. Overall, the results demonstrated that by changing the right parameters, the control over the final product characteristics is achieved, with outcomes that could be even better than those obtained from the traditional manufacture of personalized pharmaceutical dosage forms. We expect that this study will serve as a basis for the development of process validation protocols in the near future that integrate the necessary information to ensure the reliability of printed tablets in compounding pharmacies for personalized medications.

## 2.5 REFERENCES

- Abeykoon, C., Sri-Amphorn, P., Fernando, A., 2020. Optimization of fused deposition modeling parameters for improved PLA and ABS 3D printed structures. *Int. J. Light. Mater. Manuf.* 3, 284–297. <https://doi.org/10.1016/j.ijlmm.2020.03.003>
- Alhijaj, M., Nasereddin, J., Belton, P., Qi, S., 2019. Impact of Processing Parameters on the Quality of Pharmaceutical Solid Dosage Forms Produced by Fused Deposition Modeling (FDM). *Pharm.* 2019, Vol. 11, Page 633–633. <https://doi.org/10.3390/PHARMACEUTICS11120633>
- Alhnan, M.A., Okwuosa, T.C., Sadia, M., Wan, K.W., Ahmed, W., Arafat, B., 2016. Emergence of 3D Printed Dosage Forms: Opportunities and Challenges. *Pharm. Res.* 33, 1817–1832. <https://doi.org/10.1007/s11095-016-1933-1>
- Alsoufi, M.S., Elsayed, A.E., 2017. Warping deformation of desktop 3D printed parts manufactured by open source fused deposition modeling (FDM) system. *Int. J. Mech. Mechatronics Eng.* 17, 7–16.
- Araújo, M.R.P., Sa-Barreto, L.L., Gratieri, T., Gelfuso, G.M., Cunha-Filho, M., 2019. The digital pharmacies era: How 3D printing technology using fused deposition modeling can become a reality. *Pharmaceutics* 11. <https://doi.org/10.3390/pharmaceutics11030128>

- Bakar, N.S.A., Alkahari, M.R., Boejang, H., 2010. Analysis on fused deposition modelling performance. *J. Zhejiang Univ. Sci. A* 11, 972–977. <https://doi.org/10.1631/jzus.A1001365>
- Billah, K.M.M., Lorenzana, F.A.R., Martinez, N.L., Chacon, S., Wicker, R.B., Espalin, D., 2019. Thermal analysis of thermoplastic materials filled with chopped fiber for large area 3D printing. *Solid Free. Fabr. 2019 Proc. 30th Annu. Int. Solid Free. Fabr. Symp. - An Addit. Manuf. Conf. SFF 2019* 892–898.
- Chai, X., Chai, H., Wang, X., Yang, J., Li, J., Zhao, Y., Cai, W., Tao, T., Xiang, X., 2017. Fused deposition modeling (FDM) 3D printed tablets for intragastric floating delivery of domperidone. *Sci. Rep.* 7, 1–9. <https://doi.org/10.1038/s41598-017-03097-x>
- Cheng, Y.L., Zhang, L.C., Chen, F., Tseng, Y.H., 2018. Particle Emissions of Material-Extrusion-Type Desktop 3D Printing: the Effects of Infill. *Int. J. Precis. Eng. Manuf. - Green Technol.* 5, 487–497. <https://doi.org/10.1007/s40684-018-0052-3>
- Cunha-Filho, M., Araújo, M.R., Gelfuso, G.M., Gratieri, T., 2017. FDM 3D printing of modified drug-delivery systems using hot melt extrusion: A new approach for individualized therapy. *Ther. Deliv.* 8, 957–966. <https://doi.org/10.4155/tde-2017-0067>
- Cunha-Filho, M., Teixeira, M.T., Santos-Rosales, V., Sa-Barreto, L.L., Marreto, R.N., Martin-Pastor, M., García-González, C.A., Landin, M., 2019. The subdivision behavior of polymeric tablets. *Int. J. Pharm.* 568, 118554. <https://doi.org/10.1016/j.ijpharm.2019.118554>
- Durakovic, B., 2017. Design of experiments application, concepts, examples: State of the art. *Period. Eng. Nat. Sci.* 5, 421–439. <https://doi.org/10.21533/pen.v5i3.145>
- Fernandez-Vicente, M., Calle, W., Ferrandiz, S., Conejero, A., 2016. Effect of Infill Parameters on Tensile Mechanical Behavior in Desktop 3D Printing. *3D Print. Addit. Manuf.* 3, 183–192. <https://doi.org/10.1089/3dp.2015.0036>
- Ferreira-Nunes, R., Gratieri, T., Gelfuso, G.M., Cunha-Filho, M., 2018. Mixture design applied in compatibility studies of catechin and lipid compounds. *J. Pharm. Biomed. Anal.* 149, 612–617. <https://doi.org/10.1016/j.jpba.2017.11.069>
- Feuerbach, T., Kock, S., Thommes, M., 2018. Characterisation of fused deposition

- modeling 3D printers for pharmaceutical and medical applications, *Pharmaceutical Development and Technology*. Taylor & Francis. <https://doi.org/10.1080/10837450.2018.1492618>
- Fok, K.Y., Cheng, C.T., Tse, C.K., 2017. A refinement process for nozzle path planning in 3D printing. *Proc. - IEEE Int. Symp. Circuits Syst.* 1–4. <https://doi.org/10.1109/ISCAS.2017.8050471>
- Galeja, M., Hejna, A., Kosmela, P., Kulawik, A., 2020. Static and dynamic mechanical properties of 3D printed ABS as a function of raster angle. *Materials (Basel)*. 13. <https://doi.org/10.3390/ma13020297>
- Gendviliene, I., Simoliunas, E., Rekstyte, S., Malinauskas, M., Zaleckas, L., Jegelevicius, D., Bukelskiene, V., Rutkunas, V., 2020. Assessment of the morphology and dimensional accuracy of 3D printed PLA and PLA/HAp scaffolds. *J. Mech. Behav. Biomed. Mater.* 104, 103616. <https://doi.org/10.1016/j.jmbbm.2020.103616>
- Goyanes, A., Buanz, A.B.M., Hatton, G.B., Gaisford, S., Basit, A.W., 2015. 3D printing of modified-release aminosalicylate (4-ASA and 5-ASA) tablets. *Eur. J. Pharm. Biopharm.* 89, 157–162. <https://doi.org/10.1016/j.ejpb.2014.12.003>
- Goyanes, A., Fina, F., Martorana, A., Sedough, D., Gaisford, S., Basit, A.W., 2017. Development of modified release 3D printed tablets (printlets) with pharmaceutical excipients using additive manufacturing. *Int. J. Pharm.* 527, 21–30. <https://doi.org/10.1016/j.ijpharm.2017.05.021>
- Goyanes, A., Kobayashi, M., Martínez-Pacheco, R., Gaisford, S., Basit, A.W., 2016. Fused-filament 3D printing of drug products: Microstructure analysis and drug release characteristics of PVA-based caplets. *Int. J. Pharm.* 514, 290–295. <https://doi.org/10.1016/j.ijpharm.2016.06.021>
- Green, D.M., Jones, A.C., Brain, K.R., 2012. Content variability of active drug substance in compounded oral 3,4-diaminopyridine products. *J. Clin. Pharm. Ther.* 37, 53–57. <https://doi.org/10.1111/j.1365-2710.2011.01249.x>
- Hernandez, D.D., 2015. Factors affecting dimensional precision of consumer 3D printing. *Int. J. Aviat. Aeronaut. Aersp.* 2. <https://doi.org/10.15394/ijaaa.2015.1085>
- Jamróz, W., Kurek, M., Szafraniec-Szczyński, J., Czech, A., Gawlak, K., Knapik-Kowalczyk, J., Leszczyński, B., Wróbel, A., Paluch, M., Jachowicz, R., 2020. Speed

- it up, slow it down...An issue of bicalutamide release from 3D printed tablets. *Eur. J. Pharm. Sci.* 143. <https://doi.org/10.1016/j.ejps.2019.105169>
- Jamróz, W., Szafraniec, J., Kurek, M., Jachowicz, R., 2018. 3D printing in pharmaceutical and medical applications. *Pharm. Res.* 35, Article 176.
- Kempin, W., Domsta, V., Grathoff, G., Brecht, I., Semmling, B., Tillmann, S., Weitschies, W., Seidlitz, A., 2018. Immediate Release 3D-Printed Tablets Produced Via Fused Deposition Modeling of a Thermo-Sensitive Drug. *Pharm. Res.* 35. <https://doi.org/10.1007/s11095-018-2405-6>
- Li Chew, S., de Mohac, L.M., Raimi-Abraham, B.T., 2019. 3D-Printed Solid Dispersion Drug Products. *Pharmaceutics* 11, 1–12. <https://doi.org/10.3390/pharmaceutics11120672>
- Malaquias, L.F.B., Sá-Barreto, L.C.L., Freire, D.O., Silva, I.C.R., Karan, K., Durig, T., Lima, E.M., Marreto, R.N., Gelfuso, G.M., Gratieri, T., Cunha-Filho, M., 2018. Taste masking and rheology improvement of drug complexed with beta-cyclodextrin and hydroxypropyl- $\beta$ -cyclodextrin by hot-melt extrusion. *Carbohydr. Polym.* 185, 19–26. <https://doi.org/10.1016/j.carbpol.2018.01.011>
- Malaquias, L.F.B., Schulte, H.L., Chaker, J.A., Karan, K., Durig, T., Marreto, R.N., Gratieri, T., Gelfuso, G.M., Cunha-Filho, M., 2017. Hot Melt Extrudates Formulated Using Design Space: One Simple Process for Both Palatability and Dissolution Rate Improvement. *J. Pharm. Sci.* 1–11. <https://doi.org/10.1016/j.xphs.2017.08.014>
- Mathew, E., Pitzanti, G., Larrañeta, E., Lamprou, D.A., 2020. Three-dimensional printing of pharmaceuticals and drug delivery devices. *Pharmaceutics* 12, 1–9. <https://doi.org/10.3390/pharmaceutics12030266>
- Mazzanti, V., Malagutti, L., Mollica, F., 2019. FDM 3D printing of polymers containing natural fillers: A review of their mechanical properties. *Polymers (Basel)*. 11. <https://doi.org/10.3390/polym11071094>
- Melocchi, A., Parietti, F., Maroni, A., Foppoli, A., Gazzaniga, A., Zema, L., 2016. Hot-melt extruded filaments based on pharmaceutical grade polymers for 3D printing by fused deposition modeling. *Int. J. Pharm.* 509, 255–263. <https://doi.org/10.1016/j.ijpharm.2016.05.036>
- Messimer, S.L., Patterson, A.E., Muna, N., Deshpande, A.P., Pereira, T.R., 2018.

- Characterization and processing behavior of heated aluminum-polycarbonate composite build plates for the fdm additive manufacturing process. *J. Manuf. Mater. Process.* 2. <https://doi.org/10.3390/jmmp2010012>
- Micó-Vicent, B., Perales, E., Huraibat, K., Martínez-Verdú, F.M., Viqueira, V., 2019. Maximization of FDM-3D-objects gonio-appearance effects using PLA and ABS filaments and combining several printing parameters: “A case study.” *Materials (Basel)*. 12. <https://doi.org/10.3390/ma12091423>
- Neumann, U., Burau, D., Spielmann, S., Whitaker, M.J., Ross, R.J., Kloft, C., Blankenstein, O., 2017. Quality of compounded hydrocortisone capsules used in the treatment of children. *Eur. J. Endocrinol.* 177, 239–242. <https://doi.org/10.1530/EJE-17-0248>
- Norman, J., Madurawe, R.D., Moore, C.M.V., Khan, M.A., Khairuzzaman, A., 2017. A new chapter in pharmaceutical manufacturing: 3D-printed drug products. *Adv. Drug Deliv. Rev.* 108, 39–50. <https://doi.org/10.1016/j.addr.2016.03.001>
- Nukala, P.K., Palekar, S., Patki, M., Patel, K., 2019. Abuse Deterrent Immediate Release Egg-Shaped Tablet (Egglets) Using 3D Printing Technology: Quality by Design to Optimize Drug Release and Extraction. *AAPS PharmSciTech* 20. <https://doi.org/10.1208/s12249-019-1298-y>
- Öblom, H., Zhang, J., Pimparade, M., Speer, I., Preis, M., Repka, M., Sandler, N., 2019. 3D-Printed Isoniazid Tablets for the Treatment and Prevention of Tuberculosis—Personalized Dosing and Drug Release. *AAPS PharmSciTech* 20, 1–13. <https://doi.org/10.1208/s12249-018-1233-7>
- Organization), W. (World H., 2019. The international Pharmacopoeia [WWW Document]. Dept. Essent. Med. Pharm. policies. URL <https://apps.who.int/phint/en/p/docf/>
- Ou-Yang, Q., Guo, B., Xu, J., 2018. Preparation and Characterization of Poly(butylene succinate)/Polylactide Blends for Fused Deposition Modeling 3D Printing. *ACS Omega* 3, 14309–14317. <https://doi.org/10.1021/acsomega.8b02549>
- Pietrzak, K., Isreb, A., Alhnan, M.A., 2015. A flexible-dose dispenser for immediate and extended release 3D printed tablets. *Eur. J. Pharm. Biopharm.* 96, 380–387. <https://doi.org/10.1016/j.ejpb.2015.07.027>



- Pires, F.Q., Angelo, T., Silva, J.K.R., Sá-Barreto, L.C.L., Lima, E.M., Gelfuso, G.M., Gratieri, T., Cunha-Filho, M.S.S., 2017. Use of mixture design in drug-excipient compatibility determinations: Thymol nanoparticles case study. *J. Pharm. Biomed. Anal.* 137, 196–203. <https://doi.org/10.1016/j.jpba.2017.01.037>
- Richey, R.H., Hughes, C., Craig, J. V., Shah, U.U., Ford, J.L., Barker, C.E., Peak, M., Nunn, A.J., Turner, M.A., 2017. A systematic review of the use of dosage form manipulation to obtain required doses to inform use of manipulation in paediatric practice. *Int. J. Pharm.* 518, 155–166. <https://doi.org/10.1016/j.ijpharm.2016.12.032>
- Shie, M.Y., Shen, Y.F., Astuti, S.D., Lee, A.K.X., Lin, S.H., Dwijaksana, N.L.B., Chen, Y.W., 2019. Review of polymeric materials in 4D printing biomedical applications. *Polymers (Basel)*. 11, 1–17. <https://doi.org/10.3390/polym11111864>
- Solanki, N.G., Tahsin, M., Shah, A. V., Serajuddin, A.T.M., 2018. Formulation of 3D Printed Tablet for Rapid Drug Release by Fused Deposition Modeling: Screening Polymers for Drug Release, Drug-Polymer Miscibility and Printability. *J. Pharm. Sci.* 107, 390–401. <https://doi.org/10.1016/j.xphs.2017.10.021>
- Spina, R., 2019. Performance analysis of colored PLA products with a fused filament fabrication process. *Polymers (Basel)*. 11. <https://doi.org/10.3390/polym11121984>
- Tagami, T., Fukushige, K., Ogawa, E., Hayashi, N., Ozeki, T., 2017. 3D printing factors important for the fabrication of polyvinylalcohol filament-based tablets. *Biol. Pharm. Bull.* 40, 357–364. <https://doi.org/10.1248/bpb.b16-00878>
- Trenfield, S.J., Awad, A., Goyanes, A., Gaisford, S., Basit, A.W., 2018. 3D Printing Pharmaceuticals: Drug Development to Frontline Care. *Trends Pharmacol. Sci.* 39, 440–451. <https://doi.org/10.1016/j.tips.2018.02.006>
- Warsi, M.H., Yusuf, M., Al Robaian, M., Khan, M., Muheem, A., Khan, S., 2018. 3D Printing Methods for Pharmaceutical Manufacturing: Opportunity and Challenges. *Curr. Pharm. Des.* 24, 4949–4956. <https://doi.org/10.2174/1381612825666181206121701>
- Zhao, X.G., Hwang, K.J., Lee, D., Kim, T., Kim, N., 2018. Enhanced mechanical properties of self-polymerized polydopamine-coated recycled PLA filament used in 3D printing. *Appl. Surf. Sci.* 441, 381–387. <https://doi.org/10.1016/j.apsusc.2018.01.257>

### 3. CHAPTER III: IN-SITU FORMATION OF NANOPARTICLES FROM DRUG-LOADED 3D POLYMERIC MATRICES

#### 3.1. INTRODUCTION

In the past decades, the use of plastic materials as drug matrices has become increasingly common with the incorporation of new technologies for modified drug release. In fact, several market drug products are produced from polymeric substrates forming solid dispersions, adding therapeutic benefits such as modulation of drug release, as well as increased solubility and stability (Alshehri et al., 2020). Moreover, the use of different polymers in medicines has been escalated with the consolidation of hot-melt extrusion (HME) technology in pharmaceutical factories, allowing solid dispersions to be produced in a simplified, continuous, and solvent-free process (Tran et al., 2021).

Recent studies show that polymers' disaggregation in water frequently leads to micro and nanoparticles' formation. Indeed, the presence of nanoplastics derived from physical or biological decomposition processes of polymeric materials thrown into the environment has been a source of a new type of pollution found in human tissues, constituting, in this case, an invisible threat to people's health (Gigault et al., 2021). In fact, nanometric particles are known for being highly interactive structures that can easily disperse in different environments and interact with many substances, being capable of entrapping material in their surfaces or interiors and permeating through biological membranes (Mitchell et al., 2021).

In the pharmaceutical field, the *in-situ* formation of nanoparticles from polymeric-based materials is still little studied, especially considering the effect it may have on the pharmacokinetics of a drug product (Schittny et al., 2020). Indeed, in most dissolution studies with polymer-based medicines, it is assumed that the drug found in the dissolution medium is solvated and free to be absorbed by the body (Pandi et al., 2020). However, the truth is that between polymer matrix disaggregation and drug solubilization, intermediate states of nanoencapsulation and microencapsulation can occur (Nunes et al., 2022).

Such particles can be formed by multiple mechanisms leading to colloidal dispersion with the drug entrapped by the polymer. Those processes can be controlled mainly by the formulation components' dissolution profile, depending on their solubility

on the medium and the interactions among the other compounds (Nunes et al., 2022). Notably, for an oral dosage form, the presence of a nanoparticle on the dissolution medium can mean a modification of the amount of free drug available for absorption in the gastrointestinal cells, consequently changing the bioavailability of the drug (Sironi et al., 2017; Stewart and Grass, 2020). However, no literature is available regarding such unpredicted intermediates states of drug encapsulation from the polymeric solid dispersions in an *in vivo* environment (Agafonov et al., 2021) or if such systems would have the same behavior as other nanosized colloidal systems intentionally produced (Kim et al., 2021).

The spontaneous formation of nanoscale polymeric structures has gone unnoticed in medicines until now. Nevertheless, this occurrence can no longer be ignored, considering the relevance of 3D printed dosage forms, which must be the new trend in the pharmaceutical field (Karalia et al., 2021). This new way of making medicines uses almost exclusively plastic substrates, allowing high versatility in drug release with the personalization of the therapy (Pires et al., 2020). In particular, the most promising printing technique of fused deposition modeling (FDM) uses polymeric filaments obtained from HME as pharmaceutical ink (Araújo et al., 2019).

To illustrate the magnitude of this question, 30 papers have been found in the web of science database in the last five years, focusing on dissolution studies of polymeric-base dosage forms made with 3D printing and HME (Appendix A). None of them verified the possible encapsulation of the drug in nano or micro particles in the dissolution tests, assuming the drug was free in the aqueous dissolution medium. Such negligence regarding the real physical state of the drug in a simulated gastrointestinal medium may lead to the unpredictable therapeutic performance of this medicine.

Particularly for the 3D printing process of oral dosage forms, such as in tablet forms, named printlets, a high percentage of the polymeric matrix is used in the composition, with variations in the amount of the drug (Karalia et al., 2021). Based on this, the odds of particle formation are high, and it is possible that the modifications brought by the printing process and the structure of the dosage form can also change the particle formation behavior.

Faced with this scenario, there is a dramatic need to study the mechanisms involved in the *in situ* particle formation and the influence of the HME and 3D printing processes on this phenomenon. Therefore, this work aimed to study the formation of in

situ nanoparticles during the dissolution process of 3D printed pharmaceutical dosage forms. For this purpose, three systems with different solubility characteristics, and specific interactions between polymer, plasticizer, and drug, were selected. The naringenin was chosen as a model drug to be incorporated in the polymer matrices of hydroxypropylmethylcellulose acetate succinate (HPMC-AS), polyvinyl alcohol (PVA), and Eudragit RL PO<sup>®</sup> (EUD RL), using glycerol and triethyl citrate as plasticizers.

## **3.2. MATERIALS AND METHODS**

### **3.2.1. Materials**

Naringenin (NAR, (2S)-5,7-Dihydroxy-2-(4-hydroxyphenyl)-2,3-dihydro-4H-chromen-4-one, purity  $\geq$  98%, lot MKCD1056) was obtained from Sigma-Aldrich (St. Louis, MO, USA). The polymer Parateck<sup>®</sup> MXP (Polyvinyl alcohol, PVA, lot F1952064) was donated by Merck (Darmstadt, Germany). Aquasolve<sup>®</sup> MG (HPMCAS, hydroxypropylmethylcellulose acetate succinate grade M, lot SF60G410004) and Eudragit RL PO<sup>®</sup> (EUD RL, Poly(ethyl acrylate-co-methyl methacrylate-co-trimethylammonioethyl methacrylate chloride), lot G170936626) were donated by Ashland Specialty Ingredients (Covington, LA, USA), and Evonik industries (Darmstadt, Germany), respectively. The plasticizers glycerin (GLY, lot 58591) and triethyl citrate (TEC, lot S7425151) were purchased from Dinâmica<sup>®</sup> (São Paulo, Brazil) and Merck (Darmstadt, Germany), respectively. All other chemicals and solvents were of analytical grade.

### **3.2.2. Preformulation studies**

Three different polymers were selected for the filament formulation: HPMCAS, PVA, and EUD RL. Moreover, a plasticizer and the model drug NAR were also added to the formulation (Table 1). For each polymer, an appropriate plasticizer was selected according to its ability to increase the mobility of the polymer chains through the HME process, producing filaments more suitable for 3D FDM printing, i.e., it was used TEC for the polymers HPMCAS and EUD RL, and GLY for PVA (Pereira et al., 2020).

**Table 1.** Formulations composition (% , m/m) with the amount of plasticizer and model drug. HPMCAS - hydroxypropylmethylcellulose acetate succinate, PVA - Polyvinyl alcohol, EUD RL - Eudragit RL PO<sup>®</sup>, TEC - Triethyl citrate, GLY – Glycerin and NAR – Naringenin.

	Formulation	Plasticizer		Model Drug
		GLY	TEC	NAR
<b>With NAR</b>	<i>HPMCAS</i>		20%	5%
	<i>PVA</i>	20%		5%
	<i>EUD RL</i>		13%	5%
<b>Without NAR</b>	<i>HPMCAS</i>		20%	
	<i>PVA</i>	20%		
	<i>EUD RL</i>		13%	

Previously to the production, the interactions between the materials were assessed by determining the Hansen solubility parameter (HSP) and by Fourier transform infrared spectroscopy (FTIR) analysis.

The HSP for NAR was estimated by Hoftyzer and Van Krevelen group-contribution method (van Krevelen and te Nijenhuis, 2009) (Table 2). For this purpose, it was calculated the dispersion ( $\delta_d$ ), polar ( $\delta_p$ ), and hydrogen bond ( $\delta_h$ ) parameters by the equations:

$$\delta_d = \frac{\sum F_{di}}{V} \quad (1)$$

$$\delta_p = \frac{\sqrt{\sum F_{pi}^2}}{V} \quad (2)$$

$$\delta_h = \frac{\sqrt{\sum F_{hi}}}{V} \quad (3)$$

where  $F_{di}$ ,  $F_{pi}$ , and  $F_{hi}$  are, respectively, the dispersion, the polar, and the hydrogen bonding components of the molar attraction function for each contribution group “*i*”, and  $V$  is the molar volume of the respective molecule. Finally, the total Hansen solubility parameter ( $\delta_t$ ) can be obtained from the vector sum of the three components previously calculated:

$$\delta_t = \sqrt{\delta_d^2 + \delta_p^2 + \delta_h^2} \quad (4)$$

**Table 2.** Hansen solubility parameters.  $\delta_d$  – Dispersion parameter;  $\delta_p$  – Polar parameter;  $\delta_h$  – Hydrogen bonds parameter;  $\delta_t$  – Total Hansen solubility parameter. HPMCAS - hydroxypropylmethylcellulose acetate succinate, PVA - Polyvinyl alcohol, EUD RL - Eudragit RL PO<sup>®</sup>, TEC - triethyl citrate and GLY - Glycerin.

Material	Hansen solubility parameters (MPa <sup>1/2</sup> )			
	$\delta_d$	$\delta_p$	$\delta_h$	$\delta_t$
<i>NAR</i>	22.7	9.6	18.9	31.1
<i>HPMCAS</i>	20.5	5.1	14.6	25.7
<i>PVA</i>	11.2	12.4	13.0	21.1
<i>EUD RL</i>	16.9	1.0	11.1	20.2
<i>TEC</i>	16.5	4.9	12.0	20.9
<i>GLY</i>	17.4	12.1	29.3	36.2

The parameter values for HPMCAS and GLY were obtained from the studies of Klar & Urbanetz, 2016 (Klar and Urbanetz, 2016). PVA, EUD RL, and TEC were obtained from the studies of Kumar et al., 2022, Quinten et al., 2011 and Hansen, 2007, respectively (Hansen, 2007; Kumar et al., 2022; Quinten et al., 2021) (Table 2).







FTIR analyses were performed on Bruker model vertex 70 (Billerica, MA, USA), using the equipment ATR accessory, from 4,500 to 375 cm<sup>-1</sup> in a resolution of 2.0 cm<sup>-1</sup> and three scans. The FTIR spectrum of selected binary and ternary mixtures was obtained. The results were compared to the theoretical average spectrum, composed of the combination of the pure material spectra data considering the proportion of each component.

### 3.2.3. Filament production by HME

As described before, the filament formulations comprised a combination of NAR, polymers, and suitable plasticizers. The proportion of each material is described in table 1.

The mixtures were initially prepared using mortar and pestle and then extruded in a co-rotating conical twin-screw extruder with a die diameter of 1.8 mm (HAAKE MiniCTW, ThermoScientific, Waltham, MA, USA), without recirculation, coupled to a filament tractor system model FTR1 endowed with an automatic diameter gauge (Filmaq3D, Curitiba, Brazil). The rotation and temperature of the HME process were chosen to guarantee the filament diameter's uniformity and the material's correct flow (Table 3). All filaments were stored in a desiccator before the characterization.

**Table 3.** Filaments manufacturing specifications and characterization data of all formulations with and without naringenin (NAR). HPMCAS - hydroxypropylmethylcellulose acetate succinate, PVA - Polyvinyl alcohol, EUD RL - Eudragit RL PO<sup>®</sup>,  $T_{\text{extrusion}}$  – Extrusion temperature and  $V_{\text{rotation}}$  - Velocity of the screws rotation.

	<b>Formulation</b>	<b><math>T_{\text{extrusion}}</math> (°C)</b>	<b><math>V_{\text{rotation}}</math> (RPM)</b>	<b>Mean Diameter (mm)</b>	<b>Fracture Force (N)</b>	<b>Aspect</b>
<b>With NAR</b>	<i>HPMCAS</i>	140	30	1.67±0.04	28.77±1.13	
	<i>PVA</i>	150	30	1.70±0.04	28.79±2.59	
	<i>EUD RL</i>	140	40	1.46±0.06	24.34±1.38	
<b>Without NAR</b>	<i>HPMCAS</i>	140	30	1.62±0.06	30.59±1.52	
	<i>PVA</i>	150	30	1.59±0.11	28.19±1.16	
	<i>EUD RL</i>	140	40	1.59±0.07	22.29±1.82	

### 3.2.4. Filament characterization

The filament diameter was measured at every 10 cm using a digital caliper (Mitutoyo Sul Americana, São Paulo, Brazil), then the mean diameter was calculated by the arithmetic mean of the measures. The visual characteristics were evaluated by optical microscopy using a stereoscope coupled to a video camera (Laborana/SZ – SZT, São Paulo, Brazil).







The filaments' printability was tested by measuring their mechanical resistance with the fracture force data ( $n = 5$ ) (Lima et al., 2022). The analysis was performed in a universal testing machine (Shimadzu EZ test, Tokyo, Japan) equipped with a 5 kN load cell using wedge-type grips that move horizontally to tighten the grip on the filament (before analysis) and vertically to perform the elongation test. The cell moved at a constant crosshead speed of  $10 \text{ mm} \cdot \text{min}^{-1}$ . The filament size was 90 mm, the gap between the cells was 60 mm, and the initial force was 1 N.

### 3.2.5. Printlets production by FDM 3D printing

Cylinder shape printlets with a mean volume of  $0.569 \text{ cm}^3$  were designed using a free version of the software Tinkercad<sup>®</sup> (Autodesk<sup>®</sup> Inc, San Rafael, CA, USA) and were sliced using Slic3r<sup>®</sup> (Rome, Italy) software. The printlets were printed using the filaments prepared previously by HME at a Voolt FDM 3D printer model Gi3 (São Paulo, Brazil) with a brass nozzle with a diameter of 0.4 mm. The printing temperature was adapted to each polymer (Table 4). The temperature of the printing bed was fixed at  $80 \text{ }^\circ\text{C}$ , and the printlets were printed three at a time. The layer height was set at 0.2 mm, and the infill pattern was rectilinear with a density of 50%. Three extern layer shells were printed on all sides of the printlets, and the printing speed was set at  $15 \text{ mm} \cdot \text{s}^{-1}$  for printing moves and  $50 \text{ mm} \cdot \text{s}^{-1}$  for travel speed.



**Table 4.** Printlets manufacturing specifications and characterization data of all formulations with and without naringenin (NAR). HPMCAS - hydroxypropylmethylcellulose acetate succinate, PVA - Polyvinyl alcohol, EUD RL - Eudragit RL PO<sup>®</sup> and T<sub>printing</sub> – printing temperature.

Formulation	T <sub>printing</sub> (°C)	Volume (cm <sup>3</sup> )	Weight (g)	Drug content (%)	Aspect	
<i>HPMCAS</i>	180	0.579±0.005	0.408±0.01	94.9±0.8		
<b><i>With NAR</i></b>	<i>PVA</i>	180	0.605±0.005	0.637±0.03	102.5±0.8	
	<i>EUD RL</i>	190	0.551±0.007	0.523±0.02	93.2±0.9	
<b><i>Without NAR</i></b>	<i>HPMCAS</i>	180	0.568±0.004	0.463±0.01	-	
	<i>PVA</i>	180	0.563±0.009	0.525±0.01	-	
	<i>EUD RL</i>	190	0.549±0.007	0.471±0.013	-	

### 3.2.6. Printlets characterization

Printlets volumes were calculated by measuring the diameter and thickness of each printlet using a digital caliper (Mitutoyo Sul Americana, São Paulo, Brazil). The mean volume was obtained from 10 printlets for each formulation. The visual characteristics were evaluated by optical microscopy using a stereoscope coupled to a video camera (Laborana/SZ – SZT, São Paulo, Brazil).

The weight of each printlet was obtained using an analytical balance (Shimadzu, Tokyo, Japan). The individual weight and the mean weight obtained by the measure made in 10 tablets were used during the study. Drug content was determined in triplicate by dissolving the printlets in ethanol for the PLA samples and methanol for HPMCAS and EUD RL samples and determining the amount of NAR by HPLC as described in 2.9 section.

### 3.2.7. Dissolution studies and drug encapsulation

Dissolution profiles of NAR as supplied, physical mixtures of the formulations, and the printlets were determined in a dissolutor Ethik model 299 (Nova Ética, São Paulo, Brazil) using 900 mL of medium. For the HPMCAS samples, phosphate-buffer solution 0.1 mol L<sup>-1</sup> (pH 6.8) was used as the dissolution medium (Thakkar et al., 2020), whereas, for the PVA and EUD RL samples, the medium was HCl 0.1 mol L<sup>-1</sup> (Granados et al., 2022; Pietrzak et al., 2015). The temperature was maintained at 37 °C, and apparatus 2 (paddle) was used, operating at 100 rpm. Samples containing approximately 25 mg of the drug were added to the dissolution vessels. Aliquots of 5 mL were withdrawn and immediately replaced by fresh dissolution medium at 1, 2, 3, 4, 5, 6, 8, 10, 12, and 24 h. The aliquots were filtered on a paper filter using a vacuum filtration system composed of a Büchner funnel, a borosilicate filtering flask, and a vacuum pump.

After filtration, an aliquot was diluted in an appropriate organic solvent to quantify the total amount of NAR by HPLC according to the method described in section 2.8. Then, another aliquot fraction was used to determine the amount of NAR possible entrapped in the *in situ* formed particles. For that, 2 mL of the sample was inserted on a Vivaspin 2 filter (MWCO 10,000, Sartorius Lab Instruments GmbH & Co, Goettingen, Germany) and centrifuged for 10 min at a rotation of 4,000 rpm in a Z306 centrifuge (Hermle Labortechnik GmbH, Wehinger, Germany). The amount of NAR not entrapped (free NAR) was determined by the analyses of HPLC of the filtered material. Finally, the entrapped NAR was calculated according to Eq (1).

$$\text{Entrapped NAR (\% w/w)} = \frac{\text{Total amount of NAR} - \text{free NAR}}{\text{Total amount of NAR}} \times 100 \quad (5)$$

Experiments were performed in triplicate for each sample. Dissolution profiles were evaluated using their corresponding dissolution efficiency at 24 h (DE24) (Granados et al., 2022). Statistics of the dissolution efficiency were evaluated using GraphPad Prism 9 software (San Diego, CA, USA) using one-way ANOVA, followed by Turkey post-

test. The statistical analysis of the drug encapsulation data was performed by two-way ANOVA followed by Šídák post-test. The significance level ( $p$ ) for both tests was fixed at 0.05, and data normality was previously demonstrated using the Shapiro-Wilk normality test.

### 3.2.8. Characterization of the *in situ* formed particles

The particles generated from the polymeric systems were characterized in a release study under more concentrated conditions than the dissolution assay to allow the particle diameter, polydispersity index (PdI), zeta potential, and morphological assessments. In this experiment, NAR as supplied, physical mixtures of the formulations, and its printlets loaded or not with the drug were placed in a Becker containing 20 mL of the same mediums used in the dissolution studies. The systems were maintained in a water bath at  $37 \pm 3$  °C in constant magnetic stirring. Aliquots of 3 mL were withdrawn and immediately replaced by the fresh medium at 1, 4, 8, 12, and 24 h. Next, samples were filtered using the same procedure as the dissolution study and analyzed using a Zetasizer Nano ZS (Malvern, UK). Hydrodynamic diameter determinations were performed using the dynamic light scattering (DLS) method to obtain the particle diameter, PdI, and mean count rate, whereas the electrophoretic mobility method was used to determine the zeta potential. Statistics were evaluated using GraphPad Prism 9 software (San Diego, CA, USA) by two-way ANOVA, followed by Šídák post-test. The significance level ( $p$ ) was fixed at 0.05. Data normality was previously demonstrated using the Shapiro-Wilk normality test.

Additionally, the 12 h aliquot of the particle release experiments was used for morphological analysis. The samples were analyzed by transmission electron microscopy (TEM) using a JEM-1011 (JEOL, Tokyo, Japan). Before the analysis, diluted samples were deposited on Formvar-coated copper grids and received 3  $\mu$ L of uranyl acetate solution at 3% (w/v). After 3 min, the excess material was removed with filter paper, and the grids were air-dried. Then, the samples were taken to the equipment and analyzed at a magnitude of up 3,000 times.

### 3.2.9. Drug determination

NAR was quantified by a reversed-phase chromatographic method with UV detection at 290 nm using the HPLC model LC-20AT (Shimadzu, Kyoto, Japan) (Granados et al., 2022). The operating conditions of the method were as follows: 10  $\mu$ L

of injection volume; reversed-phase C18 column (LC Column, 300 × 3.9 mm, 10 μm) at 40 °C; methanol/phosphoric acid 0.01 mol.L<sup>-1</sup> (65:35, v/v) as the mobile phase; and flow rate of 0.6 mL min<sup>-1</sup>. The method was validated following the International Conference on Harmonization parameters and proved linear in the range of 0.5 to 30 μg mL<sup>-1</sup> with a correlation coefficient (r) = 0.999.

### 3.3. RESULTS AND DISCUSSION

#### 3.3.1. Preformulation studies

Polymers with different characteristics used in marketed drug products and have already been assessed for 3D printing of medicines were selected for this study, i.e., HPMCAS (pH-dependent), PVA (water-soluble polymer), and EUD RL (insoluble polymer) (Kuźmińska et al., 2021; Pandi et al., 2020). Such polymers were combined with a suitable plasticizer to enable HME and FDM 3D printing (Pereira et al., 2020), totalizing six different formulations (Table 1). Firstly, the interactions between the components of the formulations were assessed.

It is well known that the molecular interactions between the components of a particle have a decisive role in its final characteristics, such as shape, size, surface charge, and drug encapsulation (Hickey et al., 2015). Therefore, the HSP was obtained to predict those interactions. The results showed different possibilities for each polymer-based formulation (Figure 1).

Minor variations of HSP ( $\Delta\delta_t$ ) were found between the polymer HPMCAS with the drug NAR ( $\Delta\delta_t = 4.73 \text{ MPa}^{1/2}$ ) and with the plasticizer TEC ( $\Delta\delta_t = 5.44 \text{ MPa}^{1/2}$ ). Values below  $7.0 \text{ MPa}^{1/2}$  suggest strong compound interaction (Greenhalgh et al., 1999). On the other hand, for the PVA polymer, the potential interaction with NAR was considered weak ( $\Delta\delta_t = 9.97 \text{ MPa}^{1/2}$ ); however, a strong interaction between the drug and the plasticizer was noted ( $\Delta\delta_t = 5.06 \text{ MPa}^{1/2}$ ). Finally, the HSP calculations suggested a strong interaction of EUD RL with its plasticizer TEC ( $\Delta\delta_t = 0.71 \text{ MPa}^{1/2}$ ); nevertheless, a low probability of interaction was observed between this polymer and the drug or between the drug and the plasticizer.

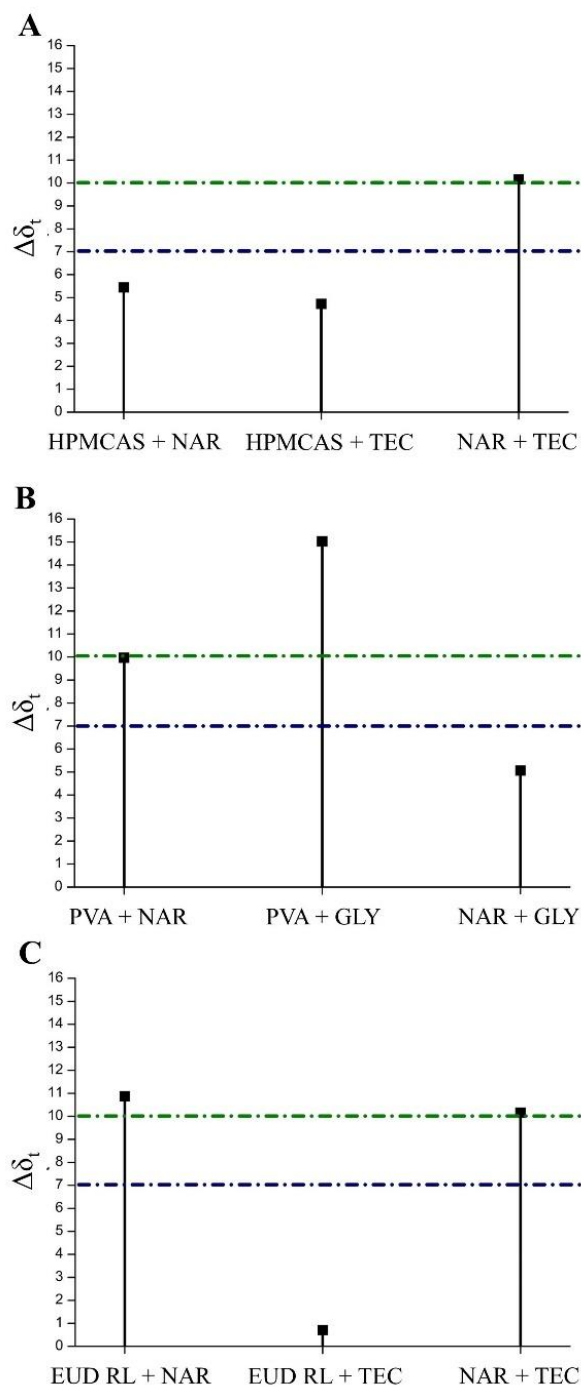


**Figure 1.** Variation of the total Hansen solubility parameter ( $\Delta\delta_t$ ) of each combination of materials related to the polymer-based formulations of hydroxypropylmethylcellulose acetate succinate (HPMCAS) and the plasticizer triethyl citrate (TEC) (A), Polyvinyl alcohol (PVA) and the plasticizer Glycerin (GLY) (B), and Eudragit RL PO<sup>®</sup> (EUD RL) and the plasticizer TEC (C). The blue line represents the limit for high interactions (up to 7.0 MPa<sup>1/2</sup>), and the green line is the limit for low interactions (up to 10.0 MPa<sup>1/2</sup>).

For a further interaction investigation, the binary mixtures with  $\Delta\delta_t < 7.0 \text{ MPa}^{1/2}$  were evaluated by FTIR (Figure 2).

In Figure 2a, all the expected bands for NAR and HPMCAS were observed for the NAR+HPMCAS physical mixture, and no shifts were identified between the calculated and experimental spectra. This result is expected since the values of the component  $\delta_d$  suggest that the interactions between NAR and HPMCAS are mainly dispersive (Table 2), not being able to promote significant dipole changes to be detected by infrared spectroscopy.

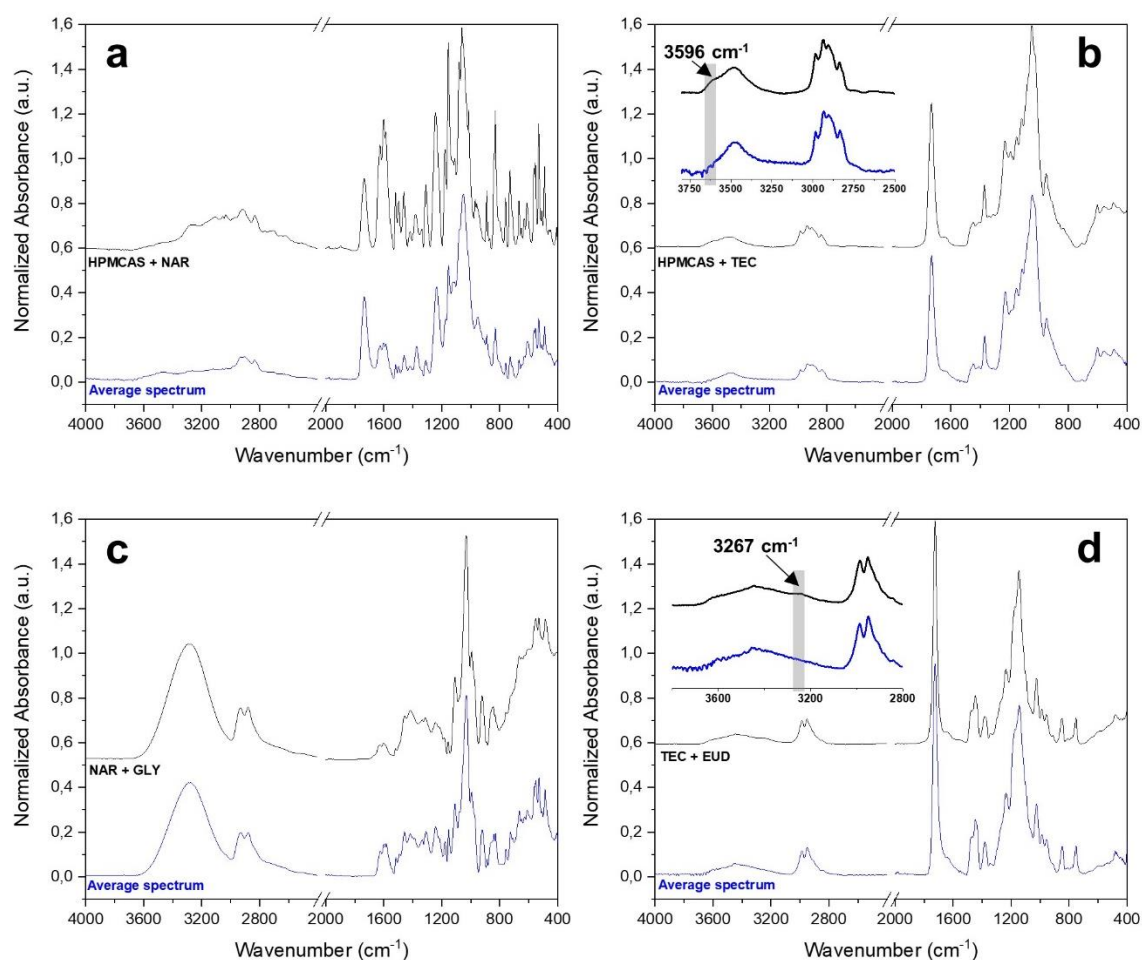


**Figure 2.** FTIR spectra of the selected samples: a) hydroxypropylmethylcellulose acetate succinate (HPMCAS) and Naringenin (NAR); b) HPMCAS and triethyl citrate (TEC); c) Glycerin (GLY) and NAR; and d) Eudragit RL PO<sup>®</sup> (EUD RL) and TEC. The theoretical average spectrum, was obtained by the combination of the pure material spectra data considering the proportion of each component.

On the other hand, as highlighted in Figure 2b, a shoulder at  $3,596\text{ cm}^{-1}$  appeared for the HPMCAS + TEC sample in the region of the O-H stretching. This finding may be associated with possible hydrogen bonds between the polymer and plasticizer, corroborating the similar  $\delta_h$  values calculated for both components (Table 2). Similarly, a shoulder was also observed at  $3,267\text{ cm}^{-1}$  for EUD + TEC sample (Figure 2d). The shoulder may be caused by the interaction between chemical groups of both molecules, most probably hydrogen bonds, since the -OH group of the plasticizer can act as a hydrogen bond donor that can interact with the many hydrogen bond acceptors presented in the polymer structure (Guerin et al., 2016).

As shown in Figure 2c, the calculated average spectrum was almost the same as obtained for the NAR + GLY sample, suggesting a low interaction and/or solubility of the NAR in glycerol. However, for the ternary physical mixture PVA + NAR + GLY (75/5/20), the FTIR spectrum (Figure 3) reveals small shifts in the C-O stretching and C-O-H bending bands, suggestive of hydrogen bond and/or other dipolar interactions.

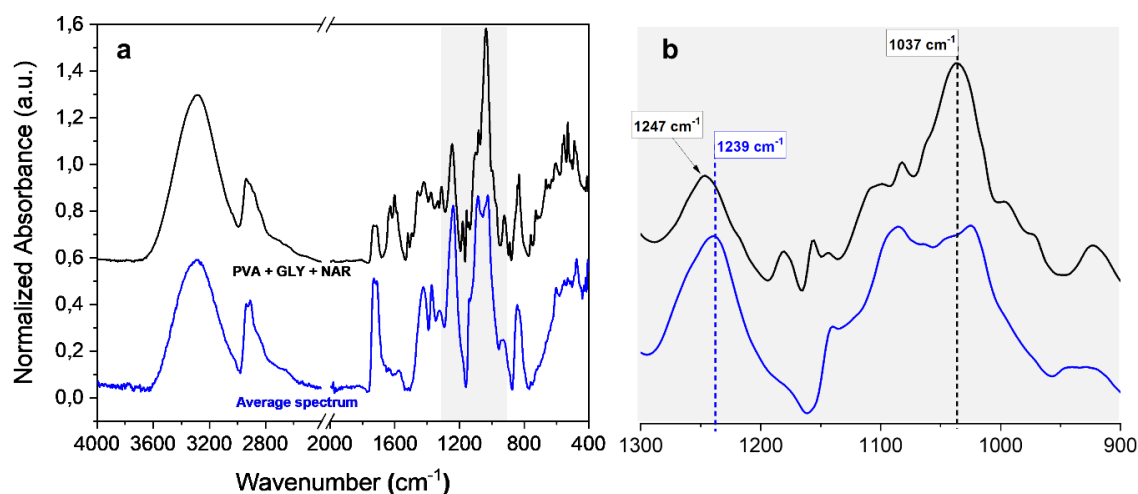


**Figure 3.** a) FTIR spectra of the physical mixture and calculated average spectrum for PVA/GLY/NAR ternary system; b) Zoom of the highlighted gray shaded rectangle region, from  $1,300$  to  $900\text{ cm}^{-1}$ . PVA - Polyvinyl alcohol, GLY – Glycerin and NAR – Naringenin.

The strong band at  $1,037\text{ cm}^{-1}$  was attributed to the glycerol C-O stretching shift observed at  $1,029\text{ cm}^{-1}$  for the pure GLY (Appendix B). In addition, the C-O-H bending of the PVA appears at  $1,247\text{ cm}^{-1}$  for the physical mixture (Figure 3b), which corresponds to a shift of  $8.0\text{ cm}^{-1}$  compared to the calculated average spectrum and the pure PVA (Appendix B). The frequency of this mode can be shifted to higher energies by increasing the bond angle or by expanding the molecule's dipole moment, which, in turn, may be associated with specific hydrogen bond interactions between the components.

It is important to emphasize that the discreet quality of those shifts evidenced that those interactions do not compromise the stability of the components. Nevertheless, it is possible that those interactions became even more expressive with the HME and 3D printing processes.

The preformulation results evidence three different scenarios for the study, with other interactions governing the behavior of those formulations, especially on the formation and characteristics of the particles, including the mutual interaction of NAR-polymer and polymer-plasticizer influencing the HPMCAS samples and the NAR-plasticizer and polymer-plasticizer affecting the PVA and EUD RL samples, respectively.

### **3.3.2. The HME filaments**

The filaments were obtained by HME, feeding the equipment with the material blend previously mixed. The constant feeding and the traction provided by filament tractor equipment allowed to produce filaments with uniform diameters, which is one of the main factors that affect the printability of the products (Bandari et al., 2021). The obtained filaments had a translucent and homogeneous aspect with a mean diameter between 1.70 and 1.46 mm (Table 3). This result is close to the ideal range recommended for the printing process (1.80 to 1.60 mm), allowing the production of appropriate printlets (Ponsar et al., 2020).

The standard deviation of the diameter of all filaments was lower than 0.11 mm (Table 3), which should allow a homogeneous feeding of the 3D printing and a better deposition of the materials (Ponsar et al., 2020). Furthermore, the filaments also had an ideal mechanical property. All the samples underwent an elastic deformation during the analysis, supporting forces higher than 22 N (Table 3), far superior to the minimum required force value for 3D printing of 5 N (Y. Yang et al., 2021). This result reinforces the probable printability of the produced filaments.



### 3.3.2. The printlets characterization

In agreement with what was expected, all the printlets obtained by the 3D printing process had a homogeneous appearance and uniformity in both weight and volume (Table 4). Furthermore, the weight and volume standard deviation were below 0.027 g and 0.009 cm<sup>3</sup>, respectively. Finally, the drug content was within the pharmacopeial range for all the printlets, ensuring health quality requirements for pharmaceutical dosage forms (Pires et al., 2020).

### 3.3.3. The dissolution assays

The nanoparticles formation over 24h was studied by dissolution assay to simulate the oral release profile of the NAR. Importantly, we analyzed the samples in order to distinguish the amount of NAR that was actually dissolved from those encapsulated in *in-situ* formed nanoparticles (Figure 4). Noteworthy, the amount of drug encapsulated almost did not change with time and is represented in Figure 4 by the mean values determined during the dissolution test.

In the case of the polymer HPMCAS and PVA, similar levels of encapsulation, around 25%, were observed both in the physical mixture of the formulation components and in the formulation submitted to the production process of extrusion and 3D printing (printlets). This effect can be attributed to an *in-situ* interaction of NAR with such polymers and/or the respective plasticizers, as predicted by the HSP simulations and confirmed by the FTIR analysis. Although NAR is more soluble in the release medium used for the HPMCAS systems (pH=6.8), the encapsulated drug content was very close to that observed in the PVA systems. This behavior can be explained by the higher polymer-drug and polymer-plasticizer interactions for the HPMCAS system, which could help maintain the cohesiveness of the nanostructure.

The drug dissolution improvement was more prominent in the physical mixture with PVA, probably due to the interactions between the NAR and the plasticizer GLY suggested by the HSP values. Furthermore, the effect may have been even more noticeable due to the slower dissolution profile of the drug in the acid medium. Indeed, for the physical mixtures containing EUD RL, such dissolution improvements did not occur due to the low interaction of the NAR with the other components of the formulation observed in the preformulation and to the low solubility of this polymer in the medium (Berg et al., 2021).

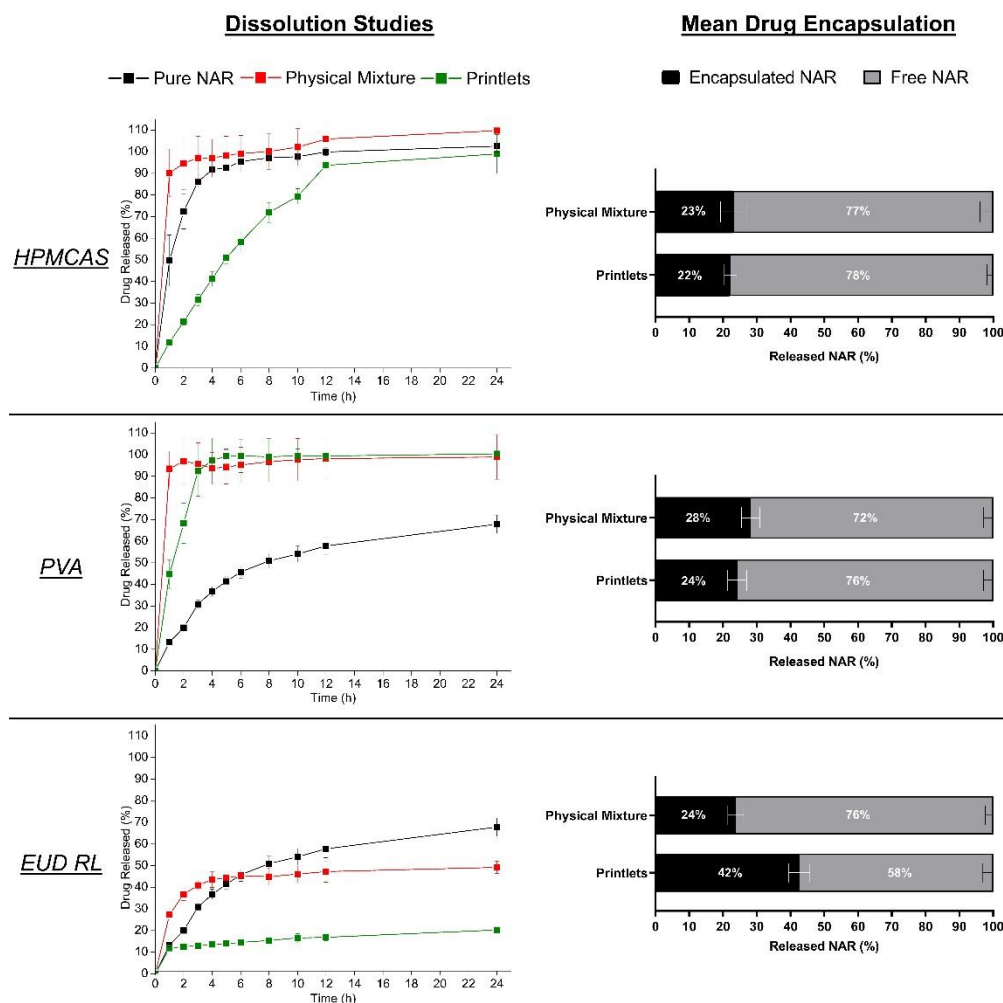


**Figure 4.** Dissolution profile and mean encapsulation of the released Naringenin (NAR) through 24 h experiment for the printlets produced with the polymers hydroxypropylmethylcellulose acetate succinate (HPMCAS), Polyvinyl alcohol (PVA), and Eudragit RL PO<sup>®</sup> (EUD RL) and the control samples, pure NAR, and physical mixture. Since the drug encapsulation values were stable, the mean drug encapsulation considers the values obtained during the experiment.

In the EUD RL system, polymer and plasticizer have strong interactions with each other and are less soluble in the release medium. In fact, the polymer-polymer and polymer-plasticizer interactions, combined with the lower solubility of these components in the medium, favor cohesive forces, inhibiting the dissolution process and keeping NAR enclosed in EUD RL/TEC matrix. As a result, NAR did not present strong interactions with the EUD/RL matrix; however, its release into the environment would depend on a diffusion process. In this context, unlike what was seen for the other polymers, the extrusion and 3D printing processes play an important role, favoring drug encapsulation.

Indeed, while EUD RL physical mixtures lead to 24% of drug encapsulation, the printlets reached 42% (Figure 4).

From these results, it is possible to suggest that the dissolution mechanism that leads to the *in-situ* formation of the nanoparticles observed in this study may depend on the following:

- i) The nature of polymer-plasticizer, polymer-drug, drug-plasticizer interactions;
- ii) The solubility of the components in the release medium;
- iii) The previous treatment of the formulation

A drug-controlled release profile was observed for the printlets produced with HPMCAS and EUD RL, as expected, due to the physical structure of the 3D printed dosage form (Figure 4). The printlets are formed by three layers of external shells and an infill of 50%, hindering a complete diffusion of the medium to the more porous inner part of the printlets. Depending on the solubility grade of the polymer on the medium, this structure can slow down the solubilization process, controlling the drug dissolution profile (Thakkar et al., 2020). In fact, in the printlets produced using PVA, a highly soluble polymer, the control of NAR release was observed only in the first 2h of the experiment, different from the other polymers that could control the drug release throughout 24h.

The polymer disintegration, together with the printing settings, can significantly modify the dissolution profile of printlets, as was observed in this study with NAR (Jamróz et al., 2020; Thakkar et al., 2020). However, the *in-situ* formation of drug-rich particles on a nanometric scale can play an important role in the bioavailability of such dosage forms. It is evidenced that having an amount of drug entrapped in the particles can directly affect the uptake process in the gastrointestinal cells, as the amount of the free drug on the absorption site depends on the drug release process from the particles. Studies show that depending on their characteristics, nanostructured drug particles can provide a more efficient release of the drug or a sustained one, directly affecting the pharmacokinetics (Sironi et al., 2017; Stewart and Grass, 2020).

One of the possible mechanisms of the formation of those nanoparticles during the dissolution process is a burst release of the amorphous drug by diffusion from the polymeric matrix. At the interface of the polymeric system with the medium, there is a region saturated with the drug, creating an environment conducive to drug encapsulation

due to the interaction with the polymer/plasticizer. Hence, particles are spontaneously formed in the dissolution medium and stabilized. This theory would explain the formation process of nanoparticles observed in physical mixture samples (Pandi et al., 2020; Schittny et al., 2020) (Figure 5). This process largely depends on the drug and the polymer characteristics, defining the profile and stability of the released particles (R. Yang et al., 2021).

Another plausible theory is the formation of the particles by an erosive process of the material. In this mechanism, the solvent enters the polymer matrix, swelling and causing the fragility of the solid structure (Figure 5). The solvent action causes erosion on the material surfaces, and nanosized pieces of the material are released on the medium. Such particles retain their structure through the molecular interactions between the components, maintaining part of the drug entrapped inside the particles. Therefore, this process is highly dependent on the intensity of those molecular interactions. (Göpferich, 1996). Regardless of the formation pathway, the investigation of how the changes undergone by the 3D printing process can affect the formation and characteristics of those particles never has been described so far.

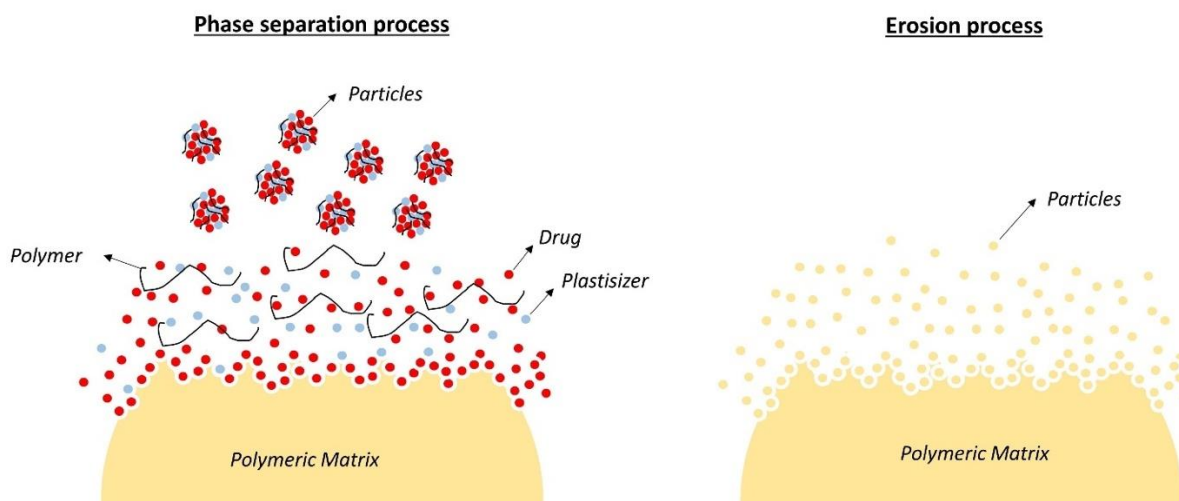


**Figure 5.** Graphical representation of the pathways of particle formation, phase separation, and erosion.

In our study, considering all the polymers, the lower mean percentage of NAR encapsulation was 22%, which is enough to impact any medical treatment. Indeed, such encapsulated drug will be released in a controlled way, directly affecting the drug uptake and its bioavailability (Qian et al., 2021).

Since the particles' formation is related to the amount of drug, plasticizer, and polymer dispersed in the medium (Schittny et al., 2020), the constant amount of drug encapsulated along the dissolution implied that the particles are formed following the same kinetics. Additionally, the stability provided by the specific molecular interactions between the components for each system kept the NAR encapsulated for 24 h, possibly directly affecting the drug uptake throughout the entire gastrointestinal tract transit.

#### **3.3.4. The particles characterization**

To assess the physical characteristics of the spontaneously formed particles, a nanoparticles release test was performed with printlets and selected control samples, including the printlets without NAR and the physical mixtures containing or not NAR. First, it was verified whether the amount of nanoparticle formation was sufficient to perform the analysis, which occurs when the count rate shows values above 100 kcps, ensuring a precise measurement of the particle's characteristics (Ullmann et al., 2019; Zheng et al., 2016).

Based on that, NAR as supplied, physical mixtures without NAR, and printlets without NAR were excluded from the data analyses of all the polymers since the count rate values for these samples did not achieve the minimum required value. In such cases, the formation of nanostructures was found to be negligible. Exceptionally, printlets produced with HPMCAS and EUD RL (Appendix C) could produce appreciable amounts of nanoparticles without NAR. In such cases, the stability of the *in-situ* nanostructures depends on the polymer-plasticizer molecular interaction, as supported by the HSP and FTIR analyses. These findings contrast with PVA samples, in which the plasticizer-drug interaction is highly significant for particle formation, generating particles only for NAR-loaded formulations.

In contrast, the samples capable of generating *in-situ* particles, even in physical mixtures (without heat treatment), reached high values of count rate, i.e., forming a considerable population of particles with a reasonable size uniformity (PdI values of around 0.6).

Considering the HPMCAS samples with NAR, a particle diameter coherence was observed between the hydrodynamic diameter and TEM determinations (Figures 6 and 7). The particles exhibited a spherical shape with well-defined borders (Figure 7) and a particle diameter between 500 and 800 nm. The particle diameter generated from physical

mixtures was relatively stable over time, with around 600 nm (Figure 6), while nanoparticles generated from printlets increased from 586 to 812 nm.

HPMCAS has shown a great tendency to interact with poorly soluble drugs such as NAR, as confirmed by HSP data. In fact, the presence of hydrophobic succinyl groups, especially for the M-grade HPMCAS used in this study, may form a strong drug-polymer interaction. Additionally, the polymer-plasticizer interaction also has a significant role in the formulation. It seems to be sensitive to the thermal treatment provided by the HME and printing processes, explaining the difference in the particle diameter between the physical mixture and printlet samples. The M-grade polymer is also rich in hydrophilic acetyl groups interacting greatly with the aqueous medium, justifying the increase in particle diameter observed on the particles during the experiment by a swollen effect, a consequence of this interaction (Nunes et al., 2022).

Still, regarding the cellulosic polymer systems with NAR, significant differentiation was also found in the zeta potential values among samples. The mean values obtained throughout the experiment for the physical mixture and printlet were -21.7 mV and -10.6 mV, respectively. These findings suggest that the differences in the particles formed between the systems are not only related to the particle diameter but also their structural conformation. Considering that the HPMCAS is a negatively charged polymer, the value difference between samples is probably related to the amount of polymer on the particle structure (R. Yang et al., 2021). As suggested by the irregular particle borders in TEM images, the physical mixture tends to have a high amount of polymeric material on the surface, which could enhance the particles' negative charge.

Regardless of the surface charge difference between the particles, such nanostructures were stable in gastrointestinal simulation conditions (dissolution assay) for 24h. Furthermore, previous studies corroborate the stability of HPMCAS nanoparticles (Wilson et al., 2021) (29).

For the HPMCAS printlets without NAR, a significative population of particles was detected by the DLS analyses only after 24 hours of the dissolution process, evidencing a low-speed kinetics on the particle's formation, only achieving a significative number after a long dissolution process. The particles had a diameter of about 770 nm and a zeta potential of about -11 mV, like previously discussed samples. Those particles are formed probably due to an erosion process of the polymeric material keeping its characteristics due to the drug-plasticizer interactions previously demonstrated by the

preformulation analysis. The occurrence of this phenomenon only on the printlets can be justified by the necessity of a more intense mixture process, provided by the thermal treatment of HME e 3D printing, enhancing the interaction between the plasticizer and the polymer.

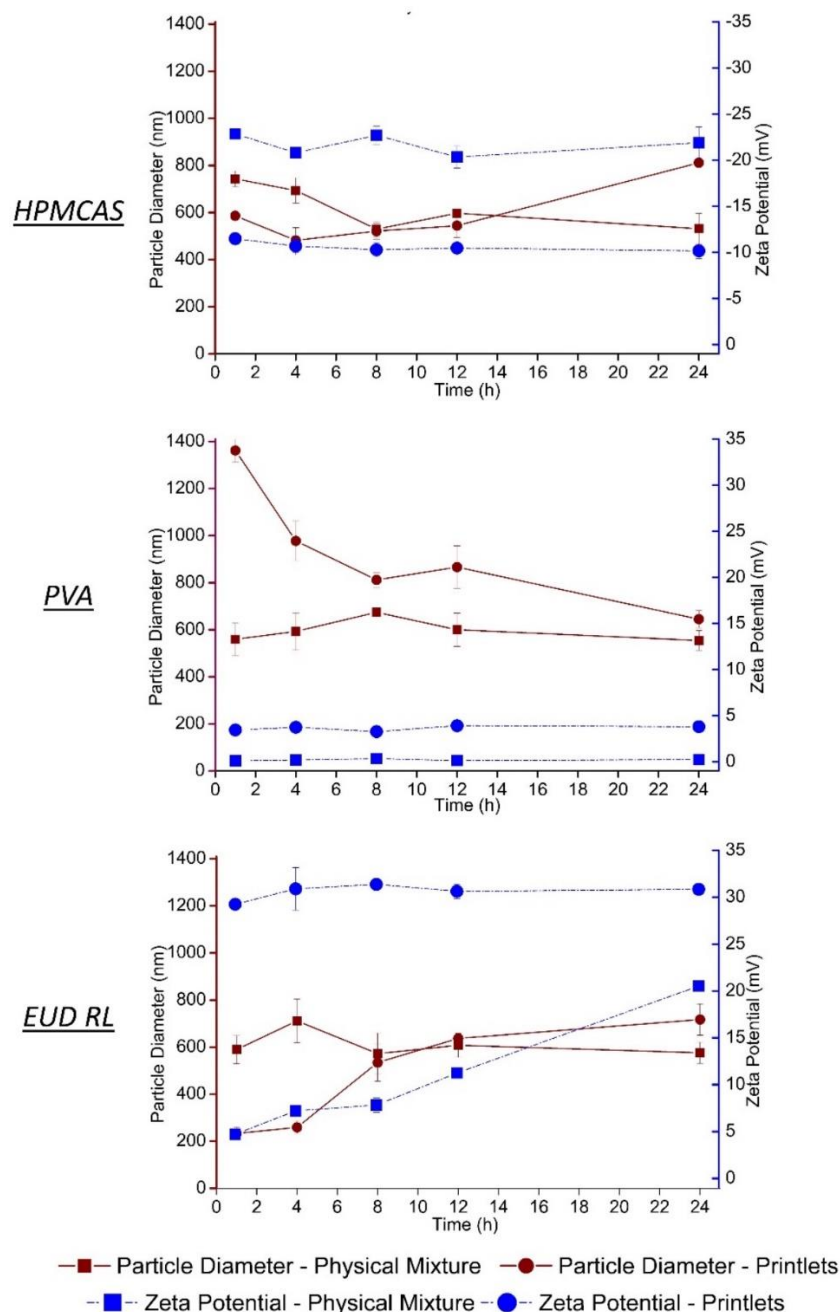


**Figure 6.** Particle diameter and zeta potential of the particles arose spontaneously from the dissolution of the physical mixtures and the printlets over 24h, produced with the polymers hydroxypropylmethylcellulose acetate succinate (HPMCAS), Polyvinyl alcohol (PVA), and Eudragit RL PO<sup>®</sup> (EUD RL).

With PVA, an important difference was observed in the mean particle diameter of physical mixtures and printlets during the first hours of the assay (596.26 and 932.71 nm, respectively). However, a progressive reduction in the particles generated from the printlets occurred practically equaled their diameter to those produced from the physical mixtures (Figure 6), probably due to the progressive solubilization of the polymer and the plasticizer in the medium, corroborating with the dissolution rate results (Figure 4) (Granados et al., 2022). Accordingly, a marked structural difference was noticed in the morphological analyses (Figure 7). Printlets produced particles with more determined border, in contrast with the physical mixtures, which exhibited particles with a less uniform and diffuse surface.

Based on the zeta potential data, PVA's physical mixtures and printlets produced neutral surface particles (Figure 6). During the dissolution assay, both samples exhibited zeta potential values  $>10\text{mV}$ , a common value found for other nanosized PVA samples since on acid medium the acetic groups on the molecule are neutralized, reducing considerably the superficial charge of the particles (Madlova et al., 2009). Yet, as occurred to the other polymers samples, the particles were preserved along 24h, probably due to the stabilization achieved thanks to the interaction between the drug and the plasticizer GLY, as suggested by the HSP and FTIR analyses analyses (Saboo et al., 2021).

Interestingly, the EUD RL samples suggested a different scenario regarding the particle formation. Since this polymer is mostly insoluble in the medium, the solvent is not too efficient in destroying the polymeric matrix. Formulations undergo a swelling process, but most of its structure is maintained throughout the 24 h. However, the formation of the particles has been observed since the dissolution beginning and is most probably resultant of the already described erosion process (Figure 5).



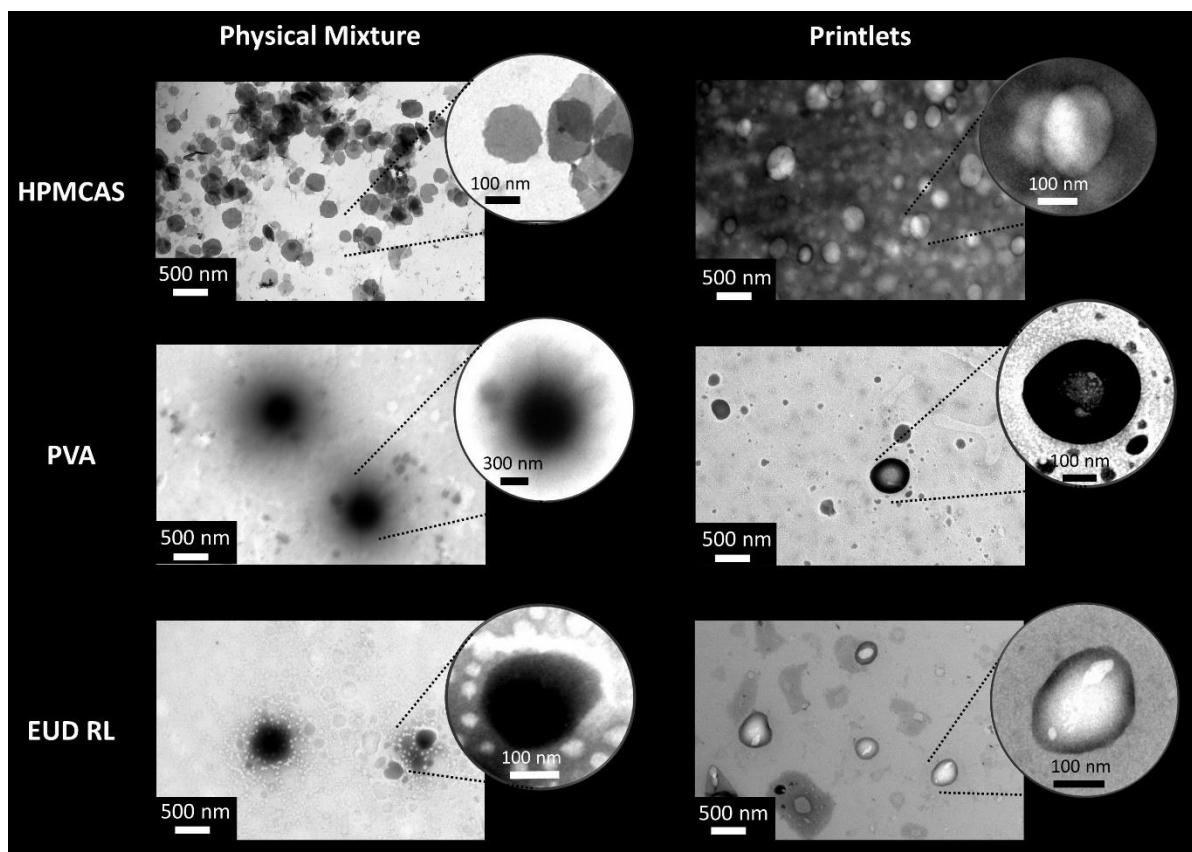


**Figure 7.** TEM images of the particles arose spontaneously from the dissolution of the physical mixtures and the printlets after 24h produced with the polymers hydroxypropylmethylcellulose acetate succinate (HPMCAS), Polyvinyl alcohol (PVA), and Eudragit RL PO<sup>®</sup> (EUD RL).

Based on the particle diameter of the samples made with NAR, a differentiation was founded during the particle's formation using EUD RL (Figure 6). The physical mixture rapidly achieved the diameter sustained during most of the experiment (about 600 nm). In contrast, the printlets started with a lower particle diameter (about 320 nm), enhancing that value until the end of the experiment, achieving a high mean diameter value of 717 nm. The slower process of nanostructuring from the printlets can be attributed to a lower degree of swelling of the polymer after heat treatment by HME and 3D printing, which should favor the polymer-plasticizer interaction, as suggested by the preformulation studies. Furthermore, the dissolution medium has less access to the compact structure of the printed object. Consequently, the erosion process is slower in such a sample affecting the particle formation process that was able to form a more stable particle only after a few hours of dissolution.

The morphological analyses of EUD RL physical mixture showed evidence of a high amount of material on the particle's surface, in the same way as with the PVA particles. In contrast, the printlets had a more delimited particle.

Still, a zeta potential difference was founded for the EUD RL samples with NAR. The physical mixture showed sustained high zeta potential throughout the experiment, with a mean of 30 mV. Such results indicate that those particles had good stability. The printlets, on the other hand, had an increasing behavior of the zeta potential during the experiment, staying most of the time on values <10 mV but achieving, after 24 h, a mean value of about >20 mV. These findings corroborate the hypotheses of slower formation and stabilization of the particles from printlets (Kamble et al., 2022). A combination of the molecular interactions and the low solubility is the most likely explanation for this behavior, i.e., the formation of the particles is delayed, producing a more uniform and stable surface after few hours of dissolution.

Similarly with the HPMCAS samples, the EUD RL printlets produced without NAR were able to form a significant amount of particles only after 24 h of the process (particle diameter of about 471 nm and Zeta potential of 7 mV), reinforcing that the interaction polymer-plasticizer intensified by the HME and 3D printing processing has a definitive role on the particle formation, probably impacting also the samples with NAR.

Based on the data collected in this study, it is possible to conclude that particle formation is highly dependent on the molecular interaction between the formulation components in association with the solubility of all the materials on the dissolution medium, probably defining the possible particle formation pathway and kinetics.

From the point of view of the bioavailability of the drug product, one of the more important characteristics to be concerned with is the amount of encapsulated drug. Our results evidenced that the HME and 3D printing process importantly influence this parameter, especially for insoluble polymers, such as EUD RL. In such cases, the particles are probably produced by a different mechanism, and the preparation process has a higher effect.

Despite the need to deepen and expand studies for other polymeric drug matrices, the results obtained here show sufficient consistency regarding the plausibility of the spontaneous generation of drug-loaded nanoparticles from these polymer-based pharmaceutical products. Thus, a study on the encapsulation of the drug seems essential

for every system that combines polymer, plasticizer, and drug, considering that, in this study, all the samples, physical mixtures, or printlets, had some amount of the total drug entrapped on the particles during 24 hours, affecting directly the amount of the drug free to be absorbed.

### 3.4. CONCLUSIONS

Although the spontaneous formation of nanoparticles from plastic matrices has attracted attention in several segments, there are practically no studies of this occurrence in the pharmaceutical field. In contrast, using polymers in drug delivery systems is becoming increasingly common, especially with the recent explosion of 3D printing drugs. The study performed here evidenced that the interactions between the drug, plasticizer, and polymer, as well as with the medium, are capable of forming mostly stable spontaneous particles during the dissolution of 3D dosage forms made with the polymers HPMCAS, PVA, and EUD RL, containing the poorly soluble NAR as the model drug.

The formed particles had spherical shapes and sizes that varied according to the drug-polymer interaction. The HME and printing processes greatly influenced those parameters forming different size particles and even affecting the superficial charge of the particles. In addition, the formed particles were able to encapsulate a considerable amount of NAR in all the samples, demonstrating that this phenomenon can directly affect the oral bioavailability of the drug and therefore needs to be further studied and monitored.

### 3.5. REFERENCES

- Agafonov, M., Ivanov, S., Terekhova, I., 2021. Improvement of pharmacologically relevant properties of methotrexate by solid dispersion with Pluronic F127. *Mater. Sci. Eng. C* 124, 112059. <https://doi.org/10.1016/j.msec.2021.112059>
- Alshehri, S., Imam, S.S., Hussain, A., Altamimi, M.A., Alruwaili, N.K., Alotaibi, F., Alanazi, A., Shakeel, F., 2020. Potential of solid dispersions to enhance solubility, bioavailability, and therapeutic efficacy of poorly water-soluble drugs: newer formulation techniques, current marketed scenario and patents. *Drug Deliv.* 27, 1625–1643. <https://doi.org/10.1080/10717544.2020.1846638>

- Araújo, M.R.P., Sa-Barreto, L.L., Gratieri, T., Gelfuso, G.M., Cunha-Filho, M., 2019. The digital pharmacies era: How 3D printing technology using fused deposition modeling can become a reality. *Pharmaceutics* 11. <https://doi.org/10.3390/pharmaceutics11030128>
- Bandari, S., Nyavanandi, D., Dumpa, N., Repka, M.A., 2021. Coupling hot melt extrusion and fused deposition modeling: Critical properties for successful performance. *Adv. Drug Deliv. Rev.* 172, 52–63. <https://doi.org/10.1016/j.addr.2021.02.006>
- Berg, S., Krause, J., Björkbom, A., Walter, K., Harun, S., Granfeldt, A., Janzén, D., Nunes, S.F., Antonsson, M., Van Zuydam, N., Skrtic, S., Hugerth, A., Weitschies, W., Davies, N., Abrahamsson, B., Bergström, C.A.S., 2021. In Vitro and In Vivo Evaluation of 3D Printed Capsules with Pressure Triggered Release Mechanism for Oral Peptide Delivery. *J. Pharm. Sci.* 110, 228–238. <https://doi.org/10.1016/j.xphs.2020.10.066>
- Gigault, J., El Hadri, H., Nguyen, B., Grassl, B., Roweczyk, L., Tufenkji, N., Feng, S., Wiesner, M., 2021. Nanoplastics are neither microplastics nor engineered nanoparticles. *Nat. Nanotechnol.* 16, 501–507. <https://doi.org/10.1038/s41565-021-00886-4>
- Göpferich, A., 1996. Mechanisms of polymer degradation and erosion I. *Biomater. Silver Jubil. Compend.* 17, 117–128. <https://doi.org/10.1016/B978-008045154-1.50016-2>
- Granados, P.A., Pinho, L.A.G., Sa-Barreto, L.L., Gratieri, T., Gelfuso, G.M., Cunha-Filho, M., 2022. Application of hot-melt extrusion in the complexation of naringenin with cyclodextrin using hydrophilic polymers. *Adv. Powder Technol.* 33, 103380. <https://doi.org/10.1016/j.apt.2021.11.032>
- Greenhalgh, D.J., Williams, A.C., Timmins, P., York, P., 1999. Solubility parameters as predictors of miscibility in solid dispersions. *J. Pharm. Sci.* 88, 1182–1190. <https://doi.org/10.1021/js9900856>
- Guerin, A.C., Riley, K., Rupnik, K., Kuroda, D.G., 2016. Determining the Energetics of the Hydrogen Bond through FTIR: A Hands-On Physical Chemistry Lab Experiment. *J. Chem. Educ.* 93, 1124–1129. <https://doi.org/10.1021/acs.jchemed.5b01014>
- Hansen, C.M., 2007. Hansen solubility parameters: A user's handbook: Second edition,

- Second Edi. ed, Hansen Solubility Parameters: A Users Handbook, Second Edition. CRC Press. <https://doi.org/10.1201/9781420006834>
- Hickey, J.W., Santos, J.L., Williford, J.-M., Mao, H.-Q., 2015. Control of Polymeric Nanoparticle Size to Improve Therapeutic Delivery. *J. Control. Release* 219, 536–547. <https://doi.org/10.1016/j.jconrel.2015.10.006>.Control
- Jamróz, W., Kurek, M., Szafraniec-Szczęsny, J., Czech, A., Gawlak, K., Knapik-Kowalczyk, J., Leszczyński, B., Wróbel, A., Paluch, M., Jachowicz, R., 2020. Speed it up, slow it down...An issue of bicalutamide release from 3D printed tablets. *Eur. J. Pharm. Sci.* 143. <https://doi.org/10.1016/j.ejps.2019.105169>
- Kamble, S., Agrawal, S., Cherumukkil, S., Sharma, V., Jasra, R.V., Munshi, P., 2022. Revisiting zeta potential, the key feature of interfacial phenomena, with applications and recent advancements. *Chemistry Sel.* 7.
- Karalia, D., Siamidi, A., Karalis, V., Vlachou, M., 2021. 3d-printed oral dosage forms: Mechanical properties, computational approaches and applications. *Pharmaceutics* 13. <https://doi.org/10.3390/pharmaceutics13091401>
- Kim, J.S., Choi, Y.J., Woo, M.R., Cheon, S., Ji, S.H., Im, D., ud Din, F., Kim, J.O., Youn, Y.S., Oh, K.T., Lim, S.J., Jin, S.G., Choi, H.G., 2021. New potential application of hydroxypropyl- $\beta$ -cyclodextrin in solid self-nanoemulsifying drug delivery system and solid dispersion. *Carbohydr. Polym.* 271, 118433. <https://doi.org/10.1016/j.carbpol.2021.118433>
- Klar, F., Urbanetz, N.A., 2016. Solubility parameters of hypromellose acetate succinate and plasticization in dry coating procedures. *Drug Dev. Ind. Pharm.* 42, 1621–1635. <https://doi.org/10.3109/03639045.2016.1160106>
- Kumar, A., Pawar, D., Late, D.J., Kanawade, R., 2022. PVA-coated miniaturized flexible fiber optic sensor for acetone detection: a prospective study for non-invasive diabetes diagnosis. *J. Mater. Sci. Mater. Electron.* 33, 2509–2517. <https://doi.org/10.1007/s10854-021-07458-1>
- Kuźmińska, M., Pereira, B.C., Habashy, R., Peak, M., Isreb, M., Gough, T.D., Isreb, A., Alhnan, M.A., 2021. Solvent-free temperature-facilitated direct extrusion 3D printing for pharmaceuticals. *Int. J. Pharm.* 598, 1–9. <https://doi.org/10.1016/j.ijpharm.2021.120305>

- Lima, A.L., Pires, F.Q., Hilgert, L.A., Sa-Barreto, L.L., Gratieri, T., Gelfuso, G.M., Cunha-Filho, M., 2022. Oscillatory shear rheology as an in-process control tool for 3D printing medicines production by fused deposition modeling. *J. Manuf. Process.* 76, 850–862. <https://doi.org/10.1016/j.jmapro.2022.03.001>
- Madlova, M., Jones, S.A., Zwerschke, I., Ma, Y., Hider, R.C., Forbes, B., 2009. Poly(vinyl alcohol) nanoparticle stability in biological media and uptake in respiratory epithelial cell layers in vitro. *Eur. J. Pharm. Biopharm.* 72, 438–443. <https://doi.org/10.1016/j.ejpb.2009.01.009>
- Mitchell, M.J., Billingsley, M.M., Haley, R.M., Wechsler, M.E., Peppas, N.A., Langer, R., 2021. Engineering precision nanoparticles for drug delivery. *Nat. Rev. Drug Discov.* 20, 101–124. <https://doi.org/10.1038/s41573-020-0090-8>
- Nunes, P.D., Pinto, J.F., Henriques, J., Paiva, A.M., 2022. Insights into the Release Mechanisms of ITZ:HPMCAS Amorphous Solid Dispersions: The Role of Drug-Rich Colloids. *Mol. Pharm.* 19, 51–66. <https://doi.org/10.1021/acs.molpharmaceut.1c00578>
- Pandi, P., Bulusu, R., Kommineni, N., Khan, W., Singh, M., 2020. Amorphous solid dispersions: An update for preparation, characterization, mechanism on bioavailability, stability, regulatory considerations and marketed products. *Int. J. Pharm.* 586, 119560. <https://doi.org/10.1016/j.ijpharm.2020.119560>
- Pereira, G.G., Figueiredo, S., Fernandes, A.I., Pinto, J.F., 2020. Polymer selection for hot-melt extrusion coupled to fused deposition modelling in pharmaceuticals. *Pharmaceutics* 12, 1–63. <https://doi.org/10.3390/pharmaceutics12090795>
- Pietrzak, K., Isreb, A., Alhnan, M.A., 2015. A flexible-dose dispenser for immediate and extended release 3D printed tablets. *Eur. J. Pharm. Biopharm.* 96, 380–387. <https://doi.org/10.1016/j.ejpb.2015.07.027>
- Pires, F.Q., Alves-Silva, I., Pinho, L.A.G., Chaker, J.A., Sa-Barreto, L.L., Gelfuso, G.M., Gratieri, T., Cunha-Filho, M., 2020. Predictive models of FDM 3D printing using experimental design based on pharmaceutical requirements for tablet production. *Int. J. Pharm.* 588, 119728. <https://doi.org/10.1016/j.ijpharm.2020.119728>
- Ponsar, H., Wiedey, R., Quodbach, J., 2020. Hot-melt extrusion process fluctuations and their impact on critical quality attributes of filaments and 3d-printed dosage forms.

- Pharmaceutics 12, 1–15. <https://doi.org/10.3390/pharmaceutics12060511>
- Qian, K., Stella, L., Jones, D.S., Andrews, G.P., Du, H., Tian, Y., 2021. Drug-rich phases induced by amorphous solid dispersion: Arbitrary or intentional goal in oral drug delivery? *Pharmaceutics* 13, 1–27. <https://doi.org/10.3390/pharmaceutics13060889>
- Quinten, T., De Beer, T., Remon, J.P., Vervaet, C., 2021. Overview of injection molding as a manufacturing technique for pharmaceutical applications. *Inject. Molding Process. Des. Appl.* 1–42.
- Saboo, S., Bapat, P., Moseson, D.E., Kestur, U.S., Taylor, L.S., 2021. Exploring the role of surfactants in enhancing drug release from amorphous solid dispersions at higher drug loadings. *Pharmaceutics* 13, 1–22. <https://doi.org/10.3390/pharmaceutics13050735>
- Schittny, A., Huwyler, J., Puchkov, M., 2020. Mechanisms of increased bioavailability through amorphous solid dispersions: a review. *Drug Deliv.* 27, 110–127. <https://doi.org/10.1080/10717544.2019.1704940>
- Sironi, D., Rosenberg, J., Bauer-Brandl, A., Brandl, M., 2017. Dynamic dissolution-/permeation-testing of nano- and microparticle formulations of fenofibrate. *Eur. J. Pharm. Sci.* 96, 20–27. <https://doi.org/10.1016/j.ejps.2016.09.001>
- Stewart, A.M., Grass, M.E., 2020. Practical Approach to Modeling the Impact of Amorphous Drug Nanoparticles on the Oral Absorption of Poorly Soluble Drugs. *Mol. Pharm.* 17, 180–189. <https://doi.org/10.1021/acs.molpharmaceut.9b00889>
- Thakkar, R., Pillai, A.R., Zhang, J., Zhang, Y., Kulkarni, V., Maniruzzaman, M., 2020. Novel on-demand 3-dimensional (3-d) printed tablets using fill density as an effective release-controlling tool. *Polymers (Basel)*. 12, 1–21. <https://doi.org/10.3390/POLYM12091872>
- Tran, P.H.L., Lee, B.J., Tran, T.T.D., 2021. Recent studies on the processes and formulation impacts in the development of solid dispersions by hot-melt extrusion. *Eur. J. Pharm. Biopharm.* 164, 13–19. <https://doi.org/10.1016/j.ejpb.2021.04.009>
- Ullmann, C., Babick, F., Stintz, M., 2019. Microfiltration of submicron-sized and nano-sized suspensions for particle size determination by dynamic light scattering. *Nanomaterials* 9. <https://doi.org/10.3390/nano9060829>
- van Krevelen, D.W., te Nijenhuis, K., 2009. Properties of polymers: Their correlation

with chemical structure; Their numerical estimation and prediction from additive group contributions., 4th Editio. ed. Elsevier Science.

Wilson, V.R., Mugheirbi, N.A., Mosquera-Giraldo, L.I., Deac, A., Moseson, D.E., Smith, D.T., Novo, D.C., Borca, C.H., Slipchenko, L. V., Edgar, K.J., Taylor, L.S., 2021. Interaction of Polymers with Enzalutamide Nanodroplets - Impact on Droplet Properties and Induction Times. *Mol. Pharm.* 18, 836–849. <https://doi.org/10.1021/acs.molpharmaceut.0c00833>

Yang, R., Mann, A.K.P., Van Duong, T., Ormes, J.D., Okoh, G.A., Hermans, A., Taylor, L.S., 2021. Drug Release and Nanodroplet Formation from Amorphous Solid Dispersions: Insight into the Roles of Drug Physicochemical Properties and Polymer Selection. *Mol. Pharm.* 18, 2066–2081. <https://doi.org/10.1021/acs.molpharmaceut.1c00055>

Yang, Y., Wang, H., Xu, X., Yang, G., 2021. Strategies and mechanisms to improve the printability of pharmaceutical polymers Eudragit® EPO and Soluplus®. *Int. J. Pharm.* 599. <https://doi.org/10.1016/j.ijpharm.2021.120410>

Zheng, T., Bott, S., Huo, Q., 2016. Techniques for Accurate Sizing of Gold Nanoparticles Using Dynamic Light Scattering with Particular Application to Chemical and Biological Sensing Based on Aggregate Formation. *ACS Appl. Mater. Interfaces* 8, 21585–21594. <https://doi.org/10.1021/acsami.6b06903>



## **4. CHAPTER IV: PRELIMINARY STUDIES ON THE COMBINATION OF IRON OXIDE NANOPARTICLES AND FDM 3D PRINTING ON THE ORAL TREATMENT OF IRON DEFICIENCY.**

### **4.1. INTRODUCTION**

The iron deficiency is one of the main sources of concern for world health organizations, affecting mainly children, women, and people in nutritional risk. It is often an asymptomatic condition, but can evolve to anemia, resulting on symptoms like fatigue, reduced concentration, dizziness, headache and even haemodynamic instability in more severe cases (Pasricha et al., 2021).

The treatment for iron deficiency is conducted mainly by oral and intravenous routes, been the oral route the most common for the less severe cases. For this route it is administered to the patient a dosage of an iron salt, most commonly ferrous sulphate, ferrous gluconate and ferrous fumarate, in a form of a tablet or a liquid suspension, and it is proved to be efficient strategy for the replenishment of the iron levels (KUMAR *et al.*, 2022). However, many problems related to the high occurrence of adverse effects and the low disponibility of specific dosages on the market have been an obstacle for the adhesion of the patient to the treatment.

The most common side effect provoked by the oral treatment of iron deficiency are the gastrointestinal events. Those events are resultant mainly from inflammatory processes on the mucosal surface of the gastrointestinal tract, provoked by residual iron products not absorbed by the cells, causing symptoms like pain, constipation, nausea and diarrhea (Bayraktar and Bayraktar, 2010). The most often used strategy to reduce those effects are the exchange for an intravenous route, that can be effective on this objective, however bring problems like the low autonomy on the treatment and the cost of production and treatment (Lo et al., 2022). Another strategy is the use of nanotechnology, specifically iron oxide nanoparticles (IONP) that have been proved to be efficient on the intravenous route and has been studied also for an oral use, with many possible advantages (Alphandéry, 2020).

Recent studies proved that small sized IONP are capable to be efficiently absorbed by the enteric cells by an endocytosis mechanism, and achieving the systemic circulation passing through the hepatic portal vein. Once on the systemic circulation the particles are

distributed to the whole body, been founded mainly on the blood and accumulated in organs like the spleen. During this process the particles have a constant loss in mass, releasing iron inside the body, replenishing the levels of the metal. Additionally, no signs of cellular damages were founded in the body sites where the particles were located, including the gastrointestinal tract, reducing considerably the possibility for the classic side effects of this type of treatment (Garcia-Fernandez et al., 2020).

The other problem associated with the current oral treatment of iron deficiency is the low availability of specific dosages necessary for a more secure and controlled treatment. It is reported that the occurrence of gastrointestinal adverse effects is heavily dose-dependent and the available doses on the market are too high for many patients, in special patients in exceptional conditions, like pregnant woman and individuals with gastrointestinal conditions (Liu and Kaffes, 2012). For those patients, again, the protocol is to recommend the use of the intravenous route, however new forms of personalization of oral dosage forms, like the 3D printing of pharmaceutical dosage forms can be a strategy to manage this problem.

The 3D printing of pharmaceutical dosage forms consists of a layer-by-layer construction of a completely personalized dosage form, using as raw material the drug or supplement incorporated in a polymeric matrix, resulting in dosage forms with different forms, sizes, dosages and release profiles, since the internal structure of the dosage form can directly affect the release profile of the active material (Thakkar et al., 2020).

For example, the fused deposit modeling 3D printing technique (FDM) uses as raw material a filament prepared by a hot melt extrusion process (HME) with the active material incorporated in a diversity of polymeric materials, including pharmaceutical grade polymers extensively tested on HME formulations (Pandey et al., 2020), with the capability of producing pharmaceutical dosage forms very similar to the classic ones, like the printlets that are tablets analogs.

On the oral treatment of iron deficiency, the use of this technology can be a possibility for the expansion of the possibilities of treatment by a complete personalization, avoiding all the problems caused by lower or higher dosages.

Thinking even forward, the combination of IONP and 3D printing can be an important step to add a new dimension for the iron deficiency treatment, with the possibility of manufacturing of an efficient and secure product, that can be completely

adaptable to the patient. To the best of our knowledge, no studies attempted to combine both techniques for this purpose and are no available information on how the release from a 3D printing dosage form can affect the availability of IONP for a possible oral absorption.

Therefore, this work aims to evaluate the combination of both technologies, focusing on the interaction between all the materials and how it can affect the availability of the iron-based materials for a gastrointestinal absorption.

## **4.2. MATERIALS AND METHODS**

### **4.2.1. Materials**

Iron(III) Chloride ( $\text{FeCl}_3 \cdot 6\text{H}_2\text{O}$ , purity  $\geq 97\%$ , lot STBJ1734) and iron(II) sulfate heptahydrate ( $\text{FeSO}_4 \cdot 7\text{H}_2\text{O}$ , purity  $\geq 99\%$ , lot MKCJ9113) was obtained from Sigma-Aldrich (St. Louis, MO, USA). The polymers Parateck<sup>®</sup> MXP (Polyvinyl alcohol, PVA, lot F1952064) were donated by Merck (Darmstadt, Germany). The plasticizers glycerin (GLY, lot 58591) was purchased from Dinâmica<sup>®</sup> (São Paulo, Brazil). All other chemicals and solvents were of analytical grade.

### **4.2.2. Iron oxide nanoparticles production**

The IONP were prepared by the co-precipitation method (Ushakov et al., 2020). On a 2% HCl solution it was added the  $\text{FeSO}_4 \cdot 7\text{H}_2\text{O}$  ( $\text{Fe}^{2+}$ ) and the  $\text{FeCl}_3 \cdot 6\text{H}_2\text{O}$  ( $\text{Fe}^{3+}$ ) on a 1:2 molar proportion to a final concentration of  $1 \text{ mol L}^{-1}$ . After the complete dissolution of the metallic compounds, a solution of  $\text{NH}_4\text{OH}$  was added to the mixture and an intense magnetic stirring was maintained for one hour.

After this, the nanoparticles, suspended on the solution, were separated by magnetic attraction. A washing procedure using ultrapure water was made five times, to eliminate all the  $\text{NH}_4\text{OH}$  from the solution. The remain particles were dried on a vacuum stove.

### **4.2.3 Filament production by hot-melt extrusion**

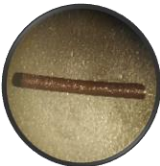
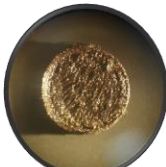
The filament formulations were composed of the combination of the IONP (15%, m/m), the plasticizer GLY (20%, m/m) and the polymer PVA and was produced by HME.

The mixtures were initially prepared using mortar and pestle and then extruded in a co-rotating conical twin-screw extruder HME with a die diameter of 1.8 mm (HAAKE MiniCTW, ThermoScientific, Waltham, MA, USA), without recirculation, coupled to a filament tractor system model FTR1 endowed with an automatic diameter gauge (Filmaq3D, Curitiba, Brazil). The temperature used on the process was 180 °C, with a screw rotation of 60 rpm.

Right after the production the filament diameter was measured at every 10 cm interval using a digital caliper (Mitutoyo Sul Americana, São Paula, Brazil), then the mean diameter was calculated by the arithmetic mean of the measures. The visual characteristics were evaluated by optical microscopy using a stereoscope coupled to a video camera (Laborana/SZ – SZT, São Paulo, Brazil) (Table 1).

The filament was stored in a desiccator sealed on a vacuum bag before further characterizations.

**Table 1.** Filaments and printlets made with the iron oxide nanoparticles (IONP) manufacturing specifications and characterization data. Textusion – Extrusion temperature; Vrotation = Velocity of the screw rotation; Tprinting – Printing temperature; Tprinting platform – Printing platform temperature.

<b>Filament Characterization</b>					
<i>Formulation</i>	<i>Textusion (°C)</i>	<i>Vrotation (RPM)</i>	<i>Mean Diameter (mm)</i>	<i>Fracture Force (N)</i>	<i>Aspect</i>
<i>IONP - Filament</i>	180	60	1,52±0,08	24,34±1.4	
<b>Printlet Characterization</b>					
<i>Formulation</i>	<i>Tprinting (°C)</i>	<i>Tprinting platform (°C)</i>	<i>Volume (cm3)</i>	<i>Weight (g)</i>	<i>Aspect</i>
<i>IONP - Printlets</i>	210	80	0,631±0,003	0,595±0,04	

#### 4.2.4 Printlets production by FDM 3D printing

Cylinder shape printlets with a mean volume of  $0.569 \text{ cm}^3$  were designed using free version of the software Tinkercad<sup>®</sup> (Autodesk<sup>®</sup> Inc, San Rafael, CA, USA) and sliced using Slic3r<sup>®</sup> (Rome, Italy) software. The printlets were printed using the filaments prepared previously at a Zmorph FAB printer (Wrocław, Poland) with a brass nozzle with a diameter of 0.4 mm. The printing temperature was 210 °C, the printing bed was maintained at 80 °C and the printlets were printed one at a time. The layer height was set at 0.2 mm, the infill pattern was rectilinear with a density of 50%. Three external layer shells were printed on all sides of the printlets and the printing speed was 15 mm/s for printing moves and  $50 \text{ mm}\cdot\text{s}^{-1}$  for travel speed.

Right after the printing process the printlets volumes were calculated using the measurements of the diameter and thickness of each printlet using a digital caliper (Mitutoyo Sul Americana, São Paulo, Brazil). In total were obtained the volume of 5 units of each printlet type to calculate the mean volume for each formulation. The visual characteristics were made by optical microscopy using a stereoscope coupled to a video camera (Laborana/SZ – SZT, São Paulo, Brazil) (Table 1).

The weight of each printlet was obtained using an analytical balance (Shimadzu, Tokyo, Japan). The individual weight and the mean weight, obtained by the measure made in 10 tablets, were used during the study (Table 1).

The printlets were stored in a desiccator sealed on a vacuum bag before further characterizations.

#### 4.2.5. Characterizations

##### 4.2.5.1. Particle diameter, pdI, mean count rate and zeta potential

IONP and released particles were analysed on particle diameter, pdI, mean count rate and zeta potential in a Zetasizer Nano ZS (Malvern, UK). Hydrodynamic diameter determinations were performed using the dynamic light scattering (DLS) method to obtain the particle diameter, polydispersity index (pdI), and mean count rate. For these analyses the samples were diluted in adequate proportion according to necessity.

For the zeta potential determination, the electrophoretic mobility method was used. The analyses were performed in three different pH, 2.0 (HCl solution), 7.0 (phosphate buffer solution) and 10.0 (Sodium tetraborate buffer solution), with the samples diluted on as adequate proportion.

#### 4.2.5.2. Thermal Analysis

Thermogravimetry (TGA) analyses were carried out in platinum pans using a DTG-60 (Shimadzu, Tokyo, Japan), which operated at a heating rate of  $10\text{ }^{\circ}\text{C min}^{-1}$  from 30 to  $800\text{ }^{\circ}\text{C}$ . Analyses were performed using crushed IONP, filaments, printlets and the formulation isolated materials samples in the range of 3-6 mg. All assays were performed under a nitrogen atmosphere (flow rate of  $50\text{ mL min}^{-1}$ ).

#### 4.2.5.3. Fourier transform infrared spectroscopy (FTIR)

FTIR-ATR analysis was performed with crushed IONP, filaments, printlets and the formulation isolated materials samples on the equipment Bruker, model vertex 70 (Billerica, MA, United States), using the equipment ATR accessory, from  $4500$  to  $375\text{ cm}^{-1}$  in a resolution of  $2.0\text{ cm}^{-1}$  and three scans.

#### 4.2.5.4. Mechanical resistance assay

The filament was tested by measuring their mechanical resistance with the fracture force data ( $n = 5$ ) (Lima et al., 2022). The analysis was performed in a universal testing machine (Shimadzu EZ test, Tokyo, Japan) equipped with a 5 kN load cell using wedge-type grips that move horizontally to tighten the grip on the filament (before analyzes) and vertically to perform the elongation test. The cell moved at a constant crosshead speed of  $10\text{ mm.min}^{-1}$ . The filament size was 90 mm, the gap between the cells was set at 60 mm, and the initial force was 1 N.

### 4.2.6. Released particles characterization

The characterization of the particles generated from the printlet's dissolution was performed in a release study under a concentrated conditions allowing the measure of particle diameter, polydispersity index (pdI), zeta potential, and morphological characterization. In this experiment, IONP and the produced printlets were inserted in a Becker containing 50 mL of HCl 0.1M. The systems were maintained in a water bath at  $37 \pm 3\text{ }^{\circ}\text{C}$  in constant magnetic stirring. Aliquots of 3 mL were withdrawn and immediately replaced by fresh medium at 2, 4 and 6 h, filtered on a paper filter using

vacuum filtration system composed of a büchner funnel, a borosilicate filtering flask, and a vacuum pump, and analyzed using a Zetasizer Nano ZS (Malvern, UK) using the already described method (Section 2.5.1). Statistics were evaluated using GraphPad Prism 9 software (San Diego, CA, USA) by two-way ANOVA, followed by Šídák post-test. The significance level ( $p$ ) was fixed at 0.05. Data normality was previously demonstrated using the Shapiro-Wilk normality test.

Additionally, all the aliquots collected from the printlet samples were used for morphological analysis. The samples were analyzed by transmission electron microscopy (TEM) using a JEM-1011 (JEOL, Tokyo, Japan). Before the analysis, diluted samples were deposited on Formvar-coated copper grids and received 3  $\mu\text{L}$  of uranyl acetate solution at 3% (w/v). After 3 min, the excess of material was removed with filter paper, and the grids were air-dried. Then, the samples were taken to the equipment and analyzed at a magnitude of up 20,000 times.

#### **4.2.7. Dissolution studies**

Dissolution profiles of IONP and the printlets were determined in a dissolutor Ethik model 299 (Nova Ética, São Paulo, Brazil) using 900 mL of medium. For all the samples it was used as dissolution medium HCl 0.1 mol L<sup>-1</sup>. Temperature was maintained at 37 °C and apparatus 2 (paddle) was used, operating at 100 rpm. Samples containing approximately 100 mg of the drug were added to the dissolution vessels. Aliquots of 5 mL were withdrawn and immediately replaced by fresh dissolution medium at 1, 2, 3, 4, 5 and 6 h. The total amount of iron was determined by atomic absorption spectroscopy (AAS) according to the method described in section 2.8.

Experiments were performed in triplicate for each sample and dissolution profiles were evaluated using their correspondent dissolution efficiency at 6 h (DE6) (Granados et al., 2022). Statistics of the dissolution efficiency were evaluated using GraphPad Prism 9 software (San Diego, CA, USA) using unpaired t test. Data normality was previously demonstrated using the Shapiro-Wilk normality test.

#### 4.2.8. Iron determination

The iron concentration was obtained on the iron content analysis of the IONP, the printlets and during the dissolution assay. The analysis was made by atomic absorption spectrometry (AAS) by flame, using a Thermo Fisher spectrometer, model iCE 3000 (Waltham, MA, United States). The samples were previously digested using a microwave reactor equipment of Anton Paar, model multiwave Pro (Graz, Austria) dispersed on a solution formed of equal parts water, hydrogen peroxide and nitric acid, using a microwave potency of 800 W to achieve a temperature of 100 °C, maintaining it for ten minutes, followed by a cooling process until the 55 °C. The digested samples were properly diluted and analyzed using the AAS equipment.

The method was validated following the International Conference on Harmonization parameters and proved to be linear in the range of 1 to 20  $\mu\text{g mL}^{-1}$  with a correlation coefficient ( $r$ ) > 0.999.

### 4.3. RESULTS AND DISCUSSION

#### 4.3.1. Characterization studies

IONP were synthesized by the co-precipitation method leading to the formation of stable magnetite with high magnetic properties. This method was selected since it is a relatively easy and efficient process, with the potential to produce particles in large scale (Besenhard et al., 2020). Besides that, the resulting particles can normally be directly dispersed in aqueous solvents without further treatments, important characteristics for this study, since the aim is a dispersion of the particles in biological gastrointestinal fluids.

The produced particles had an iron content of about  $67.15 \pm 0.58$  % and it was observed an agglomeration tendency. Initial readings by DLS shown a diameter above 200 nm, however the visual analyses made by TEM images (Figure 1) shown that this diameter is referent to agglomerations of particles, been possible to identify the real diameter of the individual particles on the images, that was between 10 and 12 nm.



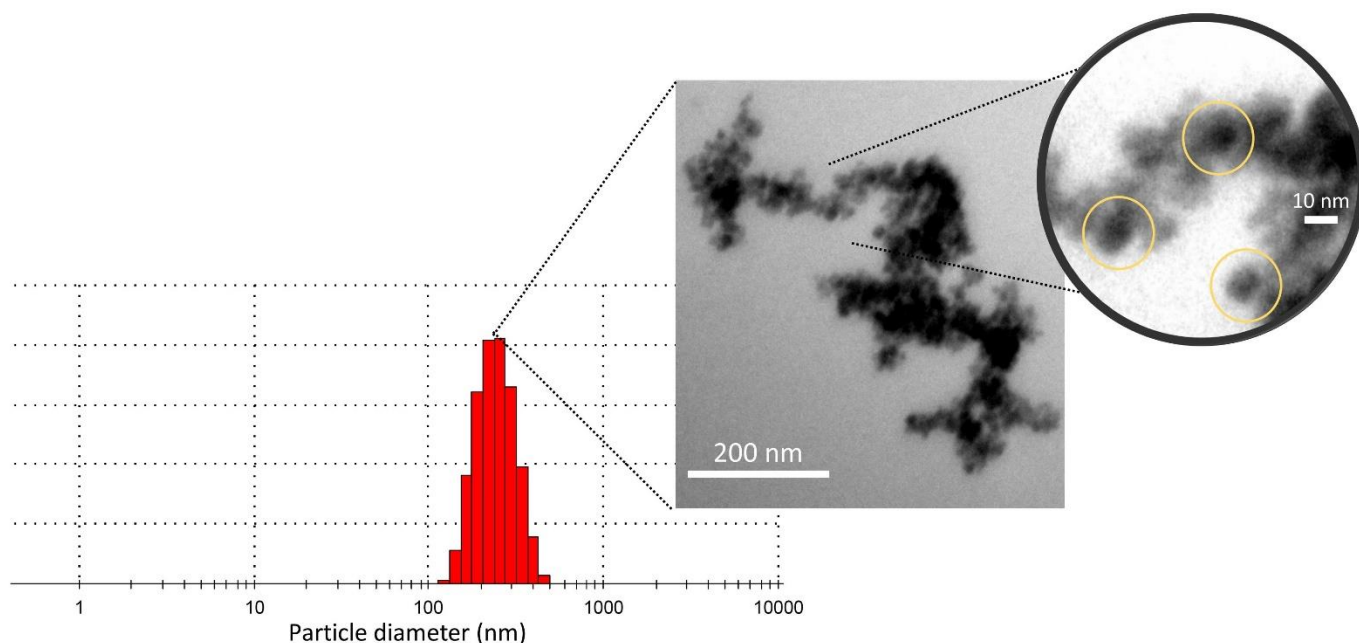


**Figure 1.** Diameter analysis by dynamic light scattering and transmission electronic microscopy analysis of the iron oxide nanoparticles.

The filament production was conducted by HME using the IONP as the active material and PVA and GLY as the polymer and plasticizer, respectively, with the constant feeding of the materials blend previously mixed in a mortar and the assistance of a traction mechanism, allowing the control over the filament diameter, factor that can directly impact the printability of the filament and uniformity of the printed dosage forms (BANDARI *et al.*, 2021).

The obtained filament had a brown coloration, similar to the IONP powder, homogeneous aspect and a mean diameter of  $1.52 \pm 0.08$  mm (Table 1). It is possible to see that, despite the good uniformity proved by the standard deviation of only 0.08 mm, the filament overall diameter was lower than the ideal range recommended for the 3D printing process, between 1.80 and 1.60 mm (Ponsar *et al.*, 2020). This is likely due to inconsistencies on the feeding and traction processes, that can lead to an fluctuation on the diameter (Gillispie *et al.*, 2020). However, even with this inconsistency the filament was able to be fed in the printer with no noticeable interference on the process.

The printability of the filament was also attested by the measure of its mechanical property. The analysis resulted on the curve shown on figure 2, and it is possible to see that the filament rapidly passes through the elastic deformation phase, marked by the rapid grown on the curve, and after the 20 N mark occurs a stability on the curve characterizing a plastic deformation phase, that goes until the complete fracture of the

filament on about  $24.3 \pm 1.45$  N. The long plastic deformation phase and the fracture force higher than 5 N indicate that the filament are ductile and has high toughness, been ideal for the application on the FDM 3D printing process (Y. Yang et al., 2021).

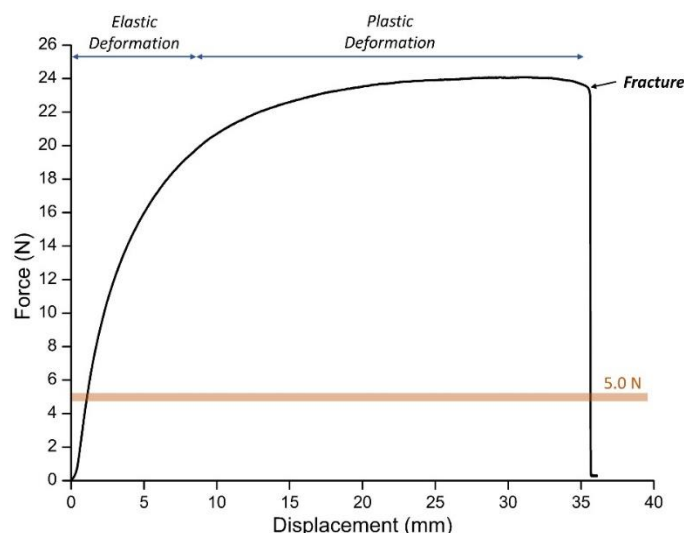


**Figure 2.** Mechanical properties of the filament. Highlighted the elastic and plastic deformation phases, the fracture and the minimal fracture force for a quality filament for fused deposit modeling 3D printing , at 5.0 N.

The filament obtained was used for the production of printlets. The printlets obtained by the FDM 3D printing process shown a slight uniformity issue, characterized by inconsistencies of infill, mainly on upper layers of the printlets (Table 1). However, this fact seems not to translate significantly to the uniformity of the printlets based on the weight and overall volume. The obtained printlets had a mean weight of  $0.595 \pm 0.047$  g, with less than 10% variation between the samples and the mean value. The mean volume was  $0.631 \pm 0.003$  cm<sup>3</sup>, showing an even lesser variation, proving the uniformity of the printlets, that can be translated to a uniformity on the iron content.

A thermal and chemical characterization of the formulation and its components, made by TGA and FTIR, respectively, was also carried, tracking any type of interaction between the components. The TGA analysis (Figure 3) was made comparing the formulations of filament and printlet forms to a theoretical thermogram made by the weighted average of the isolated materials, IONP, PVA and GLY.

On the theoretical analysis (Figure 3) a weight loss of 85% is observed on the first 400 °C, been exactly the combined proportion of PVA and GLY of the formulation, with

no other weight loss during the analysis. The remaining 15% are also the exact proportion of the IONP on the formulation, however this material do not loses any weight on the selected temperature range.

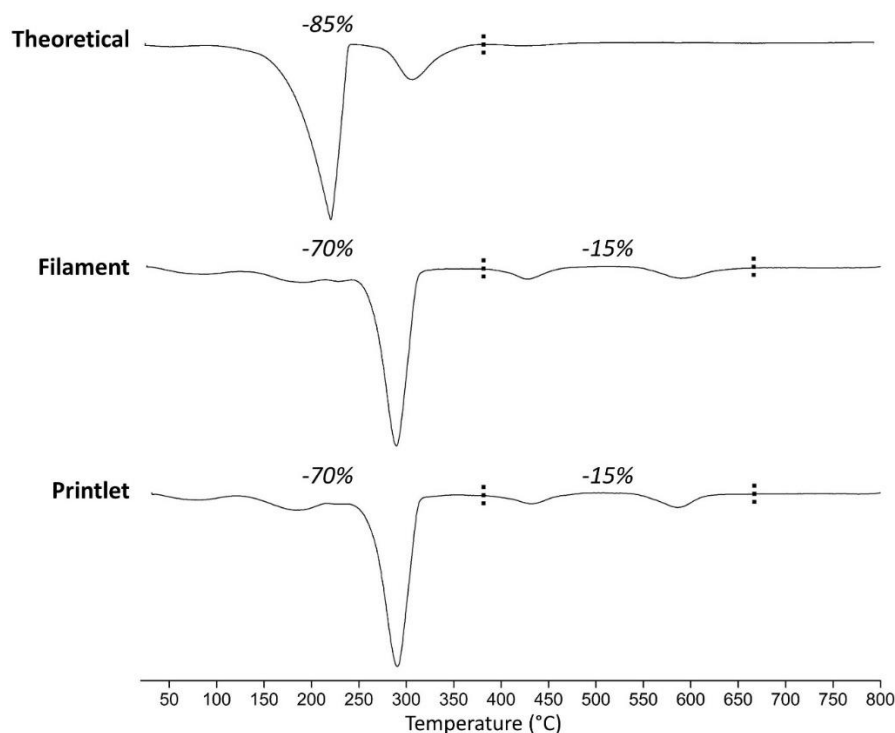


**Figure 3.** Theoretical and experimental TGA analyses of printlets formulations on the filament and printlet made with the iron oxide nanoparticles. The theoretical thermogram was obtained considering the contribution of each formulation compound on the mass loss events.

On the formulations the thermal behavior was the same on the filament and printlet forms. Like on the theoretical thermogram, there is an important weight loss on the first 400 °C, however on the formulations this loss is of about 70%, followed with a weight loss of the remaining 15% on higher temperatures, resulting on the 85%, that is exactly correspondent to the total amount of PVA and GLY.

This behavior is a clear indication of interactions, probably between the PVA and the IONP, since the GLY is normally completely lost on temperatures below 250 °C. A polymeric coating process are the most probable cause of this shift, with the 15% of material lost on temperatures higher than 400 °C been most probably the remained PVA adsorbed on the particles surfaces by interaction like hydrogen bonds (Silva S and Moraes D, 2016).

On the FTIR analysis (Figure 4) the IONP was identified by the presence of peaks related to two structures, the O-H group of the surface of the particles, marked by the bending on about  $3350\text{ cm}^{-1}$  and the Fe-O interaction stretching on about  $545\text{ cm}^{-1}$ , confirming that the particle is formed by iron oxide. This last group was also spotted on the filament and printlet analysis without any significant changes on the position, proving the stability of the particles after the HME and 3D printing processes.

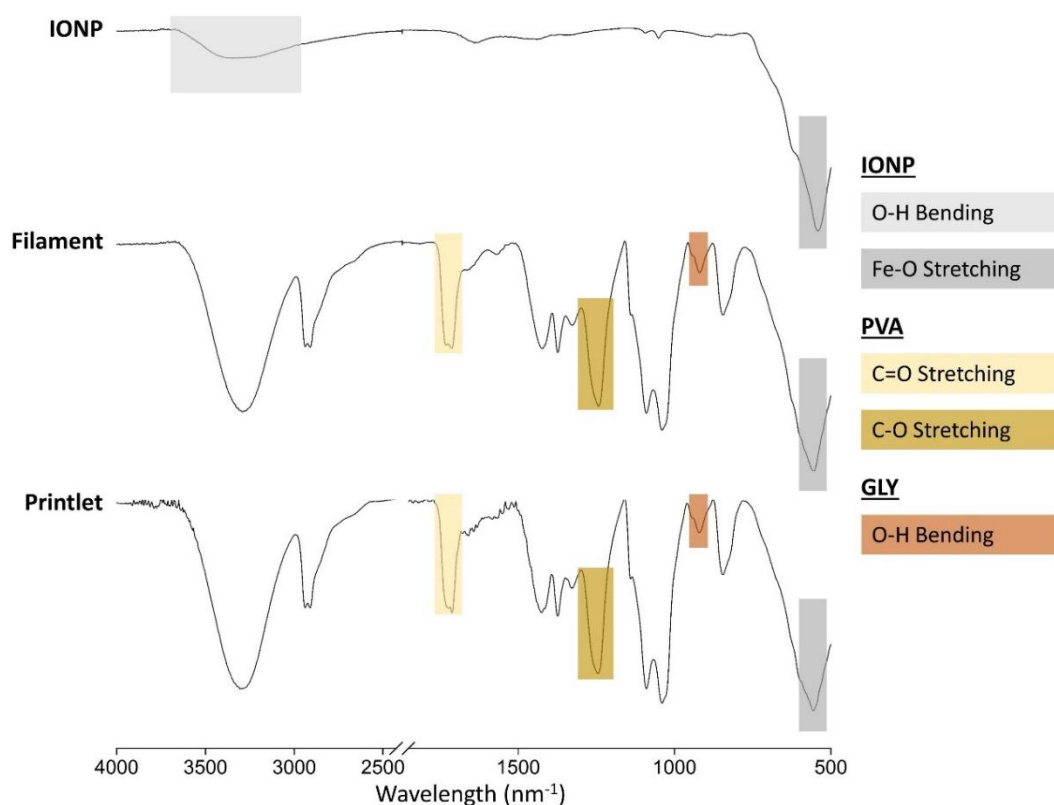


**Figure 4.** FTIR of the iron oxide nanoparticles (IONP), filament and printing. Highlighted the most identifiable peaks of the IONP, the polymer Polyvinyl alcohol (PVA) and the plasticizer glycerin (GLY) on all the spectrums.

On the filament and printlet analysis the presence of the polymer PVA and the plasticizer GLY was also well marked on the FTIR analyses. The ester groups C=O and C-O of PVA stretching on about  $1720$  and  $1250\text{ cm}^{-1}$ , respectively and the O-H bending of the hydroxyl groups of GLY on  $920\text{ cm}^{-1}$ , demonstrated the presence of the materials and the stability of both during the printlets production, since the peaks didn't suffered any significative displacement. The interaction between the PVA and IONP detected on the TGA analysis was not detected on the FTIR probably because the high proportion of the non-linked PVA on the formulation.

### 4.3.2. Characterization of the released particles

The physical characteristic of the particles released from the printlets during the dissolution process was assessed during a small-scale dissolution, in order to determine any changes on the particles that can affect its overall performance. The process was made with the printlet samples, and a control sample formed by the IONP powder, analyzing the particle diameter, pDI, count rate and zeta potential.

In particular, the zeta potential analysis was conducted in three different conditions of pH. It is a well-known fact that pH is the factor that affects the most the zeta potential, on account of the ionic exchanges that happens when the pH is changed. With that in mind, shifts on the pH can provide information like the environments where the particles are most and less stable and how formulation components, like the 3D polymer and plasticizer, can affect these behaviors (Veloso et al., 2020).

In all the samples analyzed the particle formation was more than sufficient to qualify the analysis as reliable, considering that the count rate values was always above the mark of 250 kcps (Zheng et al., 2016). It was also seen that the population of particles formed had a reasonable uniformity, with the mean PdI value of about 0.6.

Starting by the control samples, it is possible to see a good stability on the diameter of the IONP on the dissolution medium (Figure 5). Until the fourth hour of experiment the diameter was nearly constant, and in the last two hours only a small rise on the diameter is observed, getting to about  $187 \pm 39$  nm, making the difference between the initial diameter and the value obtained at end of the dissolution only of about 31 nm. Considering the error of the experiment a constancy on the diameter may be assumed.

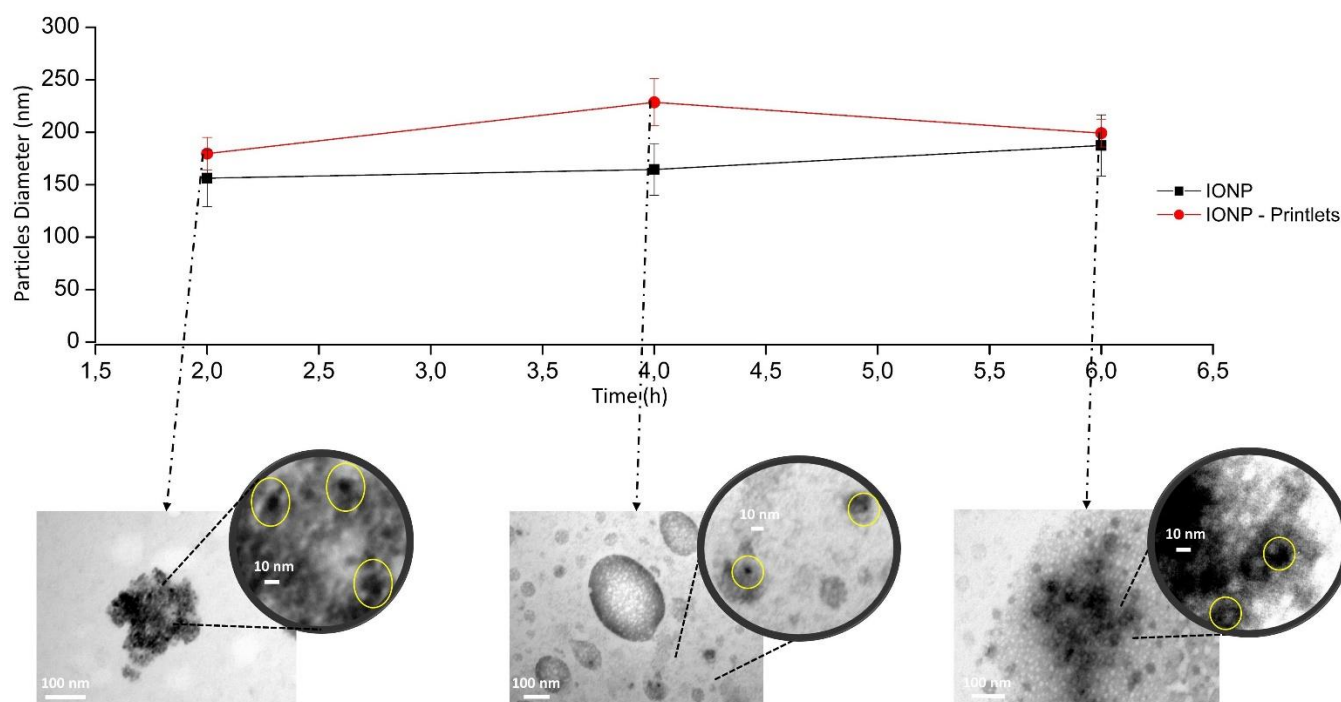


**Figure 5.** Particle diameter of the particles released from the dissolution of the iron oxide nanoparticles (IONP) powder and printlets along 6h. Additionally, transmission electronic microscopy images of printlets aliquots.

That stability was also suggested by the zeta potential analysis (Figure 6). In acidic medium the zeta potential of the IONP maintained a value of  $25.19 \pm 1.47$  mV during the whole six hours of dissolution, suggesting a high electrostatic repulsion between the nanostructures detected on this medium.

Also in this analysis, changes on the pH suggested a stability of the particle in the two extreme pH values tested, 2 and 10 (Figure 6). On the acidic environment, with high concentration on positive charges, the particle surfaces present a highly positive value, suggesting a low chances of further aggregation on environments like the intestinal fluid. Enhancing the pH a rapid change on the superficial charges was observed, with the complete neutralization happening on a pH of about 4.7, the so-called isoelectric point, implying that at this pH the particles are highly susceptible to aggregation and flocculation (Bhattacharjee, 2016).

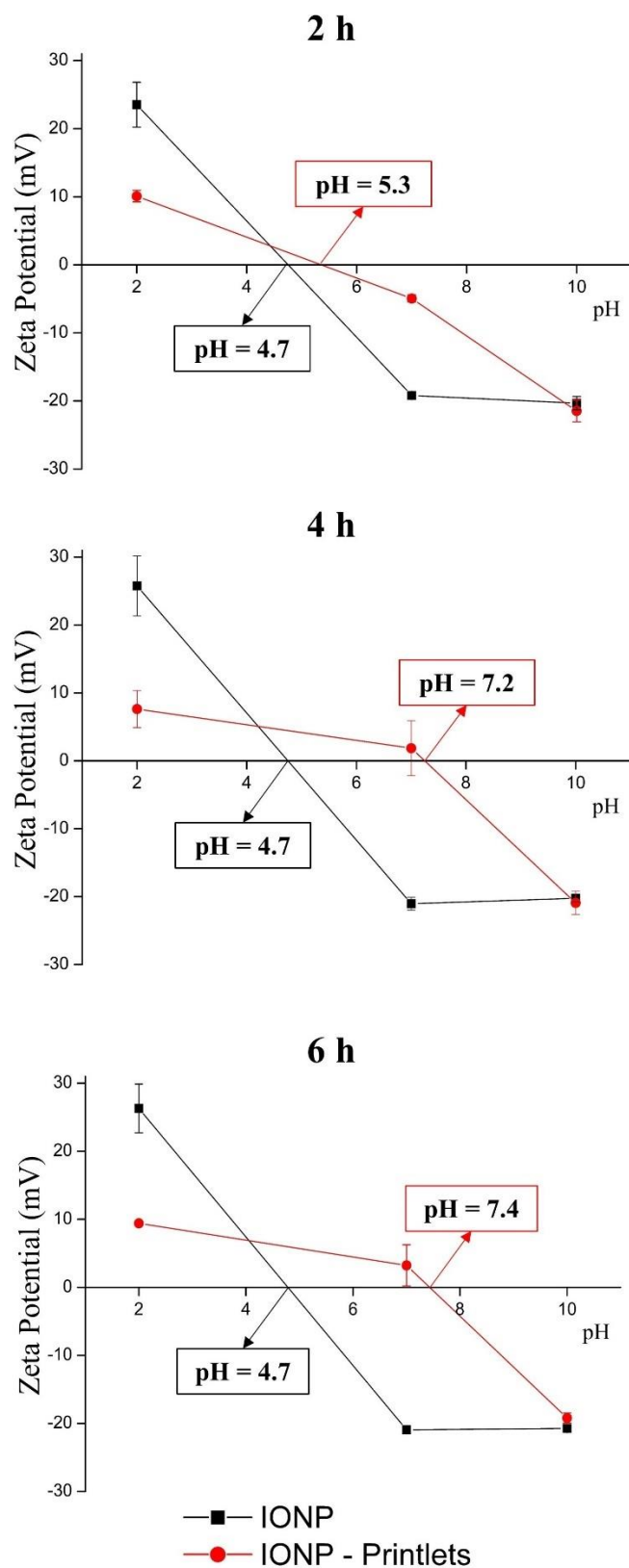


**Figure 6.** Zeta potential analysis in three different pH, 2.0, 7.0 and 10.0 of the particles released from the dissolution of the iron oxide nanoparticles (IONP) powder and printlets along 6h.

With the higher concentration of negative charges provided by the high alkaline environment the particle surface assumed a negative charge with values that can peak on about  $20.43 \pm 1.47$  mV, suggesting a good stability on environments with high pH. With that the isolated particles tested demonstrated a good stability in extreme environments, like the stomach and intestinal environments, being a positive characteristic for an oral administration.

On the printlet samples analysis of diameter and zeta potential it is confirmed a direct interference provided by interaction with the printlet formulation (PVA and GLY), already suggested by the TGA analysis (Figure 3). On the beginning of the diameter analysis (Figure 5) the obtained diameter was very similar to what was observed on the control samples, with the TEM images showing an agglomeration very alike the IONP powder isolated (Figure 1). It is possible to see that the small particles, with a size of about 12 nm (Highlighted for yellow circles on Figure 5) are visible on the structures, with a mass of a clearer appearance material between the particles, suggesting the presence of the polymeric matrix around the agglomerated particles.

The presence of the polymer on the two hours mark is also suggested by the zeta potential analysis (Figure 6). Unlike the IONP powder, on the acidic medium the zeta potential value of the released material had a slightly shifts between the hours of experiment and the values were less than half of what was observed on the control samples, about  $9.04 \pm 1.27$  mV. That can be explained not by a sudden loss of stability, but by the presence of the polymeric matrix, formed mainly by the polymer PVA, on the released material. The interaction between polymer and the particles, previously suggested by TGA analyses, is possible by the formation of hydrogen bonds between the polymer groups and the hydroxyl groups of the particle surfaces, resulting in an adsorption process forming a small polymeric layer around the particles, that causes a shift of slipping plane from the surface and a reduction of the zeta potential (Kallay et al., 2006; Wiśniewska et al., 2015).

The isoelectric point was achieved on a pH of 5.3, higher than what was observed on the IONP powder, probably also because of the influence of the small layer of the polymer, PVA. And with the rising of the pH a zeta potential value similar to the control sample was attained, about  $20.53 \pm 1.18$  mV, suggesting a stability of the released material on high pH, like the intestinal environments.



This initial data is already clear evidence of a spontaneous formation of a type of polymeric coating on the particles during the dissolution process, resultant from a direct molecular interaction between the polymeric matrix and the IONP, probably intensified by the HME and 3D printing processes. A phenomenon like that can mean a potential change on the characteristics of the particles without the necessity of an additional steps on the synthesis process, like coating.

On the fourth hour samples there is a clear differentiation on the mean particle diameters of the released material, if compared to the second hour samples. On the TEM analyses (Figure 5) it is noticeable the presence of polymeric structures in a shape of particles. Those structures are probably formed by the erosion process that occurs with the printlet during the dissolution process of its polymeric matrix (Figure 7). During this erosion the IONP are carried inside those eroded structures, been dispersed on the dissolution environment. That can be clearly seen on the TEM image on figure 5 by the presence of small black dots on the interior of the polymeric structure. The consequence of this interaction is a thicker layer of polymeric material around the IONP resulting in readings with higher diameters and can also make a difference on how the particles going to be dispersed on the medium.

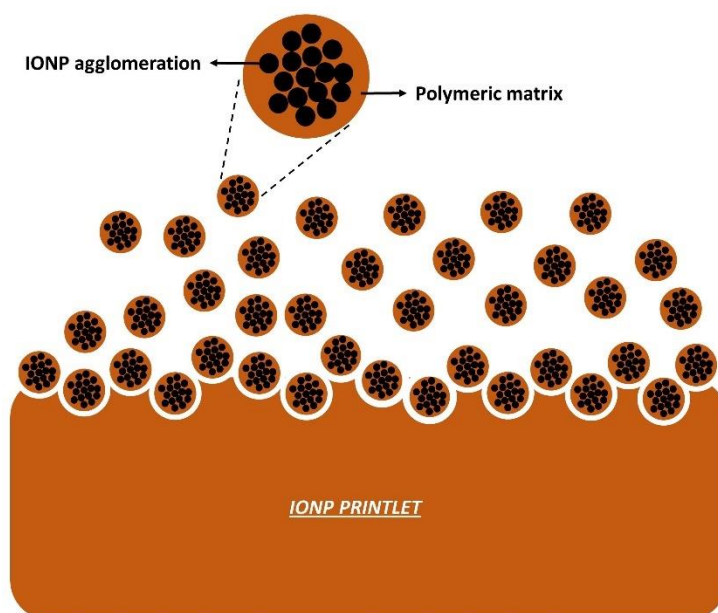


**Figure 7.** Illustration of the erosion process of the polymeric matrix of the printlets, forming polymeric nanosized structures that can carry the iron oxide nanoparticles (IONP) agglomerations.

On the zeta potential analysis, the effect of this thicker layer of polymer directly affects the surface charge behavior of the released materials. On the acidic medium it is possible to observe a slightly lower value of zeta potential, reduced by the more impactful presence of the polymeric matrix. But the more prominent change is demonstrated by the shift of the isoelectric point. The neutral charge polymer is capable to maintain the positive values of zeta potential for a longer time controlling the changes of the superficial charge and achieving full neutrality only on a pH value of 7.4. This pH is close to the values observed on the intestinal environment, suggesting a higher possibility of agglomeration of the released materials on these medium. On higher pH environments the particles again achieved values of zeta potential lower than -20 mV suggesting a good stability of the released materials on those environments.

On the six hour mark the diameter suffers a reduction on the values, probably due to a dissolution process of the polymeric materials. On the TEM images it is possible to see a reduction of the polymeric particles formed with the erosion process, probably caused by the high solubility of the PVA on the medium, leading to a loss of on the mass of those structures, returning to values like what was observed on the beginning of the experiment.

The zeta potential analyses of the six hours demonstrate that the PVA is still present, coating the released IONP, with stronger interactions between the polymeric matrix and the IONP, resulting in a slightly thicker layer of coating, sufficient to alters the zeta potential in a similar way to the four hour samples. Also raising the concern about the high probability of agglomeration of those released materials in slightly alkaline environments.

With that, it is possible to conclude that the polymeric material used to fabricate the 3D printed material can form a strong bond with the IONP, due to the intense processing by HME and 3D printing, creating a type of coating that can directly affect the diameter and the stability of the particles released during a dissolution process. In special, the presence of the polymeric layer seems to interfere heavily on the charge of the released particles, making those particles more susceptible to agglomeration on some types of environments and more stable in others, opening a possibility for the manipulation of the particles characteristics by changes on the 3D printing formulation.

This strategy of manipulating the characteristics of the particles to attained an objective is very popular on nanoscience, been the formation of polymeric layers around

the particles, coating, one of the main strategies used for this objective (Bachhar and Bandyopadhyaya, 2016). The use of a polymeric coating, like the observed on this study, is one of the strategies proved to have a positive impact on the stability of the particles, acceptability of the product and the interaction with the biological structures.

A PVA coating, for example, is validated as a good strategy to protect the particle against the environment of the gastrointestinal tract (Samide et al., 2019). It is also a well-known fact that the presence of a layer of polymeric material on inorganic particles like the IONP, are a way to enhance the biocompatibility of the product, since polymeric materials like PVA are largely more accepted by the biological structures than inorganic compounds like iron oxides, reducing considerably the possibility of toxicity and inflammatory responses (Kayal and Ramanujan, 2010; Salunkhe et al., 2013). And studies shown that the presence of polymeric coating, including PVA, had the potential to enhance the mucoadhesive of the particles on the gastrointestinal cells, facilitating the uptake process (Yang et al., 2014; Yin Win and Feng, 2005).

With all that information, the administration of IONP by 3D printing on the oral treatment of iron deficiency can be a strategy for a more stable, secure and efficient administration, facilitating the absorption of a higher quantity of iron and reducing even more the occurrence of adverse effects, because of the enhance on the biocompatibility, all because the formation of a stable polymeric coating around the particles only by the dissolution of the printlets, avoiding any type of additional coating processes.

#### **4.3.3. The dissolution assays**

The dissolution assay was also carried out with the object of identify possible changes that the already assessed interaction between the IONP and the printlets formulation can cause on the iron disponibility throughout a dissolution proceed in a simulated biological environment. And, like the characterization of the released particles, the dissolution profile was obtained for the printlets made with the IONP and a control sample made with the IONP powder.

On the dissolution profile (Figure 8) is possible to identify a limitation on the dispersion of the IONP on the dissolution medium in both powder and printlets forms. In both cases the samples weren't capable to attain a complete dispersion of the particles and, consequently, the iron concentration in the end of the experiment was way lower than

the maximum, achieving a value of  $31.22\pm 2.30\%$  and  $62.92\pm 5.47\%$  of iron dispersed in the medium for the IONP powder and the printlets samples, respectively. That happened probably due to the fact that the particles obtained have physical characteristics, like the intense aggregation, that makes difficult the complete dispersion of the material, a established problem of this type of particles (Szpak et al., 2013).

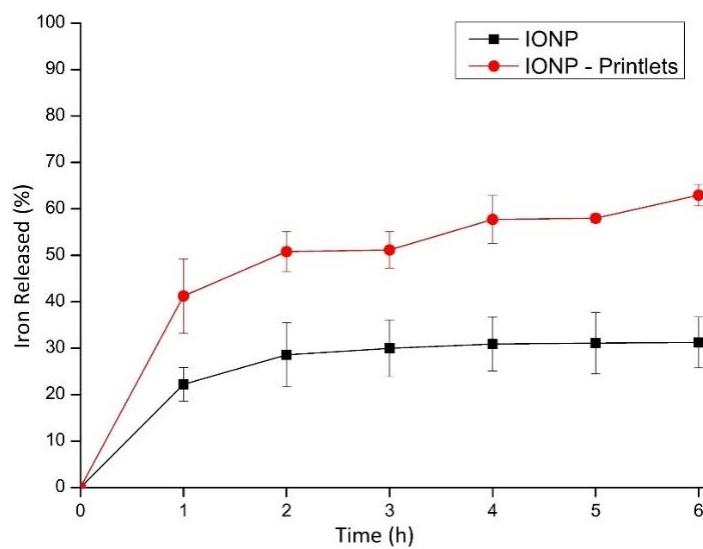


**Figure 8.** Dissolution profile of the iron oxide nanoparticles (IONP) powder and printlets along 6h.

However, the maximum iron concentration in the end of the six hours show a clear superiority on the printlet samples. At the end of the experiment the iron concentration on the dissolution vessels containing those samples was more than double, comparing with the IONP powder, maintaining a constant rising of that concentration throughout the whole process. The most probable justification for this behavior is founded on the results of the released particles characterization. With the dissolution the particles are released with a type of coating formed by the polymeric matrix of the printlet and this material can influence directly the behavior of the particles on the medium.

One of the main strategies used as an answer for the poor dispersion of inorganic particles, in special IONP, are the coating process of the particles with a material that can enhance the dispersion of the particles in aqueous solvent, been the most popular coating materials the polymers, including PVA (Che Mohamed Hussein et al., 2022). With that, it is possible that the polymeric matrix of the printlet, adsorbed on the particles, works in

the same way as this type of coating, facilitating the dispersion of the particles in the medium.

Additionally, the erosion process of the polymeric matrix, illustrated on figure 6, can also synergically act with the formed coating, facilitating even more the dispersion of the particles.

This characterizes another important advantage of the oral administration of IONP by a 3D dosage form. The polymeric matrix adsorption on the IONP during the dissolution process is capable to enhance the dispersion of the particles and combined to a erosive process of the 3D printing dosage form during dissolution it can make the particles more available for the absorption on the gastrointestinal tract.

#### 4.4. CONCLUSIONS

The oral treatment of iron deficiency can benefit from the combination of the enhanced security provided by the use of IONP and the versatility of the 3D printing technique, with a final product that is going to be much more accepted by the user.

This study proved that, in addition, the processing composed of the HME and 3D printing, part of a printlet production by FDM 3D printing, is capable to enhance the interaction between polymeric matrix of the 3D formulation and the IONP, creating a type of coating on the particles that was capable to change some physical-chemical characteristics of the particles, altering its stability and dispersion on aqueous medium.

With that, the resultant product has the potential to be applied to an oral administration of iron supplement, benefiting from the advantages brought by the IONP, the 3D printing, with an additional advantage of a *in situ* coating process, that can facilitate the production by eliminating additional coating procedures.

#### 4.5. REFERENCES

- Alphandéry, E., 2020. Iron oxide nanoparticles for therapeutic applications. *Drug Discov. Today* 25, 141–149. <https://doi.org/10.1016/j.drudis.2019.09.020>
- Bachhar, N., Bandyopadhyaya, R., 2016. Role of coating agent in iron oxide nanoparticle formation in an aqueous dispersion: Experiments and simulation. *J. Colloid Interface Sci.* 464, 254–263. <https://doi.org/10.1016/j.jcis.2015.11.006>

- Bandari, S., Nyavanandi, D., Dumpa, N., Repka, M.A., 2021. Coupling Hot Melt Extrusion and Fused Deposition Modeling: Critical Properties for Successful Performance. *Adv. Drug Deliv. Rev.* 172, 52–63. <https://doi.org/10.1016/j.addr.2021.02.006>. Coupling
- Bayraktar, U.D., Bayraktar, S., 2010. Treatment of iron deficiency anemia associated with gastrointestinal tract diseases. *World J. Gastroenterol.* 16, 2720–2725. <https://doi.org/10.3748/wjg.v16.i22.2720>
- Besenhart, M.O., LaGrow, A.P., Hodzic, A., Kriechbaum, M., Panariello, L., Bais, G., Loizou, K., Damilos, S., Margarida Cruz, M., Thanh, N.T.K., Gavriilidis, A., 2020. Co-precipitation synthesis of stable iron oxide nanoparticles with NaOH: New insights and continuous production via flow chemistry. *Chem. Eng. J.* 399, 125740. <https://doi.org/10.1016/j.cej.2020.125740>
- Bhattacharjee, S., 2016. DLS and zeta potential - What they are and what they are not? *J. Control. Release* 235, 337–351. <https://doi.org/10.1016/j.jconrel.2016.06.017>
- Che Mohamed Hussein, S.N., Amir, Z., Jan, B.M., Khalil, M., Azizi, A., 2022. Colloidal Stability of CA, SDS and PVA Coated Iron Oxide Nanoparticles (IONPs): Effect of Molar Ratio and Salinity. *Polymers (Basel)*. 14, 4787. <https://doi.org/10.3390/polym14214787>
- Garcia-Fernandez, J., Turiel, D., Bettmer, J., Jakubowski, N., Panne, U., Rivas García, L., Llopis, J., Sánchez González, C., Montes-Bayón, M., 2020. In vitro and in situ experiments to evaluate the biodistribution and cellular toxicity of ultrasmall iron oxide nanoparticles potentially used as oral iron supplements. *Nanotoxicology* 14, 388–403. <https://doi.org/10.1080/17435390.2019.1710613>
- Gillispie, G., Prim, P., Copus, J., Fisher, J., Mikos, A.G., Yoo, J.J., Atala, A., Lee, S.J., 2020. Assessment methodologies for extrusion-based bioink printability. *Biofabrication* 12. <https://doi.org/10.1088/1758-5090/ab6f0d>. Assessment
- Granados, P.A., Pinho, L.A.G., Sa-Barreto, L.L., Gratieri, T., Gelfuso, G.M., Cunha-Filho, M., 2022. Application of hot-melt extrusion in the complexation of naringenin with cyclodextrin using hydrophilic polymers. *Adv. Powder Technol.* 33, 103380. <https://doi.org/10.1016/j.apt.2021.11.032>
- Kallay, N., Kovačević, D., salac, S., 2006. Chapter 6 Thermodynamics of the solid/liquid

- interface - its application to adsorption and colloid stability. *Interface Sci. Technol.* 11, 133–170. [https://doi.org/10.1016/S1573-4285\(06\)80050-5](https://doi.org/10.1016/S1573-4285(06)80050-5)
- Kayal, S., Ramanujan, R. V., 2010. Doxorubicin loaded PVA coated iron oxide nanoparticles for targeted drug delivery. *Mater. Sci. Eng. C* 30, 484–490. <https://doi.org/10.1016/j.msec.2010.01.006>
- Kumar, A., Sharma, E., Marley, A., Samaan, M.A., Brookes, M.J., 2022. Iron deficiency anaemia: Pathophysiology, assessment, practical management. *BMJ Open Gastroenterol.* 9. <https://doi.org/10.1136/bmjgast-2021-000759>
- Lima, A.L., Pires, F.Q., Hilgert, L.A., Sa-Barreto, L.L., Gratieri, T., Gelfuso, G.M., Cunha-Filho, M., 2022. Oscillatory shear rheology as an in-process control tool for 3D printing medicines production by fused deposition modeling. *J. Manuf. Process.* 76, 850–862. <https://doi.org/10.1016/j.jmapro.2022.03.001>
- Liu, K., Kaffes, A.J., 2012. Iron deficiency anaemia: A review of diagnosis, investigation and management. *Eur. J. Gastroenterol. Hepatol.* 24, 109–116. <https://doi.org/10.1097/MEG.0b013e32834f3140>
- Lo, J.O., Benson, A.E., Martens, K., Hedges, M.A., McMurry, H.S., DeLoughery, T., Aslan, J.E., Shatzel, J.J., 2022. Oral iron treatment in adult iron deficiency. *Eur. J. Haematol.* 1–8. <https://doi.org/10.1111/ejh.13892>
- Pandey, M., Choudhury, H., Fern, J.L.C., Kee, A.T.K., Kou, J., Jing, J.L.J., Her, H.C., Yong, H.S., Ming, H.C., Bhattamisra, S.K., Gorain, B., 2020. 3D printing for oral drug delivery: a new tool to customize drug delivery. *Drug Deliv. Transl. Res.* 10, 986–1001. <https://doi.org/10.1007/s13346-020-00737-0>
- Pasricha, S., Tye-din, J., Muckenthaler, M.U., Swinkels, D.W., 2021. Iron deficiency. *Lancet* 397, 233–248.
- Pires, F.Q., Alves-Silva, I., Pinho, L.A.G., Chaker, J.A., Sa-Barreto, L.L., Gelfuso, G.M., Gratieri, T., Cunha-Filho, M., 2020. Predictive models of FDM 3D printing using experimental design based on pharmaceutical requirements for tablet production. *Int. J. Pharm.* 588, 119728. <https://doi.org/10.1016/j.ijpharm.2020.119728>
- Ponsar, H., Wiedey, R., Quodbach, J., 2020. Hot-melt extrusion process fluctuations and their impact on critical quality attributes of filaments and 3d-printed dosage forms. *Pharmaceutics* 12, 1–15. <https://doi.org/10.3390/pharmaceutics12060511>

- Salunkhe, A.B., Khot, V.M., Thorat, N.D., Phadatare, M.R., Sathish, C.I., Dhawale, D.S., Pawar, S.H., 2013. Polyvinyl alcohol functionalized cobalt ferrite nanoparticles for biomedical applications. *Appl. Surf. Sci.* 264, 598–604. <https://doi.org/10.1016/j.apsusc.2012.10.073>
- Samide, A., Stoean, R., Stoean, C., Tutunaru, B., Grecu, R., Cioatera, N., 2019. Investigation of polymer coatings formed by polyvinyl alcohol and silver nanoparticles on copper surface in acid medium by means of deep convolutional neural networks. *Coatings* 9, 1–14. <https://doi.org/10.3390/COATINGS9020105>
- Silva S, P. da, Moraes D, C. de, 2016. Iron Oxide Nanoparticles Coated with Polymer Derived from Epoxidized Oleic Acid and Cis-1,2-Cyclohexanedicarboxylic Anhydride: Synthesis and Characterization. *J. Mater. Sci. Eng.* 05, 1–7. <https://doi.org/10.4172/2169-0022.1000247>
- Szpak, A., Kania, G., Skórka, T., Tokarz, W., Zapotoczny, S., Nowakowska, M., 2013. Stable aqueous dispersion of superparamagnetic iron oxide nanoparticles protected by charged chitosan derivatives. *J. Nanoparticle Res.* 15. <https://doi.org/10.1007/s11051-012-1372-9>
- Thakkar, R., Pillai, A.R., Zhang, J., Zhang, Y., Kulkarni, V., Maniruzzaman, M., 2020. Novel on-demand 3-dimensional (3-d) printed tablets using fill density as an effective release-controlling tool. *Polymers (Basel)*. 12, 1–21. <https://doi.org/10.3390/POLYM12091872>
- Ushakov, M. V, Sousa, M.H., Morais, P.C., Kuzmann, E., 2020. Effect of iron oxide nanoparticles functionalization by citrate analyzed using Mössbauer spectroscopy. *Hyperfine Interact.* 241, 1–9.
- Veloso, C.H., Filippov, L.O., Filippova, I. V., Ouvrard, S., Araujo, A.C., 2020. Adsorption of polymers onto iron oxides: Equilibrium isotherms. *J. Mater. Res. Technol.* 9, 779–788. <https://doi.org/10.1016/j.jmrt.2019.11.018>
- Wiśniewska, M., Ostolska, I., Szewczuk-Karpisz, K., Chibowski, S., Terpiłowski, K., Gun'ko, V.M., Zarko, V.I., 2015. Investigation of the polyvinyl alcohol stabilization mechanism and adsorption properties on the surface of ternary mixed nanooxide AST 50 (Al<sub>2</sub>O<sub>3</sub>–SiO<sub>2</sub>–TiO<sub>2</sub>). *J. Nanoparticle Res.* 17. <https://doi.org/10.1007/s11051-014-2831-2>



- Yang, M., Lai, S.K., Yu, T., Wang, Y.Y., Happe, C., Zhong, W., Zhang, M., Anonuevo, A., Fridley, C., Hung, A., Fu, J., Hanes, J., 2014. Nanoparticle penetration of human cervicovaginal mucus: The effect of polyvinyl alcohol. *J. Control. Release* 192, 202–208. <https://doi.org/10.1016/j.jconrel.2014.07.045>
- Yang, Y., Wang, H., Xu, X., Yang, G., 2021. Strategies and mechanisms to improve the printability of pharmaceutical polymers Eudragit® EPO and Soluplus®. *Int. J. Pharm.* 599. <https://doi.org/10.1016/j.ijpharm.2021.120410>
- Yin Win, K., Feng, S.S., 2005. Effects of particle size and surface coating on cellular uptake of polymeric nanoparticles for oral delivery of anticancer drugs. *Biomaterials* 26, 2713–2722. <https://doi.org/10.1016/j.biomaterials.2004.07.050>
- Zheng, T., Bott, S., Huo, Q., 2016. Techniques for Accurate Sizing of Gold Nanoparticles Using Dynamic Light Scattering with Particular Application to Chemical and Biological Sensing Based on Aggregate Formation. *ACS Appl. Mater. Interfaces* 8, 21585–21594. <https://doi.org/10.1021/acsami.6b06903>

## 5. CONCLUSION

3D printing and nanotechnology are two fields in the front line of pharmaceutical development on modern days. 3D printing brought to the field the possibility of a complete personalization of dosage forms. Nanotechnology brought a way to manipulate the action of drugs, making the treatment more secure and efficient in many ways. The combination of these two technologies has the potential for an even more open possibility of treatment, benefiting directly the user. With that, this work had the objective of investigating the combination of these technologies in different scenarios, with good results.

In order to fully understand the 3D printing process, still new to the market, the study started with the investigation on how the printing parameter can affect the printed dosage forms. With the use of quality-by-design tools it was possible to select the most impactful parameters, that can directly affect many characteristics of a printed dosage form and it was seen that with a full validation process it is possible to ensure the printing of dosage forms with specific characteristics with little deviation.

Understanding the 3D printing process, it was possible to start the production of 3D printed dosage forms with pharmaceutical grade polymers and investigate the first intersection between 3D printing and nanotechnology. The in-situ formation of nanoparticles by the dissolution process of a 3D printing dosage form was proved by this study, being the magnitude of molecular interaction between the components of the formulation the main factor that governs the formation of those particles. It was determined that a great amount of active was trapped inside particles for a period of 24 hours, potentially impacting the drug availability for absorption. With that, the neglected analysis of those particles has to become fundamental on the study of any new 3D printed dosage forms, simulating in a more realistic way the dissolution and absorption process.

With those results the necessity of a more careful investigation of the interaction of the polymeric matrix of a printed material and the active material was a priority and that was applied for another combination of the 3D printing and nanotechnology. The use of iron oxide nanoparticles inserted on a 3D printed model for oral delivery can be a great strategy for the treatment of iron deficiency, with personalization, security and efficiency being the main qualities. In addition, this study demonstrated that the interaction between

the polymer and the particles resulted in a in-situ coating process, with the potential of manipulate the physical-chemical and biological characteristics of the dosage forms.

As a conclusion, the combination of 3D printing and nanotechnology can be more than the combination of its combine benefits, bringing new horizons not just for the iron deficiency treatment, but the pharmaceutical field in general.

## APPENDIX A – BIBLIOGRAPHICAL SEARCH

**Table 1.** Bibliographic search on polymeric based 3D printed dosage forms evaluating the investigation on the in-situ formation of nano/micro compounds.

Year	Product	Technique	Polymer	Target	Investigation of nano/micro compounds	Reference
2020	Floating Printlets	FDM 3D printing	Hydroxypropyl Cellulose (HPC)	Oral Delivery	No	(Giri et al., 2020)
2020	Printlets	FDM 3D printing	Polycaprolactone	Oral Delivery	No	(Elbadawi et al., 2020)
2020	Printlets	FDM 3D printing	Hydroxypropyl Cellulose (HPC)	Oral Delivery	No	(EGORKEM BUYUKGOZ <i>et al.</i> , 2020a)
2022	Printlets	FDM 3D printing	Poly(2-ethyl-tetra-oxazoline) (PETOx)	Oral Delivery	No	(Raje et al., 2022)
2022	Printlets	FDM 3D printing	Soluplus® and Eudragit® E PO	Oral Delivery	No	(Hoffmann et al., 2022)
2018	Chewable Printlets	FDM 3D printing	Hydroxypropylmethylcellulose acetate succinate (HPMCAS)	Oral Delivery	No	(Scoutaris et al., 2018)
2020	Capsules	FDM 3D printing	Polyvinyl alcohol (PVA) and Polylactic acid (PLA)	Oral Delivery	No	(Cotabarren and Gallo, 2020)
2021	Printlets	FDM 3D printing	Eudragit® E PO	Oral Delivery	No	(Fanous et al., 2021)
2021	Printlets	FDM 3D printing	Polyvinyl alcohol (PVA)	Oral Delivery	No	(Sharma et al., 2021)

2021	Capsules	FDM 3D printing	Polyvinyl alcohol (PVA) and Hydroxypropylmethylcellulose (HPMC)	Oral Delivery	No	(Gaurkhede et al., 2021)
2019	Printlets	FDM 3D printing	Polyvinyl alcohol (PVA)	Oral Delivery	No	(Ibrahim et al., 2019)
2019	Caplets	FDM 3D printing	Polyvinyl alcohol (PVA)	Oral Delivery	No	(Nukala et al., 2019)
2021	Mini-Printlets	FDM 3D printing	Polyvinyl alcohol (PVA)	Oral Delivery	No	(Ayyoubi et al., 2021)
2021	Vaginal ring	FDM 3D printing	Polylactic acid (PLA)	Vaginal Delivery	No	(Arany et al., 2021)
2020	Implants	FDM 3D printing	Polylactic acid (PLA), antibacterial polylactic acid (Anti PLA), polyethylene terephthalate glycol (PETG) and poly(methyl methacrylate) (PMMA)	Multifunctional delivery system	No	(Arany et al., 2020)
2022	Printlets	FDM 3D printing	Hydroxypropyl Cellulose (HPC)	Oral Delivery	No	(Nashed et al., 2022)
2022	Printlets	FDM 3D printing	Polylactic acid (PLA) and Hydroxypropylmethylcellulose (HPMC)	Oral Delivery	No	(Parulski et al., 2022)
2022	Bento Box	FDM 3D printing	Polyvinyl alcohol (PVA)	Oral Delivery	No	(Kraisit et al., 2022)
2018	Vaginal ring	FDM 3D printing	Polylactic acid (PLA)	Vaginal Delivery	No	(Fu et al., 2018)
2019	Suppository	FDM 3D printing	Polyvinyl alcohol (PVA)	Rectal Delivery	No	(Tagami et al., 2019)
2020	Floating Printlets	FDM 3D printing	Hydroxypropyl Cellulose (HPC)	Oral Delivery	No	(Dumpa et al., 2020)

2020	Caplets	FDM 3D printing	Hydroxypropyl Cellulose (HPC)	Oral Delivery	No	(Tan et al., 2020)
2020	Printlets	FDM 3D printing	Kollidon® VA 64 and Soluplus®	Oral Delivery	No	(SAYDAM and TAKKA, 2020)
2021	Printlets	FDM 3D printing	Polyvinyl alcohol (PVA) and Hydroxypropylmethylcellulose (HPMC)	Oral Delivery	No	(Đuranović et al., 2021)
2020	Printlets	FDM 3D printing	Kollicoat® IR and Polylactic acid (PLA)	Oral Delivery	No	(Jamróz et al., 2020)
2022	Printlets	FDM 3D printing	Hydroxypropylmethylcellulose (HPMC), Hydroxypropylmethylcellulose acetate succinate (HPMCAS) and Hydroxypropyl Cellulose (HPC)	Oral Delivery	No	(Hu et al., 2022)
2020	Printlets	FDM 3D printing	Hydroxypropyl Cellulose (HPC) and Kollidon VA64	Oral Delivery	No	(Fanous et al., 2020)
2020	Printlets	FDM 3D printing	Hydroxypropyl Cellulose (HPC) and Polylactic acid (PLA)	Oral Delivery	No	(GORKEM BUYUKGOZ <i>et al.</i> , 2020b)
2021	Printlets	FDM 3D printing	Hydroxypropylmethylcellulose acetate succinate (HPMCAS) and Hydroxypropyl Cellulose (HPC)	Oral Delivery	No	(Ghanizadeh Tabriz et al., 2021)
2021	Implants	FDM 3D printing	Polylactic acid (PLA)	Multifunctional delivery system	No	(Cui et al., 2021)

- Arany, P., Papp, I., Zichar, M., Csontos, M., Elek, J., Regdon, G., Budai, I., Béres, M., Gesztelyi, R., Fehér, P., Ujhelyi, Z., Vasvári, G., Haimhoffer, Á., Fenyvesi, F., Váradi, J., Miklós, V., Bácskay, I., 2020. In Vitro Tests of FDM 3D-Printed Diclofenac Sodium-Containing Implants. *Molecules* 25, 1–31. <https://doi.org/10.3390/MOLECULES25245889>
- Arany, P., Papp, I., Zichar, M., Regdon, G., Béres, M., Szalóki, M., Kovács, R., Fehér, P., Ujhelyi, Z., Vecsernyés, M., Bácskay, I., 2021. Manufacturing and examination of vaginal drug delivery system by fdm 3d printing. *Pharmaceutics* 13. <https://doi.org/10.3390/pharmaceutics13101714>
- Ayyoubi, S., Cerda, J.R., Fernández-García, R., Knief, P., Lalatsa, A., Healy, A.M., Serrano, D.R., 2021. 3D printed spherical mini-tablets: Geometry versus composition effects in controlling dissolution from personalised solid dosage forms. *Int. J. Pharm.* 597. <https://doi.org/10.1016/j.ijpharm.2021.120336>
- Cotabarren, I., Gallo, L., 2020. 3D printing of PVA capsular devices for modified drug delivery: design and in vitro dissolution studies. *Drug Dev. Ind. Pharm.* 0, 1416–1426. <https://doi.org/10.1080/03639045.2020.1791166>
- Cui, M., Pan, H., Li, L., Fang, D., Sun, H., Qiao, S., Li, X., Pan, W., 2021. Exploration and Preparation of Patient-specific Ciprofloxacin Implants Drug Delivery System Via 3D Printing Technologies. *J. Pharm. Sci.* 110, 3678–3689. <https://doi.org/10.1016/j.xphs.2021.08.004>
- Dumpa, N.R., Bandari, S., Repka, M.A., 2020. Novel gastroretentive floating pulsatile drug delivery system produced via hot-melt extrusion and fused deposition modeling 3D printing. *Pharmaceutics* 12. <https://doi.org/10.3390/pharmaceutics12010052>
- Đuranović, M., Madžarević, M., Ivković, B., Ibrić, S., Cvijić, S., 2021. The evaluation of the effect of different superdisintegrants on the drug release from FDM 3D printed tablets through different applied strategies: In vitro-in silico assessment. *Int. J. Pharm.* 610. <https://doi.org/10.1016/j.ijpharm.2021.121194>
- Elbadawi, M., Gustaffson, T., Gaisford, S., Basit, A.W., 2020. 3D printing tablets: Predicting printability and drug dissolution from rheological data. *Int. J. Pharm.* 590, 119868. <https://doi.org/10.1016/j.ijpharm.2020.119868>
- Fanou, M., Bitar, M., Gold, S., Sobczuk, A., Hirsch, S., Ogorka, J., Imanidis, G., 2021.

- Development of immediate release 3D-printed dosage forms for a poorly water-soluble drug by fused deposition modeling: Study of morphology, solid state and dissolution. *Int. J. Pharm.* 599, 120417. <https://doi.org/10.1016/j.ijpharm.2021.120417>
- Fanous, M., Gold, S., Hirsch, S., Ogorka, J., Imanidis, G., 2020. Development of immediate release (IR) 3D-printed oral dosage forms with focus on industrial relevance. *Eur. J. Pharm. Sci.* 155, 105558. <https://doi.org/10.1016/j.ejps.2020.105558>
- Fu, J., Yu, X., Jin, Y., 2018. 3D printing of vaginal rings with personalized shapes for controlled release of progesterone. *Int. J. Pharm.* 539, 75–82. <https://doi.org/10.1016/j.ijpharm.2018.01.036>
- Gaurkhede, S.G., Osipitan, O.O., Dromgoole, G., Spencer, S.A., Pasqua, A.J.D., Deng, J., 2021. 3D Printing and Dissolution Testing of Novel Capsule Shells for Use in Delivering Acetaminophen. *J. Pharm. Sci.* 110, 3829–3837. <https://doi.org/10.1016/j.xphs.2021.08.030>
- Ghanizadeh Tabriz, A., Nandi, U., Hurt, A.P., Hui, H.W., Karki, S., Gong, Y., Kumar, S., Douroumis, D., 2021. 3D printed bilayer tablet with dual controlled drug release for tuberculosis treatment. *Int. J. Pharm.* 593, 120147. <https://doi.org/10.1016/j.ijpharm.2020.120147>
- Giri, B.R., Song, E.S., Kwon, J., Lee, J.H., Park, J.B., Kim, D.W., 2020. Fabrication of intragastric floating, controlled release 3D printed theophylline tablets using hot-melt extrusion and fused deposition modeling. *Pharmaceutics* 12. <https://doi.org/10.3390/pharmaceutics12010077>
- Gorkem Buyukgoz, G., Soffer, D., Defendre, J., Pizzano, G.M., Davé, R.N., 2020a. Exploring tablet design options for tailoring drug release and dose via fused deposition modeling (FDM) 3D printing. *Int. J. Pharm.* 591. <https://doi.org/10.1016/j.ijpharm.2020.119987>
- Gorkem Buyukgoz, G., Soffer, D., Defendre, J., Pizzano, G.M., Davé, R.N., 2020b. Exploring tablet design options for tailoring drug release and dose via fused deposition modeling (FDM) 3D printing. *Int. J. Pharm.* 591. <https://doi.org/10.1016/j.ijpharm.2020.119987>



- Hoffmann, L., Breitzkreutz, J., Quodbach, J., 2022. Fused Deposition Modeling (FDM) 3D Printing of the Thermo-Sensitive Peptidomimetic Drug Enalapril Maleate. *Pharmaceutics* 14, 2411. <https://doi.org/10.3390/pharmaceutics14112411>
- Hu, Z., Xu, P., Zhang, J., Bandari, S., Repka, M.A., 2022. Development of controlled release oral dosages by density gradient modification via three-dimensional (3D) printing and hot-melt extrusion (HME) technology. *J. Drug Deliv. Sci. Technol.* 71, 103355. <https://doi.org/10.1016/j.jddst.2022.103355>
- Ibrahim, M., Barnes, M., McMillin, R., Cook, D.W., Smith, S., Halquist, M., Wijesinghe, D., Roper, T.D., 2019. 3D Printing of Metformin HCl PVA Tablets by Fused Deposition Modeling: Drug Loading, Tablet Design, and Dissolution Studies. *AAPS PharmSciTech* 20, 1–11. <https://doi.org/10.1208/s12249-019-1400-5>
- Jamróz, W., Kurek, M., Szafraniec-Szczęsny, J., Czech, A., Gawlak, K., Knapik-Kowalczyk, J., Leszczyński, B., Wróbel, A., Paluch, M., Jachowicz, R., 2020. Speed it up, slow it down...An issue of bicalutamide release from 3D printed tablets. *Eur. J. Pharm. Sci.* 143. <https://doi.org/10.1016/j.ejps.2019.105169>
- Kraisit, P., Limpamanoch, P., Hirun, N., Limmatvampirat, S., 2022. Design and development of 3D-printed bento box model for controlled drug release of propranolol HCl following pharmacopeia dissolution guidelines. *Int. J. Pharm.* 628, 122272. <https://doi.org/10.1016/j.ijpharm.2022.122272>
- Nashed, N., Lam, M., Ghafourian, T., Pausas, L., Jiri, M., Majumder, M., Nokhodchi, A., 2022. An Insight into the Impact of Thermal Process on Dissolution Profile and Physical Characteristics of Theophylline Tablets Made through 3D Printing Compared to Conventional Methods. *Biomedicines* 10, 1–18. <https://doi.org/10.3390/biomedicines10061335>
- Nukala, P.K., Palekar, S., Solanki, N., Fu, Y., Patki, M., Shohatee, A.A., Trombetta, L., Patel, K., 2019. Investigating the application of FDM 3D printing pattern in preparation of patient-tailored dosage forms. *J. 3D Print. Med.* 3, 23–37. <https://doi.org/10.2217/3dp-2018-0028>
- Parulski, C., Gresse, E., Jennotte, O., Felten, A., Ziemons, E., Lechanteur, A., Evrard, B., 2022. Fused deposition modeling 3D printing of solid oral dosage forms containing amorphous solid dispersions: How to elucidate drug dissolution mechanisms through surface spectral analysis techniques? *Int. J. Pharm.* 626.

<https://doi.org/10.1016/j.ijpharm.2022.122157>

Raje, V., Palekar, S., Banella, S., Patel, K., 2022. Tunable Drug Release from Fused Deposition Modelling (FDM) 3D-Printed Tablets Fabricated Using a Novel Extrudable Polymer. *Pharmaceutics* 14.

<https://doi.org/10.3390/pharmaceutics14102192>

SAYDAM, M., TAKKA, S., 2020. Improving the dissolution of a water-insoluble orphan drug through a fused deposition modelling 3-Dimensional printing technology approach. *Eur. J. Pharm. Sci.* 152, 105426.

<https://doi.org/10.1016/j.ejps.2020.105426>

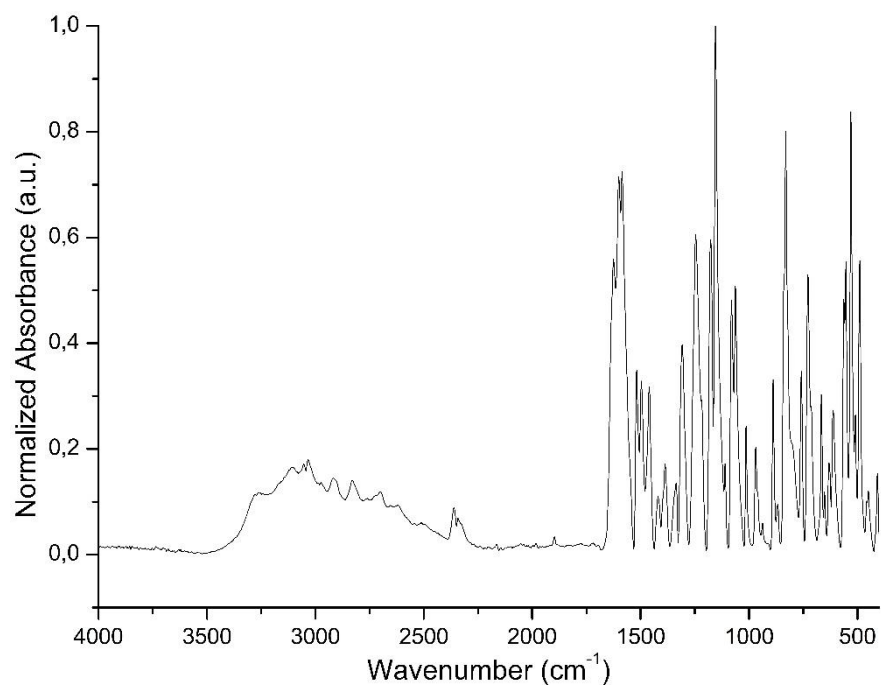
Scoutaris, N., Ross, S.A., Douroumis, D., 2018. 3D Printed “Starmix” Drug Loaded Dosage Forms for Paediatric Applications. *Pharm. Res.* 35.

<https://doi.org/10.1007/s11095-017-2284-2>

Sharma, V., Shaik, K.M., Choudhury, A., Kumar, P., Kala, P., Sultana, Y., Shukla, R., Kumar, D., 2021. Investigations of process parameters during dissolution studies of drug loaded 3D printed tablets. *Proc. Inst. Mech. Eng. Part H J. Eng. Med.* 235, 523–529. <https://doi.org/10.1177/0954411921993582>

Tagami, T., Hayashi, N., Sakai, N., Ozeki, T., 2019. 3D printing of unique water-soluble polymer-based suppository shell for controlled drug release. *Int. J. Pharm.* 568, 118494. <https://doi.org/10.1016/j.ijpharm.2019.118494>

Tan, D.K., Maniruzzaman, M., Nokhodchi, A., 2020. Development and Optimisation of Novel Polymeric Compositions for Sustained Release Theophylline. *Polymers (Basel)*. 12, 1–18.

**APPENDIX B – FTIR ISOLATED MATERIALS**

**Figure 1.** FTIR spectrum of naringenin (NAR) as supplied.

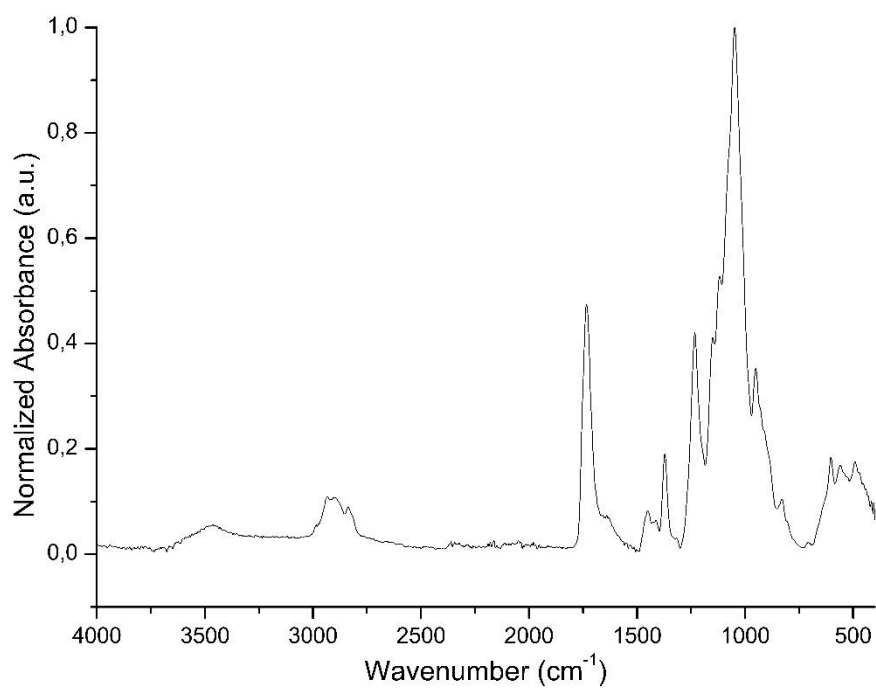


**Figure 2.** FTIR spectrum of hydroxypropylmethylcellulose acetate succinate (HPMCAS) as supplied.

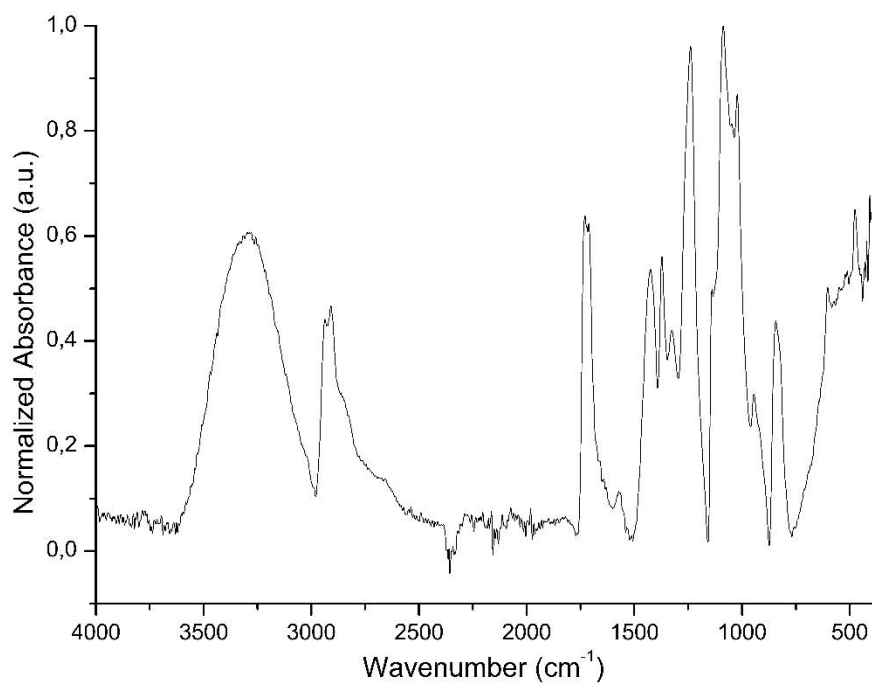


**Figure 3.** FTIR spectrum of Polyvinyl alcohol (PVA) as supplied.

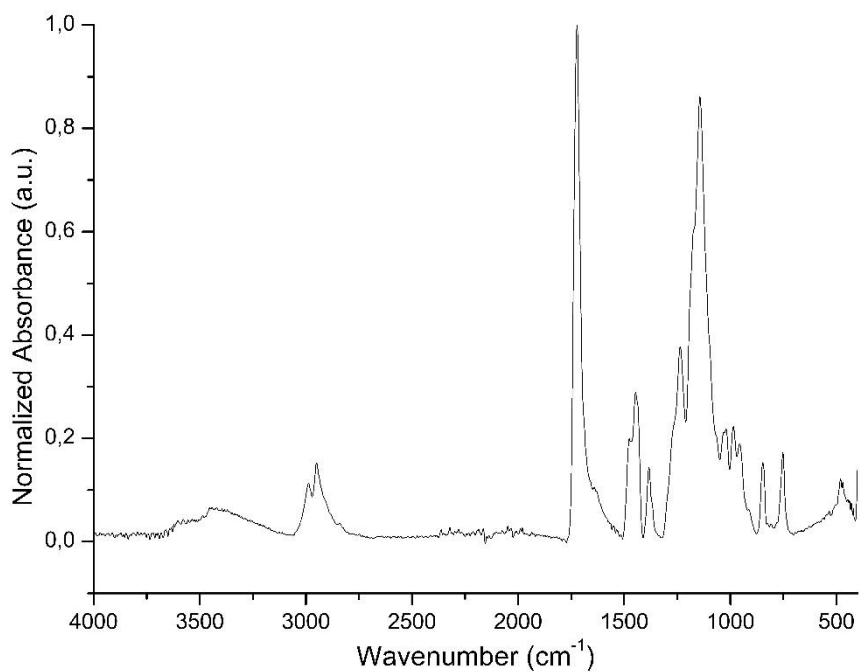


**Figure 4.** FTIR spectrum of Eudragit RL PO (EUD RL) as supplied.

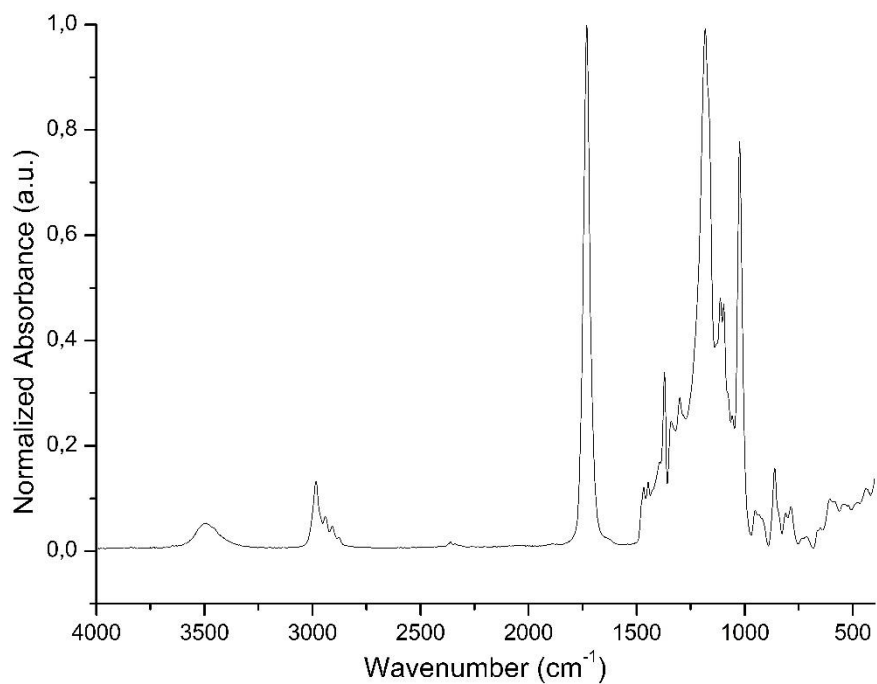


**Figure 5.** FTIR spectrum of Triethyl citrate (TEC) as supplied.

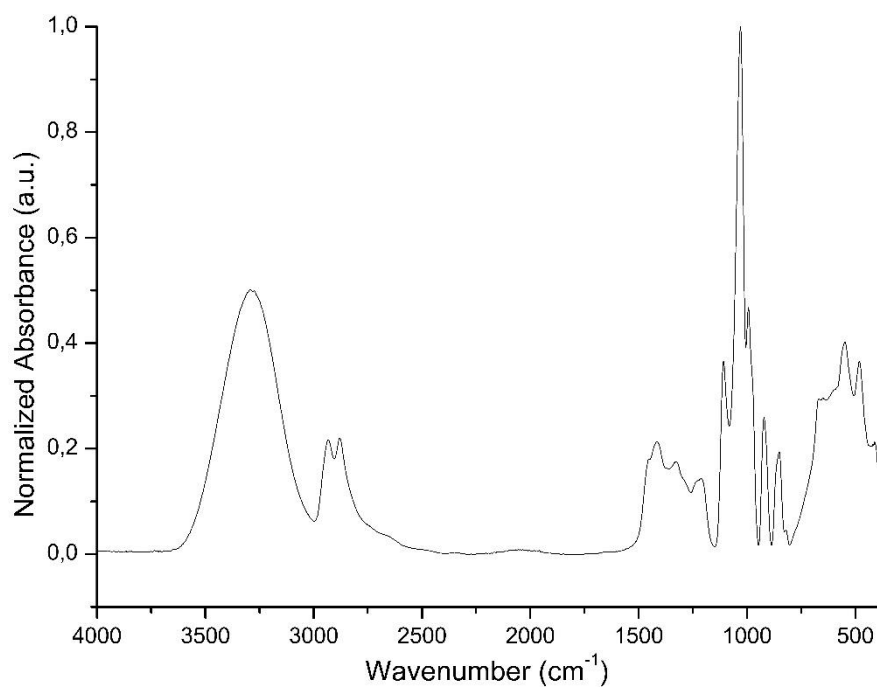


**Figure 6.** FTIR spectrum of glycerin (GLY) as supplied.

## APPENDIX C – PARTICLE RELEASE OF SAMPLES WITHOUT NARINGENIN

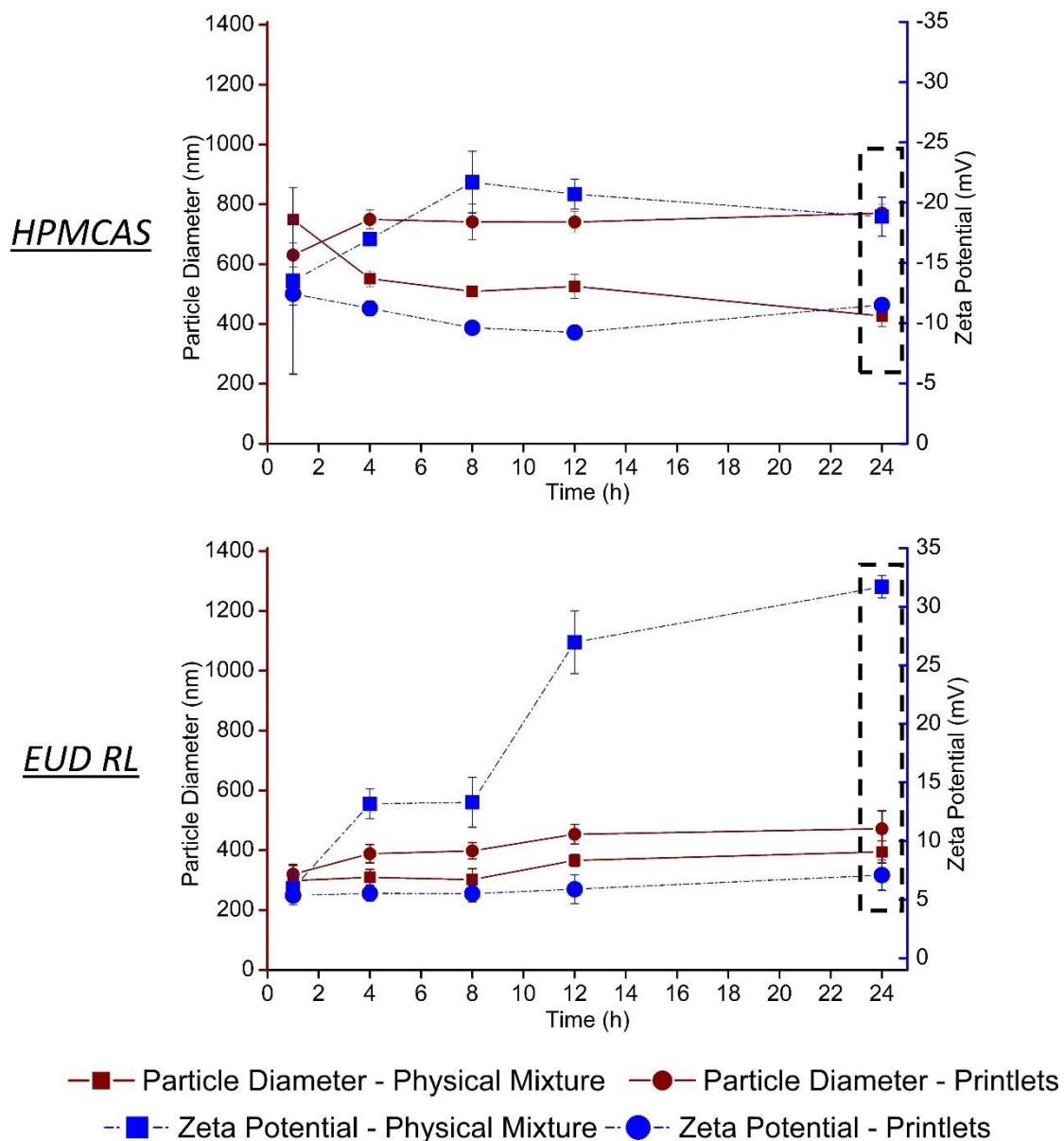


**Figure 1.** Particle diameter and zeta potential of the particles arose spontaneously from the dissolution of the physical mixtures and the printlets over 24h, produced with the polymers hydroxypropylmethylcellulose acetate succinate (HPMCAS) and Eudragit RL PO<sup>®</sup> (EUD RL) without the model drug naringenin (NAR). The highlighted data are the only ones with count rate higher than 100 kcps, been the only reliable data.